



TECHNISCHE
UNIVERSITÄT
WIEN
Vienna University of Technology

DIPLOMARBEIT

Modelling Block Of Excitation Of A Retinal Ganglion Cell Stimulated With Microelectrodes Using Python And Neuron

Ausgeführt am Institut für
ANALYSIS UND SCIENTIFIC COMPUTING
TECHNISCHE UNIVERSITÄT WIEN

unter der Anleitung von
ao. Univ.-Prof. Dipl.-Ing. DDDr. Frank Rattay

durch
Andreas Fellner
Jubiläumsallee 13
4861 Schörfling

Wien, am 15. Mai 2017

*Dedicated to my grandparents Eleonore and Ludwig,
Ludwig graduated at TU Wien 85 years ago*

Abstract

Selective stimulation of retina ganglion cells is a great challenge for the next generation of inner eye prostheses. One strategy to stimulate only certain target cells, is the utilization of a specific stimulation window, a lower and upper limit for stimulus strength to force an action potential. Stimulation strengths above the given upper limit are causing a block of excitation.

Such a stimulus window is not only defined by physiological and geometrical properties of the neuronal cell, but also depends on the geometry and location of the electrode itself. There are two hypotheses for the block of excitation: the *Anodal Surround Block* and the *Stimulation Upper Threshold*. However, there is a controversy about the physical principles that are causing the block of excitation for higher stimulus amplitudes.

The implemented multi compartment model in *Neuron* and *Python* supports active membrane mechanisms based on the Hodgkin-Huxley and the Fohlmeister-Miller model. It allows to simulate intra- and extracellular stimulation of a modelled retinal ganglion cell or parts of it. Besides a highly interactive user interface, also systematic test procedures are supported for analysing results of thousands of model runs with variations in geometrical or biophysical properties.

Based on the model, different analyses were performed. First, the direct effects of an electric field on a neuron during extracellular stimulation were investigated. For a spherical soma, a nearly equipotential state of the intracellular potential was found. Further, we were able to confirm experimental and computational results of another research about the time constant to reach intracellular potential equilibrium of a spherical soma within an electric field.

Then, the stimulation window for extracellular stimulation for a spherical soma was investigated in detail. We could find a correlation between the diameter of a spherical structure and the electrode distance which together define the stimulation window. Further, we were able to mathematically formulate the relationship between stimulation windows determined for different diameters of the spherical soma.

Also, we analysed the Na^+ current reversal and the total ionic Na^+ current flux during the stimulation and its consequences for action potential generation. We found a significant large zone within the stimulation win-

dow where a Na^+ current reversal happened during stimulation. Further, according to our model results, the relative portion of a Na^+ current reversal zone within the respective stimulation window seems to be constant for all stimulation amplitudes. Additionally, we found some stimulation configurations which initiated an action potential in spite a net Na^+ ion outflux occurred during the stimulation because of a Na^+ current reversal.

Finally, different electrode positions were tested on a retinal ganglion cell (without dendrites) and evaluated regarding blocking phenomena. For certain electrode geometries which influenced the retinal ganglion cell at different sections with comparable stimulation strengths simultaneously, we were able to reproduce total or partial blocking of the neuron. However, we were not able to distinguish in detail on which blocking phenomena (*Anodal Surround Block*, *Stimulation Upper Threshold*, or a combination of both) the determined blocking zones are based on. Out of a computational point of view, at the moment there are still many uncertainties regarding the consequences of the Na^+ current reversal on the generation or blocking of action potentials. Therefore, an exact classification was not possible yet.

The results of this thesis shall give some insight views on blocking phenomena helping to understand the mechanisms when applying extracellular stimulation to a neuronal cell with a spherical soma.

Kurzfassung

Die selektive Stimulation von Ganglienzellen in der Netzhaut ist eine der Herausforderung für die nächste Generation von Netzhautimplantaten. Eine der Strategien um nur bestimmte Zellen zu stimulieren, ist die Ausnutzung eines spezifischen Stimulationsfensters. Das Stimulationsfenster ist durch eine untere und obere Grenze für die Stimulationsintensität definiert innerhalb derer Aktionspotentiale generiert werden können. Bei einer Stimulationsintensität die über dem oberen Limit liegt, kommt es zu einer neuronalen Blockierung.

Das Stimulationsfenster ist nicht nur durch physiologische und geometrische Eigenschaften der Nervenzelle definiert, sondern hängt auch von der Geometrie und Lage der Elektrode selbst ab. Es gibt zwei verschiedene Hypothesen welche die neuronale Blockierung erklären, der *Anodal Surround Block* und der *Stimulation Upper Threshold*. Allerdings gibt es eine Kontroverse über die physikalischen Prinzipien, die zur neuronalen Blockierung bei hohen Stimulationsintensitäten führen.

Das in *Neuron* und *Python* implementierte Multi-Compartment Modell unterstützt aktive Membranmechanismen auf Basis des Hodgkin-Huxley und des Fohlmeister-Miller-Modells. Mit diesem Modell wird die intra- und extrazelluläre Stimulation einer modellierten retinalen Ganglienzelle (oder Teile davon) simuliert. Das Modell beinhaltet eine interaktive Benutzeroberfläche zur Auswertung von Zelldynamiken. Weiters werden auch systematische Testverfahren zur Analyse von unterschiedlichen geometrischen oder biophysikalischen Eigenschaften unterstützt.

Mit diesem Modell wurden verschiedene Untersuchungen durchgeführt. Zuerst wurden die direkten Effekte eines elektrischen Feldes auf ein Neuron während der extrazellulären Stimulation untersucht. Für ein kugelförmiges Soma wurde ein nahezu isoelektrischer Zustand im Inneren der Zelle ausgemacht. Weiters konnten wir experimentelle und modellierte Ergebnisse einer Studie über die Zeitkonstante zur Erreichung des Gleichgewichtszustands im elektrischen Feld eines kugelförmigen Soma bestätigen.

Anschließend wurde das Stimulationsfenster für die extrazelluläre Stimulation eines kugelförmigen Soma genauer betrachtet. Wir konnten eine Korrelation zwischen dem Durchmesser des kugelförmigen Soma und dem Stimulationsfenster nachweisen. Zusätzlich formulierten wir den mathema-

tischen Zusammenhang zwischen individuellen Stimulationsfenster für unterschiedliche Kugeldurchmesser.

Darüber hinaus analysierten wir auch die Na^+ Stromumkehr und den ionischen Na^+ Stromfluss während der Stimulation bezüglich deren Auswirkungen auf die Initiierung eines Aktionspotentials. Wir fanden eine durchaus signifikant große Zone innerhalb des Stimulationsfensters, in denen es während einer Stimulation zur Na^+ Stromumkehr kam. Die relative Größe einer solchen Na^+ Stromumkehrzone innerhalb des Stimulationsfensters ist für alle Stimulations-Stärken konstant. Zusätzlich fanden wir einige Fälle in denen auch Aktionspotentiale initiiert wurden, obwohl es zu einem netto Na^+ Ionen-Ausstrom während des Stimulus kam.

Schließlich wurden verschiedene Elektrodenpositionen für eine retinale Ganglienzelle (ohne Dendriten) hinsichtlich neuronaler Blockierung ausgewertet. Für gewisse Elektrodenkonfiguration welche unterschiedliche Bereiche der Nervenzelle zeitgleich mit vergleichbaren Stimulationsintensitäten beeinflussten, konnten wir neuronale Blockierungen der Zelle oder zumindest in Teilen der Zelle nachvollziehen. Allerdings konnten wir nicht im Detail unterscheiden, welche physikalische Effekte (*Anodal Surround Block* oder *Stimulation Upper Threshold* oder eine Kombination von beiden) diese Blockierungen verursachten. Dafür muss die Rolle der Na^+ Stromumkehr und deren Auswirkung auf die Generierung oder Blockierung von Aktionspotentialen erst genauer untersucht werden.

Die Ergebnisse dieser Arbeit sollen dabei helfen ein besseres Verständnis über die Vorgänge und Abläufe von verschiedenen Arten der neuronalen Blockierungen während der extrazellulären Stimulation von Nervenzellen mit kugelförmigen Soma zu bekommen.

Contents

Abstract	ii
Kurzfassung	iv
Acknowledgements	ix
Symbols, Glossary, Abbreviations	x
1 Introduction	1
1.1 Motivation	1
2 Overview	3
2.1 Neuronal Cells	3
2.2 Neuron Structure	5
2.3 Ion Channels	7
2.4 Action Potential	9
2.5 Electrical Stimulation	10
2.6 Retina	12
2.6.1 Retinal Ganglion Cells	14
3 Models	16
3.1 Cable Model	16
3.2 Hodgkin-Huxley Model	18
3.3 Fohlmeister-Miller Model	20
3.4 Compartment Model	22
3.5 Activating Function	23
3.6 Longitudinal and Transversal Modelling	24
4 Blocking Phenomena	26
4.1 Stimulation Window	26
4.2 Anodal Surround Block	28
4.2.1 Electric Field	29
4.2.2 Cathodic Stimulation	30
4.2.3 Activating Function	31

4.2.4	Magnitude of Polarizations	33
4.2.5	Anodic Stimulation	34
4.3	Stimulation Upper Threshold	34
4.3.1	Sodium Current Reversal	35
4.3.2	In-vitro Stimulation	37
4.3.3	Computational Modelling	37
4.4	Controversy	41
5	Neuron Software	42
5.1	Spatial Discretization	43
5.2	Biophysical Mechanisms	44
5.3	Temporal Discretization	45
6	Methodology	46
6.1	Cell Overview	47
6.2	Cell Morphology	48
6.3	Cell Biophysics	49
6.4	Spherical Soma	51
6.4.1	Membrane Potentials	51
6.4.2	Compartments	53
6.4.3	Axis of Soma	55
6.5	Cylindrical Structures	56
6.5.1	Membrane Potentials	56
6.5.2	Connection to Soma	58
6.6	Electrode	59
6.6.1	Extracellular Mechanism	59
6.6.2	Electrode Position	61
6.6.3	Electric Field	61
6.7	Neuron Models	64
6.8	Compiling of Neuron	64
6.9	Neuron Recording	64
6.10	Action Potential Detection	65
6.11	Automatic Test Procedures	67
6.12	User Interface	69
7	Results	73
7.1	Hypotheses	73
7.2	Direct Effects of Stimulus	75
7.2.1	Cylindrical Structure	75
7.2.2	Spherical Structure	79
7.3	Effects of Ionic Currents	83
7.4	Stimulation Window Spherical Soma	85
7.4.1	Geometric Relations Analysis	86
7.4.2	Sodium Current Reversal	90

CONTENTS

viii

7.5	Stimulation Window Retinal Ganglion Cell	96
7.5.1	Electrode above Soma	96
7.5.2	Electrode above Axon Hillock	98
7.5.3	Electrode lateral to Soma	100
8	Discussions	102
8.1	Summary	102
8.2	Further Work	104
	Bibliography	105

Acknowledgements

First, I need to thank Prof. Frank Rattay who advised this thesis. In countless meetings, we were working together not only on the major topics, but also on all those little details this thesis is finally based on. I always enjoyed our interesting discussions and scientific discourses. Frank, thanks a lot for all your support and motivation throughout this research, but also thanks a lot for letting me participate in your enthusiasm about neuronal science.

Further, I would like to thank Prof. Eugenijus Kaniusas, Dr. Paul Werginz and Hassan Bassereh Moosaabadi for their discussions and contributions during this research.

Some very special thanks goes to my family and especially my girlfriend Dani for accompanying and supporting me on my way. I am very grateful for all your trust and love!

Finally, I need to mention my friend Christoph Schöneegger. For many years now we are having long discussions about electrical topics and phenomena. Also, for this work he provided me some valuable information to understand the physics behind it.

Symbols, Glossary, Abbreviations

C	Capacity
F	Force, Faraday's constant
I	Current
Q	Charge
R	Resistance, gas constant
T	Temperature
t	Time
V	Voltage
C'	Transmembrane capacity length related
C''	Transmembrane capacity area related
E_{Na}	Nernst potential for Na^+ ions
E_K	Nernst potential for K^+ ions
E_L	Nernst potential for leakage current
G'	Transmembrane conductance length related
G''	Transmembrane conductance area related
R'_i	Intracellular resistance length related
R'_e	Extracellular resistance length related
R_x	Transfer resistance of extracellular stimulus
V_e	Extracellular potential/voltage
V_i	Intracellular potential/voltage
V_m	Membrane voltage
V_r	Resting voltage

g_{ion}	Conductance of an ion channel
\bar{g}_{ion}	Maximum Conductance of an ion channel
i_{ion}	Current density for ionic currents
i_K	Current density for ionic K^+ currents
i_L	Current density for ionic leakage currents
I_L	Leakage current
i_m	Current density total membrane
I_m	Membrane current
i_{Na}	Current density for ionic Na^+ currents
i_{st}	Current density for stimulus current
I_{st}	Stimulus current
k	Temperature coefficient
m, h, n	Gating variables
$[ion]$	Concentration of an ion
$[ion]_e$	Extracellular concentration of an ion
$[ion]_i$	Intracellular concentration of an ion
P_{ion}	Permeability of an ion
\vec{F}_d	Chemical diffusion force
\vec{F}_e	Electrical force
A	Area
d	Diameter
l	Length
r	Radius
τ	Time constant
AH	Axon Hillock
D	Distance between Electrode and Soma
DA	Distal section of an axon
ES	Extracellular space
FM	Fohlmeister Miller model
HD	Horizontal dendrite section
HH	Hodgkin-Huxley model

RGC	Retinal Ganglion Cell
SOCB	Sodium channel band of an axon
TS	Thin section of an axon
VD	Vertical dendrite section
Hodgkin-Huxley model	Active cell membrane mechanisms as described by Hodgkin and Huxley (1952) for the giant squid axon but with reversed current flows and changed resting potential to $V_r = -65mV$
Fohlmeister model	Active cell membrane mechanisms as described by Fohlmeister and Miller (1997) for tiger salamander retina ganglion cells
Anodal Surround Block	The propagation of an action potential is prevented by hyperpolarized zones
Compartment model	A model where geometric structures are described as interconnected smaller units. Each compartment implements the same functionality, but may differ in its properties
Current-distance relation	The dependency between a stimulus current amplitude and the distance between an electrode and neuron which determines the stimulation strength
Electrode pole	Pole of a spherical neuronal structure next/nearest to an extracellular electrode
Nernst potential	The membrane voltage for a certain type of ion (or generally for leakage ion flux) at which chemical diffusion force because of intra- and extracellular concentration and electrical force are in equilibrium
Section	A part of a neuronal structure which can be clearly distinguished by its anatomical or biophysical properties (soma, axon hillock, etc.)

Segment	A compartment of a section
Stimulation Upper Threshold	The initiation of an action potential is blocked in the first place because of a Na^+ current reversal
Stimulation window	Upper and lower limit for stimulus strength in extracellular stimulation
Strength-duration relation	The dependency between a stimulus strength the duration of the stimulus which determines the excitation of a neuronal cell

Variables used with limited context are not listed here, instead they are explained within the actual scope. Further, dot notation for differentiation is used throughout the whole thesis, e. g. , $\dot{V} \rightarrow \frac{dV}{dt}$

Chapter 1

Introduction

*“The universe perceives itself through us,
or to be more specific, through our neurons”*
- Abhijit Naskar

1.1 Motivation

While the electrical activity of the nervous system was already known in the late 18th century, the action potential was detected in the mid of the 19th century. An action potential is the electrical signal propagating along the axon of a neuron used to transmit information. The action potential is caused by ions passing the cell membrane via voltage sensitive ion channels. The main driving force is the chemical diffusion because of a concentration gradient between the intra- and extracellular space.

After first researches in electrical stimulation by Galvani, Volta, and others, the mechanisms and dynamics of an action potential were mathematically described by Hodgkin and Huxley in 1952 as a system of non-linear differential equations (Hodgkin and Huxley, 1952). Today, the principles of the Hodgkin-Huxley model are still used as basis of many neuronal models, including compartment models where every segment of the cell is characterized by specific biophysical and geometric properties.

There are different methods for stimulating a neuron. The target of a stimulation is always to activate the neuron's own mechanism of signal generation and propagation - therefore trigger an action potential. This research is focusing on extracellular stimulation with a micro-electrode in the vicinity of a neuron. The established electric field will change the potential differences between the intra- and extracellular space, forcing voltage sensitive ion channels to react on the stimulus. This may cause either the firing or the blocking of an actions potential.

The specific reaction of a neuronal cell on the stimulation depends on its physiology, the properties of the electrical stimulus, but also on the location

of the micro-electrode. Different cases of blocking the initiation or propagation of an action potential are described in literature like the *Anodal Surround Block* (or cathodic block phenomenon) (Ranck, 1975; Rattay, 1990) or the *Stimulation Upper Threshold* (Boinagrov et al., 2012). The focus on this research will lie in investigating different blocking phenomena based on a retinal ganglion cell model realized in *Python* and the neural modelling software *Neuron*, the most used software in the neuroscience community. For modelling the mechanisms and dynamics of the cell, the original Hodgkin-Huxley model (Hodgkin and Huxley, 1952), but also the specific Fohlmeister model for retinal ganglion cells (Fohlmeister et al., 1990; Fohlmeister and Miller, 1997) will be taken into account.

Chapter 2

Overview

“Neurons that fire together wire together”
- Donald Hebb

This chapter will give an overview about the scientific fields this work is related to. Biological mechanisms of neuronal cells including its very basic physics will be described, further the principles of electrical stimulation will be outlined.

2.1 Neuronal Cells

A neuronal cell has a cell membrane which mainly consists of a lipid bilayer. This membrane separates the intracellular from the extracellular space. Besides the lipids, the cell membrane incorporates different protein structures. Two types of such protein structures (macromolecules) are of special interest, the ion channels and the sodium-potassium pumps. (Mulroney et al., 2009)

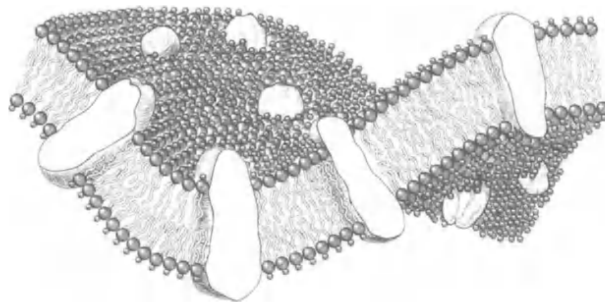


Figure 2.1: Visualization of a cell membrane. The figure shows the lipid bilayer with incorporated protein complexes used for ion transport (figure and parts of caption from Pfützner (2003)).

The cell is surrounded by the extracellular fluid, the inside of the cell contains the intracellular fluid, mainly cytosol. Both fluids are electrolytic solutions which contain certain ions in different concentrations. (Hille, 1992; Pfützner, 2003; Mulrone et al., 2009)

Electrochemically, the cell membrane is an isolating layer. However, because of the ion channels, there is an exchange of molecules between the inside and outside of the cell. This makes the membrane semipermeable. Taking into account the different concentrations of ions in the intra- and extracellular space, ions will move through ion channels once they are open. The two main driving forces are chemical diffusion \vec{F}_d and electrical force \vec{F}_e (Pfützner, 2003; Kaniusas, 2012):

- \vec{F}_d is caused by concentration gradients of ions between intra- and extracellular space.
- \vec{F}_e is caused by the voltage across the cell membrane because of different intra- and extracellular potentials.

Chemical diffusion is a thermodynamic force, molecules are moving from places with high concentration to places with low concentration. This flux would establish an equilibrium of molecules in the long run. By reaching an equilibrium of concentrations, the entropy of a system is maximized as stated in the thermodynamic laws.

As ions are electrical charged, the electrical force will also affect the ions transported through the cell membrane. Ions will be attracted or repelled depending on the charge of the ion itself and actual potential difference across the cell membrane.

Most significant ion concentration differences between intra- and extracellular space can be observed for sodium Na^+ which is dominant in the extracellular space and for potassium K^+ which is dominant in intracellular space. In general, the chemical diffusion forces and electrical forces would create an equilibrium of ion concentrations which would lead to electrical dysfunctionality. To keep the necessary unbalance upright, excitable cells need special mechanisms, e.g., the sodium-potassium pump. The sodium-potassium pump is constantly pumping Na^+ ions back to extracellular space, while K^+ ions are transported back to the inside of the cell. The necessary energy for these pumps is provided by adenosine triphosphate (ATP). (Pfützner, 2003; Mulrone et al., 2009)

Other ions playing a role are Ca^{2+} and Cl^- which can also be found in this environment. Further protein complexes found inside the cell like DNA or RNA will also influence the total charge of a cell. Considering all these compositions of charged molecules, a negative resting potential between the inside and the outside of a cell is present, typically in a range of around $-50mV$ to $-70mV$ for neuronal cells (Rattay, 1990). The actual

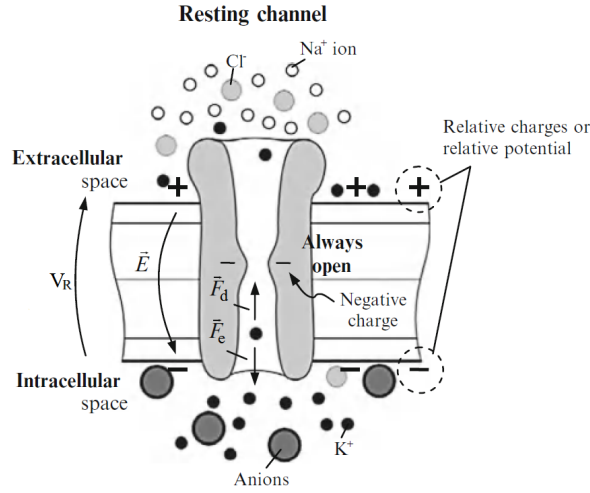


Figure 2.2: Forces driving an ion through an ion channel. Within the channel, the net transport of K^+ ions across the membrane is governed by an equilibrium between the diffusional force \vec{F}_d because of the concentration difference and electrical force \vec{F}_e because of the voltage difference (related to the electric field \vec{E}) (figure and parts of caption from Kaniusas (2012)).

voltage can be approximated based on the Goldman-Hodgkin-Katz equation (Goldman, 1943; Hodgkin and Katz, 1949):

$$V_m = \frac{R \cdot T}{F} \cdot \ln \frac{P_{Na}[Na^+]_e + P_K[K^+]_e + P_{Cl}[Cl^-]_i}{P_{Na}[Na^+]_i + P_K[K^+]_i + P_{Cl}[Cl^-]_e} \quad (2.1)$$

where V_m is the membrane potential, R the gas constant, T the temperature, and F the Faraday's constant. P_{ion} is the permeability for a certain ion, while $[ion]_e$ describes the extracellular concentration and $[ion]_i$ the intracellular concentration.

In case of any flux of ions through the cell membrane because of diffusion force \vec{F}_d and electrical force \vec{F}_e , the concentrations of ions are changing. Therefore, current is transported and the electrical potentials between in- and outside of the cell are changed. These local current flows and voltage changes are propagating inside the cell as axial currents. But, because of the thin cell membrane is a dielectric layer, any currents within the cell also leads to currents along the outer cell membrane (capacitive currents).

2.2 Neuron Structure

Neuronal cells have typically four morphological regions (see also figure 2.3) (Kaniusas, 2012):

- **Soma** or cell body: contains the organelles of the cell body.

- **Dendrites:** Branches that provide a receptive area.
- **Axon:** Single cylindrical extension which is used for signal propagation. The region an axon is connected to the soma is called axon hillock. An axon may be myelinated, isolating layers of Schwann cells which support signal propagation.
- **Terminal:** Branches that serve as cellular output.

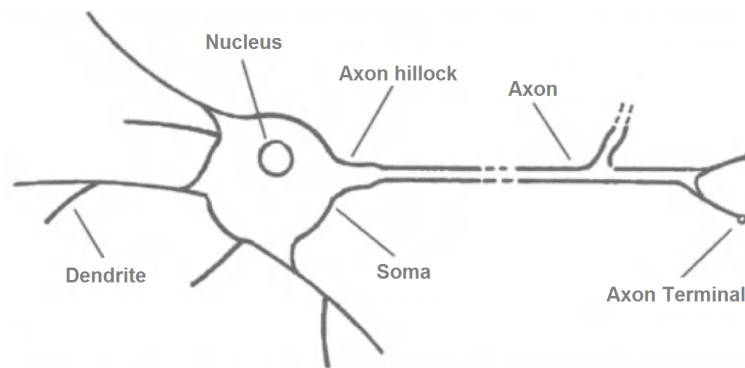


Figure 2.3: Morphological regions of a neuronal cell (modified from Pfützner (2003)).

The dendrites are typically branched and open for synaptic input from other neurons. Neurotransmitter which are released by source cells into the synaptic cleft open active ligand gated ion channels in the dendrites of a target cell. Ion influx through the channels lead to small local changes of the membrane voltage. Besides ligand gated ion channels, nowadays there are indications that most dendrites also have voltage sensible ion channels. These channels are reacting on small changes in the extracellular potential and have the ability to amplify these potential changes. (Kaniusas, 2012)

The resulting and summed up depolarization fronts from dendrites passively propagates toward to more sensible zones in the neuron, like the soma or the unmyelinated area of the axon near the axon hillock (Kaniusas, 2012). The reason for more or less sensible zones at different locations in a neuron is found in the cell membrane. Dendrites are usually considered as passive structures, meaning the density of ion channels in the membrane is small. In contrast to the soma which already has a notable density of ion channels. But, especially near the axon hillock, there is usually a region which has a much higher sodium channel density than the soma. Therefore, the axon proximal to the soma is the most excitable region of a neuron. (Carras et al., 1992; Nowak and Bullier, 1998; Fohlmeister et al., 2010; Jeng et al., 2011)

The axon is responsible for propagating a signal over distance. There are unmyelinated and myelinated axons. Myelinated axons are covered by

isolating sheaths of Schwann cells. The additional isolation maximizes the velocity of an electrical signal travelling through the axon as there are less losses because of capacitive currents charging the cell membrane. In between single myelin sheaths there are areas which are not myelinated, called nodes of Ranvier. These unmyelinated gaps have a high density of ion channels. An electrical current travelling through the axon therefore jumps rapidly from node to node (saltatory conduction) where it is regenerated by voltage sensitive ion channels for further propagation. (Rattay and Wenger, 2010; Kaniusas, 2012)

2.3 Ion Channels

Ion channels are pores which are incorporated in the cell membrane. They are composed of proteins which together form the macromolecular channel. There are many different types of such channels providing different functionality. Two characteristics are of special interest in this context, the selective permeability of ion channels for certain ions and the gating of these channels. (Hille, 1992)

The exact gating mechanisms of ion channels are extremely complex and research is difficult as all takes place on a molecular basis. Already Alan Hodgkin and Andrew Huxley stated (Hodgkin and Huxley, 1952):

"Details of the mechanism will probably not be settled for some time ..."

While there are ion channels which are open for different kind of ions, others are highly selective regarding the type of ions passing the channel. However, even a selective ion channel may be passed by different types of ions (Hille, 1992), but there are different mechanisms to discriminate for certain ions, known as selectivity filters (Hille, 1992; Doyle et al., 1998; MacKinnon, 2004):

- **Size of ions:** Different types of ions also have different sizes, so the geometry of a channel can exclude ions of different sizes than the desired one.
- **Charge and charge density of ions:** The charging of walls and/or entries of an ion channels may filter ions according their charge or charge density. Further, repelling effects of multiple ions entering the pore at the same time might be an active part of the filtering too.
- **Conformation changes:** Charged ions can cause conformation changes at other molecules which are also passing the pore. Such conformation changes lead to thermodynamic consequences for all molecules actually in the channel.

While still many details of the selective filters are not known at the moment, the gating mechanisms are better understood. Basically, following gating mechanisms can be distinguished (Hille, 1992; Kaniusas, 2012):

- **No gating:** Some channels have no active gating mechanism, meaning they are constantly open for ion flux. Such channels are for example leakage channels.
- **Voltage gating:** Voltage sensitive ion channels react on changes in the transmembrane voltage by a conformation change of the own structure. In case these conformation changes are severe enough, the ion channel opens.
- **Ligand gating:** Transmitters can bind to receptors of an ion channel which changes the conformation and forces the channel to open (molecular activity). This kind of gating is used for neuron to neuron signalling where neurotransmitters are released in the synaptic cleft to open channels at the target neuron.
- **Other gating:** There is a wide range of other mechanisms, like temperature gating or ion channels which react on mechanical influences like pressure or stretch.

While ligand-gated or different other gating mechanisms are responsible to translate a sensory input into a (weak) signal, the voltage gated ion channels will amplify and propagate the electrical signal. For the excitation of a neuronal cell, especially the voltage sensitive Na^+ and K^+ ion channels are of interest.

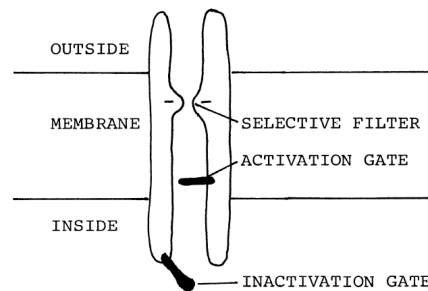


Figure 2.4: A simplified Na^+ ion channel: The activation gate controls the *open* and *closed* states. The additional inactivation gate also has the ability to close the channel (*inactive* state). Ion flux is only possible if both gates are open (figure and parts of caption from Rattay (1990)).

Besides the general functionality of selective voltage sensitive ion channels, also other physical properties are influencing the electrical behaviour

of the membrane. Differences in timing of different kinds of ion channels are crucial for the signal generation and its propagation. Typically, most types of Na^+ ion channels are considered to react faster on changes in voltage than K^+ ion channels. Also, the maximum permeability may differ between channels for different kind of ions. The total permeability of an area of cell membrane of course also depends on the density of ion channels there. Further, the possible conformational states of a channel needs to be considered. While a K^+ channel typically only knows the states *open* and *closed*, a Na^+ ion channel has an additional third state *inactive*. (Rattay, 1990; Pfützner, 2003; Kaniusas, 2012)

2.4 Action Potential

The temporal (major) change of the cell membrane voltage caused by fluxes of molecules through ion channels is called action potential¹. An action potential is an electrical signal propagating inside the cell to transmit information (Rattay, 1990).

Excitable cells are influenced/disturbed by the surrounding environment. They are susceptible for different kinds of molecules called neurotransmitter which may bind to special receptors of the cell by different mechanisms. Typically, those receptors trigger the opening of highly selectively ion channels. The caused ion fluxes influence the cell membrane voltage. As stated before, each cell has a resting potential around $-50mV$ to $-70mV$ which gets disturbed by entering and leaving ions.

In case the disturbance is severe enough, the voltage driven ion channels will open. This is often described by reaching a certain threshold voltage more positive than the resting potential. However, the dynamics of ion channels are influenced by many different factors (e. g. , time course of voltage change), therefore, the actual threshold voltage is fluctuating and should not be seen as a constant threshold.

The opening of these Na^+ ion channels will cause a huge amount of Na^+ ions enter the cell driven by diffusion and electrical forces. This leads to a net influx of positive charged ions. The membrane voltage will become more and more positive, this change in voltage is called depolarization.

During depolarization, the Na^+ ion channels close again², while the

¹It must be clearly stated that many different forms and characterizations of action potentials exist. For example, cardiac muscle cells underlie different dynamics than typical neuronal cells. Therefore, a cardiac action potential has a different form and timing than an action potential of a retinal ganglion cell for example. The general theoretical descriptions as found in physiological text books or in this section are only simplifications of very complex dynamics and physical phenomena which take place across the cell membrane.

²Both, the activation gate but also the inactivation gate of a Na^+ ion channel are closing the channel, but with different time constants. Gating dynamics for both gates are membrane voltage driven.

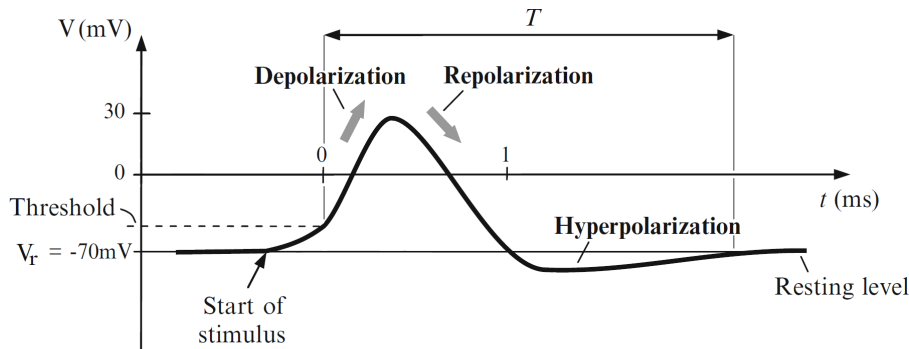


Figure 2.5: Typical action potential. After a stimulus started, the threshold level at around -50mV is reached. The Na^+ ion channels open and the depolarization starts. The membrane voltage is driven for a short time into positive range. Because the slower K^+ ion channels are working against the depolarization and the Na^+ ion channels are closing again, a repolarization sets in to bring the membrane voltage back to its resting potential. Before returning to the resting level, a short period of hyperpolarization can be seen. The duration T of the action potential is given in this case by exceeding the threshold level and returning back to resting voltage. However, there is no general accepted rule to identify a start or end or the total duration of an action potential (figure modified from Kaniusas (2012)).

slower K^+ ion channels will open. Because of the excess of K^+ ions in the intracellular space the K^+ ions will leave the cell, a net outflux of positive K^+ ions will take place, the voltage will become more negative again. This change is called repolarization and often ends in a hyperpolarization - meaning the voltage is short time below the normal resting level. After hyperpolarization, the voltage goes back to its resting level. During de-, re-, and hyperpolarization a cell might be incapable to initiate another action impulse also known as refractory period. (Kaniusas, 2012)

2.5 Electrical Stimulation

In nature, normally the excitation is initiated by neurotransmitters released by synapses into the synaptic cleft which open ligand gated ion channels of the target cell. Entering ions will disturb the intracellular potential locally. This result in intracellular currents transported inside the neuron. If there are many local trigger zones involved, summed up currents are travelling towards global trigger zones. A global trigger zone is a zone which is highly excitable. At the global trigger zone the voltage sensitive Na^+ ion channels rapidly open and initiate an action potential.

However, in experimental environment, but also for neuroprostheses, the electrical stimulation of a target cell is the preferred method to trigger an

action potential. An electrical stimulus inside or in the vicinity of a neuronal cell will influence the membrane potential by establishing an electric field by producing polarizations in the membrane voltage. In case of a serious depolarization over the threshold membrane voltage, the voltage sensitive Na^+ ion channels are forced to react and initiate an action potential. Ligand based ion channels are omitted this way as voltage sensible ion channels are targeted directly.

The membrane voltage V_m is the difference of the intracellular potential V_i and the extracellular potential V_e ($V_m = V_i - V_e$). At rest, the resting voltage V_r is around $V_r \approx -65mV$. A typical threshold voltage to force a voltage sensible Na^+ ion channel to open rapidly is around $-50mV$. To exceed the membrane threshold voltage there are basically two ways (Rattay, 1990; Pfützner, 2003; Kaniusas, 2012):

- **Intracellular stimulation:** The V_i potential must be increased locally to reach the threshold voltage. This can be realized by injecting current into the cell by one or more electrodes.
- **Extracellular stimulation:** The V_e potential must be decreased in order to get a local depolarization of the cell. This can be archived by establishing an electric field in the vicinity of the neuronal cell which directly influences the membrane voltage V_m . Different kind of electrodes and electrodes geometries are possible.

Ohm's law ($V = R \cdot I$) states that voltage V is proportional to current I . So, in electrical stimulation either the membrane voltage or the current itself is controlled. While first experiments³ were voltage based, the current based approach is more comprehensible as all membrane mechanism are current based (ion fluxes) and the voltage is just a result of these ionic current transports (Kaniusas, 2012).

Basically, there are two important relations which determine the generation of an action potential in extracellular stimulation (Ranck, 1975):

- **Current-distance relation:** The resistivity of the extracellular medium will weaken the stimulus along its way. For short distances between a neuron and an electrode, only a small amplitude of stimulus current is required to initiate an action potential. In contrast to long distances where higher amplitudes are necessary. The essential factor is the current/voltage which is directly influencing the cell membrane. Therefore, the strength of stimulus always depends on the current in combination with the distance to a possible trigger zone. The minimum strength necessary to excite a neuronal structure is called *rheobase*.

³Kenneth Cole invented the voltage clamp in 1947.

- **Strength-duration relation:** For a given stimulation strength a minimum stimulation time is required to reach the threshold voltage and to open the voltage sensitive ion channels. The required conformation change of an opening ion channel takes some time. Therefore, the gating dynamics have time delays which need to be exceeded by the stimulus. The minimum duration for twice *rheobase* strength is called *chronaxie*.

However, electrical stimulation is underlying several more limitations. One of these limitations is a specific stimulation window, a lower and upper limit for the strength of a stimulus to trigger an action potential. Such a stimulus window is not only defined by the cell type (physiological and geometrical properties), but also the geometry and location of the electrode itself (see also chapter 4):

- **Lower limit:** A stimulus intensity below this limit is not resulting in a depolarization severe enough to initiate an action potential. The reason is a too weak stimulus to overcome the threshold voltage of a cell because (i) a too weak stimulus amplitude, (ii) a too short time the stimulus is applied, or (iii) the distance between electrode and target zone is too large.
- **Upper limit:** A stimulus strength above the upper limit is blocked by the neuronal cell. One reason is known as *Anodal Surround Block*⁴ (Ranck, 1975; Rattay, 1990). Shortly, this phenomenon is characterized by a strong depolarized local zone opening its Na^+ ion channels, but next to the depolarized region there are strongly hyperpolarized regions preventing the propagation of the action potential.

Another reason is known as the *Stimulation Upper Threshold* (Boinagrov et al., 2012). Here, a very strong stimulus is causing the Na^+ ion channels to open but leading to a Na^+ current reversal (outflow of Na^+ ions instead of inflow as usual) preventing the generation of an action potential in the first place. The Na^+ current reversal is given if an outward directed electrical force exceeds the inward directed chemical diffusion force.

Further there is also an absolute upper limit given by a stimulus strength which leads to a cellular damage (Durand, 1999).

2.6 Retina

The retina is part of the visual perception system and coats the eyeball on the inner side. In the retina, any stimuli from light (photons) are transferred into

⁴Also known as cathodic block phenomenon.

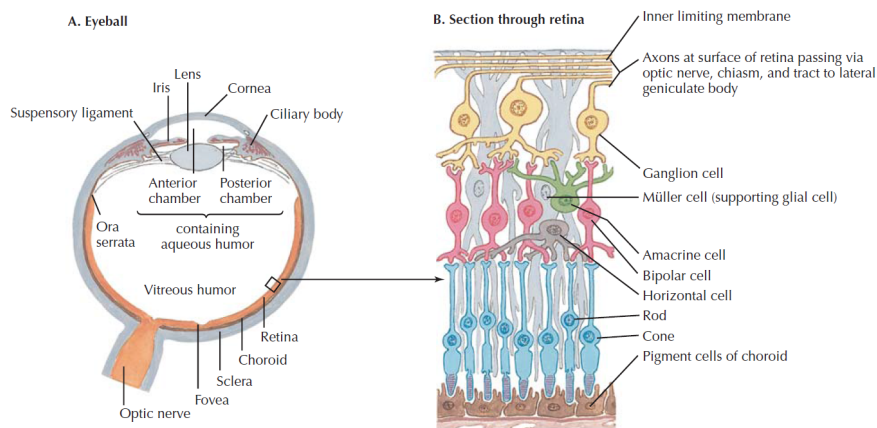


Figure 2.6: Anatomy of the human eye and details of the structure of the retina. Light is entering the eye through the cornea. The lens is projecting and focusing the light onto the retina which will convert the input of photons into neuronal signals passing to brain via optical nerve. The photons will first pass the neuronal structures of retinal ganglion cells and bipolar cells until finally the rods and cones are stimulated. Rods and cones have photoreceptors which will react on any stimulus of photons with inhibition. Bipolar cells are synaptic connected to rods and cones and are responsible to transmit signals to the ganglion cells. Finally, the retinal ganglion cells react on the neuronal signals of surrounding bipolar and amacrine cells and response with action potentials passed into optical nerve (figure and parts of caption from Mulroney et al. (2009)).

neuronal signals which are passed into brain via the optical nerve (see figure 2.6). The most important neuronal structures in the retina are (Kandel et al., 2000; Mulroney et al., 2009):

- **Rods and cones:** Photoreceptors on rods and cones will inhibit these cells in case of stimulation by photons. In case of excitation (less light), they are releasing neurotransmitters processed by the bipolar cells.
- **Horizontal cells:** Build functional networks between rods and cones. These networks are summing up signals from rods and cones and are influencing signal flow and routing between these structures.
- **Bipolar cells:** Transmit signals from rods/cones or horizontal cells to the retinal ganglion cells. Instead of action potential their signal is propagating by voltage gradients. There are on and off bipolar cells meaning they are reacting in exactly opposite way on the same stimulus.
- **Amacrine cells:** Build functional networks between bipolar cells and retinal ganglion cells. They are influencing the signal of bipolar cells

to ganglion cells by routing the signal. This way functional units of ganglion cell are built.

- **Retinal ganglion cells:** They are processing the neuronal input of bipolar and amacrine cells by summing them up. If the total input is strong enough to excite the retinal ganglion cell they react with an action potential which is passed via the optical nerve to the brain.

2.6.1 Retinal Ganglion Cells

Basically, a retinal ganglion cell consists of a soma, dendrites, and an axon. The shape of the soma is a complex 3D structure of spherical form, its dendrites are widely branched. The axons are forming the optical nerve which is heading from the retina into the brain (thalamus and then visual cortex). (Kandel et al., 2000)

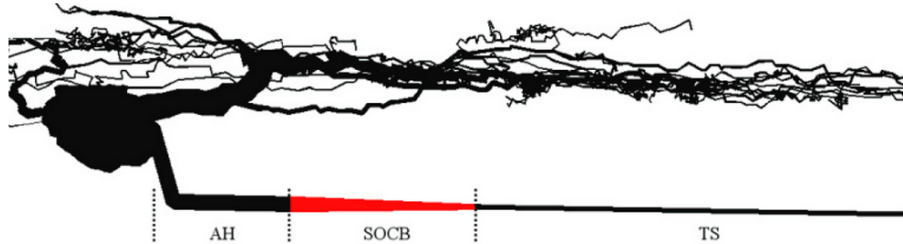


Figure 2.7: Schematic of a retinal ganglion cell with dendrite tree, spherical soma, axon hillock (AH), the sodium channel band (SOCB) with very high density of Na^+ ion channels, and rest of axon referred as thin section (TS). Distal axon (DA) region after thin segment (TS) is not shown (figure and parts of caption from Jeng et al. (2011)).

Regarding biophysical properties different section of the retinal ganglion cell must be considered (Carras et al., 1992; Kandel et al., 2000; Fried et al., 2009; Fohlmeister et al., 2010; Jeng et al., 2011):

- **Dendrites:** They have a very low conductivity and are usually referred to be passive structures or active structures with low Na^+ conductivity. Therefore, it is not likely an action potential is initiated there. The dendrites will react on neurotransmitters released by bipolar cells with small currents. These currents are transferred into the soma where they are summed up.
- **Soma:** The more or less spherical soma is the center of the cell. The dendrites are entering the soma, while the axon leaves from there. It is not very excitable compared to the sodium channel band of the axon with its high densities of Na^+ ion channels.

- **Axon Hillock:** The first region of the axon proximal to soma with similar electrical properties as the soma itself. Typically, it incorporates a bend where leaving the soma.
- **Sodium channel band:** This is the most excitable region of the whole neuronal structure placed proximal to the soma after the axon hillock. Because of the high density of voltage sensitive ion channels, it is the most responsive part of a neuron to electrical stimulation.
- **Thin section:** A short thin segment right after the sodium channel band, with slightly increased conductivities compared to the rest of the axon.
- **Axon:** The region of the axon after the sodium channel band may be classified into further segments, however, in general it is assumed to have more or less same biophysical membrane properties as the soma.

Typical conductivities and other biophysical properties can be found in following table 2.8:

	Axon				Soma	Dendrites
	AH	SOCB	TS	DA		
Diameter (μm) (proximal end)	3	3	0.8	1		
Diameter (μm) (distal end)	3	0.8	0.8	1		
Length (μm)	41	40	90	5300		
\hat{G}_{Na} ($E_{\text{Na}}=+35\text{mV}$)	70	350–2800	100	70	80	25
$\hat{G}_{\text{K,DR}}$ ($E_{\text{K}}=-75\text{mV}$)	18	9–72	18	18	18	12
\hat{G}_{A} ($E_{\text{K}}=-75\text{mV}$)		54	54		54	36
\hat{G}_{Ca} ($E_{\text{Ca}}=132\text{mV}$)		1.5			1.5	2
$\hat{G}_{\text{K,Ca}}$	0.065	0.065	0.065	0.065	0.065	0.001
\hat{G}_{I}	0.005	0.005	0.005	0.005	0.005	0.005
Conductances are in pS/cm^2						
Number of segments	99	21	21	354	21	536

Figure 2.8: Biophysical and morphological properties for a retinal ganglion cell. Conductivities for different channels are given by \hat{G}_{ion} , the corresponding Nernst potentials with E_{ion} . The conductivity for Na^+ ions in the sodium channel band (SOCB) is much higher than on any other section because of the high density of Na^+ ion channels. This is the region with highest excitability (figure and parts of caption from Jeng et al. (2011)).

Chapter 3

Models

Mathematical models are used to describe the mechanisms and dynamics of neuronal cells. Different types of cells have different properties, still very general approaches of modelling allow good projections for a particular type of cell one is interested in. To model a certain type of cell, not only the electrochemical behaviour is of interest, also its geometry plays an important role. Further, it must be considered that a cell is composed of different sections having different characteristics. A serious model needs to be able to incorporate these characteristics and deal with them over all sections correctly including boundary conditions at the terminals.

3.1 Cable Model

The cable model is describing the biophysical properties of a cell (see figure 3.1) behaviour of a small part (Δx) of cell membrane by using classical electrical components⁵ (Rattay, 1990; Pfützner, 2003; Kaniusas, 2012):

- **Intra- and extracellular resistance R'_i and R'_e :** The resistances are given by the electrolytic solutions in the intra- and extracellular space. Not only the respective mobility of ions influence the specific resistivity, but also the limited cross-sectional area in the intracellular space (and therefore limited amount of charge carrier) has direct implications for R'_i .
- **Transmembrane conductance G' :** The membrane is an isolating layer, but it is not isolating not perfectly. Therefore, some leakage current can pass the membrane which is modelled by a resistor.
- **Transmembrane resting voltage V_r :** The membrane resting potential is modelled with a battery in series to the transmembrane resistance G' .

⁵All notations are related to Δx .

- **Transmembrane capacity C' :** The cell membrane with its dielectric characteristics is separating two conductive fluids. This is equivalent to a plate capacitor, where charge is directly stored at the cell membrane (+ Q and $-Q$).

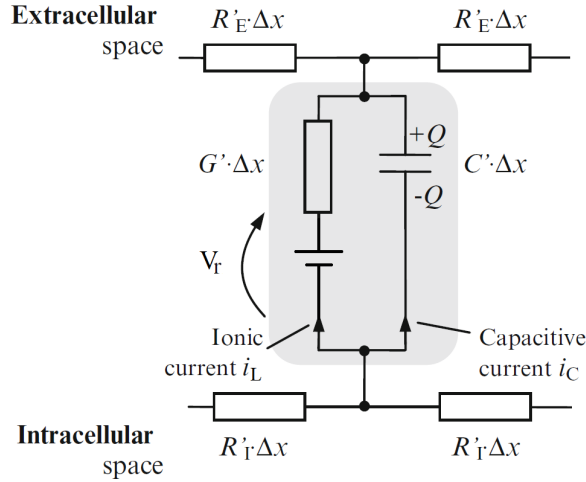


Figure 3.1: Classical cable model for a passive cell of small size. A voltage V_m is established between the intra- and extracellular space (V_r for resting state). The gray area represents the modelled cell membrane with a leakage current i_L and a capacitive current i_C (figure and parts of caption from Kaniusas (2012)).

The passive cable model can always be used to describe the resting state of a membrane or used for sub-threshold stimulation (no action potential initiated). The dielectric lipid bilayer is modelled as a capacitor with a resistor for leakage current in parallel. Mathematically, the capacitor charge Q is equal to capacitance C multiplied with the membrane voltage V_m . By differentiation, the current I_C can be determined (Hille, 1992):

$$Q = C \cdot V_m \rightarrow \dot{Q} = C \cdot \dot{V}_m \rightarrow I_C = C \cdot \dot{V}_m \quad (3.1)$$

The leakage current I_L can be rewritten by Ohm's law:

$$I_L = V_m/R \quad (3.2)$$

Because the capacitor is in parallel, Kirchhoff's law must be applied, stating:

$$I_L + I_C = 0 \rightarrow V_m/R + C \cdot \dot{V}_m = 0 \rightarrow \dot{V}_m = -\frac{V_m}{R \cdot C} \quad (3.3)$$

$R \cdot C$ can be replaced by the time constant τ , the solution of the differential equation will result in an exponential decay:

$$\dot{V}_m = -\frac{V_m}{\tau} \rightarrow V_m(t) = V_{m,0} \cdot e^{-\frac{t}{\tau}} \quad (3.4)$$

3.2 Hodgkin-Huxley Model

In the beginning of the 1950's Alan Lloyd Hodgkin and Andrew Fielding Huxley were performing electrical stimulation on a giant squid's axon with a voltage clamp. This resulted in the Hodgkin-Huxley model which describes the active cell membrane electrical behaviour - the action potential.

In contrast to the passive mechanism as described in section 3.1, two additional ion channels for Na^+ and K^+ are added to the leakage channel. These ion channels are voltage sensitive, so their conductivity is not fixed any more and changes over time. Instead of a resistor, a potentiometer is now used for modelling the gating of these channels. The ion channel for leakage current does not have any gating and is therefore modelled by a resistor. (Hodgkin and Huxley, 1952)

Note the reversed battery for the Na^+ ion channel, the reason is found in the concentration gradient for Na^+ ions⁶ which results an inflow of Na^+ at a membrane voltage in normal ranges. This inflow is caused by the diffusion force because of concentration gradient (see also section 2.3).

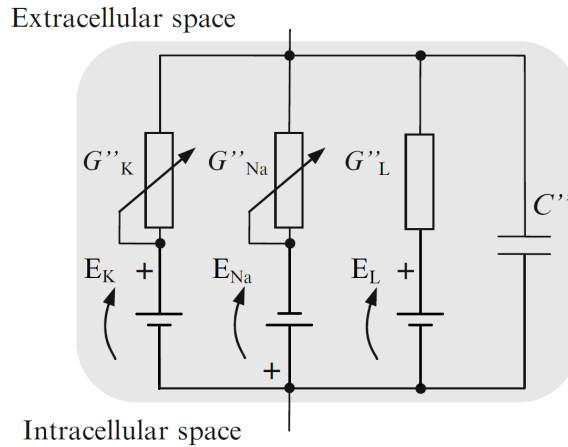


Figure 3.2: Classical cable model of a cell membrane during excitation (action potential). Two ion channels (Na^+ and K^+) are modelled by potentiometer with area related conductivities G''_{Na} and G''_K . An additional leakage channel modelled with a resistor (area related conductivity G''_L). The membrane voltage at time t is greater than the resting membrane voltage ($V_m(t) > V_r$) during an action potential (figure modified from Kaniusas (2012)). An equivalent circuit can also be found in the original Hodgkin and Huxley (1952) paper.

Mathematically⁷ the Hodgkin-Huxley model describes the voltage to cur-

⁶Extracellular:Intracellular sodium ion concentration is 460:50 for squid axon according to Pfützner (2003).

⁷Compared to the original publication, all formulas are fitted to a resting state voltage $V_r = -65mV$, voltages are given absolutely.

rent relation in a neuron by a set of nonlinear differential equation. Basically, the membrane voltage is defined as V_m whereas i describes the current density and c the capacity density:

$$\dot{V}_m = [i_{st} - i_{ionic}]/c \rightarrow \dot{V}_m = [i_{st} - i_{Na} - i_K - i_R]/c \quad (3.5)$$

Using densities⁸ allows to define a model independent of actual geometry (Rattay, 1990). The voltage to current relation then is given by:

$$\dot{V}_m = [i_{st} - \bar{g}_{Na}m^3h(V_m - E_{Na}) - \bar{g}_Kn^4(V_m - E_K) - \bar{g}_L(V_m - E_L)]/c \quad (3.6)$$

Constants were determined in experiments (Hodgkin and Huxley, 1952):

$$c = 1 \frac{\mu F}{cm^2}$$

$$\bar{g}_{Na} = 120 \frac{mS}{cm^2}, \bar{g}_K = 36 \frac{mS}{cm^2}, \bar{g}_L = 0.3 \frac{mS}{cm^2}$$

$$E_{Na} = 50mV, E_K = -77mV, E_L = -54.4mV$$

The maximal conductance \bar{g}_{ion} describes the permeability of the respective ion channel while the E_{ion} stands for the voltage generated by ionic chemical diffusion currents. E_{ion} is given by the Nernst⁹ equation (Nernst, 1888):

$$E_{ion} = \frac{R \cdot T}{z \cdot F} \cdot \ln \frac{[Na]_e}{[Na]_i} \quad (3.7)$$

with R denotes the gas constant, T the temperature, F the Faraday's constant, and z the valence of an ion ($z = 1$ for Na^+). The concentrations for extracellular and intracellular space are given by $[Na]_e$ and $[Na]_i$.

The variables m , h , and n are gating variables. A gating variable models the probability of an ion channel's conformational state. For voltage sensitive ion channels as used in this model, the probability only depends on the membrane Voltage V . While the K^+ ion channel only requires one gating variable n for its conformational states *open* and *closed*, the Na^+ ion channel has two gating variables m and h where h is used to model the additional *inactive* state:

$$\dot{m} = [\alpha_m(1 - m) - \beta_m m] \cdot k \quad (3.8)$$

$$\dot{n} = [\alpha_n(1 - n) - \beta_n n] \cdot k \quad (3.9)$$

$$\dot{h} = [\alpha_h(1 - h) - \beta_h h] \cdot k \quad (3.10)$$

⁸E.g. $i_{st} = I_{inj}/2\pi rl$, current injected from a stimulus to area of the membrane.

⁹Walther Nernst (1864-1941) was a German physicist and was awarded the Nobel Prize in chemistry for his work in thermochemistry.

Above differential equations were extended by a temperature coefficient $k = 3^{0.1T-0.63}$. The experiments and therefore archived constants of Hodgkin and Huxley (1952) where performed at $T = 6.3^\circ C$. This temperature coefficient¹⁰ is used to fit the model to a certain temperature T . This is necessary as the thermodynamic forces determining the temporal dynamics of an ion channel are temperature sensible (Rattay, 1990). The α_{state} and β_{state} are:

$$\alpha_m = 0.1 \frac{(V + 40)}{1 - e^{-(V+40)/10}} \quad (3.11)$$

$$\beta_m = 4e^{-(V+65)/18} \quad (3.12)$$

$$\alpha_n = 0.01 \frac{(V + 55)}{1 - e^{-(V+55)/10}} \quad (3.13)$$

$$\beta_n = 0.125e^{-(V+65)/80} \quad (3.14)$$

$$\alpha_h = 0.07e^{-(V+65)/20} \quad (3.15)$$

$$\beta_h = \frac{1}{1 + e^{-(V+35)/10}} \quad (3.16)$$

The dynamics of the model are a direct result of the gating variables (see also section 2.3). The K^+ channel just knows the *open/closed* state which is modelled by the gating variable n . Figure 3.3 (a) shows that the K^+ ion channel opens soon after threshold voltage is reached. Above the threshold level it stays in an open state. The respective time constant of the K^+ ion channel reacts very slowly compared to the fast Na^+ ion channel.

The *open/close* state of the Na^+ ion channel is represented by the m gating variable. It opens at significant lower voltages than the K^+ ion channels (see figure 3.3) (a), the curve progression is similar to the one of K^+ . However, the time constants (b) show that the Na^+ ion channel is much faster, according to Malmivuo and Plonsey (1995) a typical Na^+ channel opens around 10 times faster than a K^+ channel. This difference in timing is the reason an action potential can occur at all, as the cell has some time to depolarize before K^+ ions are working against the depolarization.

However, besides the m gating variable, there is a second one, the h . A Na^+ ion channel can be *inactive*, meaning there is another mechanism in the pore that prevents the flux of ions. The total current of Na^+ ions is given by $\bar{g}_{Na}m^3h(V_m - E_{Na})/c$ (see equation 3.6). While the m gating variable will cause an increase of current, the h variable slows down and finally stops the flux of Na^+ ions again (Malmivuo and Plonsey, 1995).

3.3 Fohlmeister-Miller Model

A modification of the Hodgkin-Huxley model was presented by Fohlmeister et al. (1990) for a tiger salamander ganglion cell using four voltage gated ion

¹⁰Also referred to Q_{10} coefficient in literature.

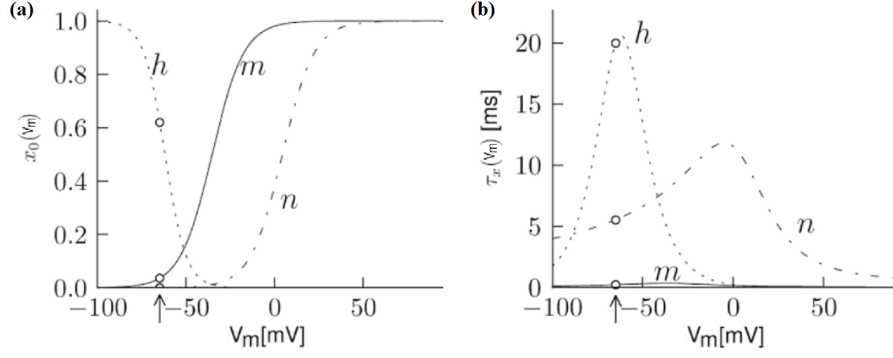


Figure 3.3: Hodgkin-Huxley model gating variables in relation to the membrane voltage. The left figure (a) shows the probability of the gating variables (equilibrium functions). Note the two Na^+ ion channel gating variables: While m opens rapidly when threshold voltage is reached, the *active/inactive* state variable h is starting to prevent Na^+ ions to pass the channel at early stage again. The right figure (b) shows the respective temporal behaviours of the ion channels. The arrows mark the resting voltage $V_r = -65mV$ (figure modified from Gerstner et al. (2014)).

channel (Na^+ , Ca^{2+} , non-inactivating K^+ , and inactivating A-type¹¹ K^+). Further, another ligand gated K^+ channel activated by the Ca^{2+} concentration of the intracellular space is considered. After continuous research the Fohlmeister et al. (1990) model was slightly adapted and extended by a leakage channel which led to the Fohlmeister and Miller (1997) model.

The voltage current relation for this model is (Fohlmeister and Miller, 1997):

$$\begin{aligned} \dot{V}_m = & [i_{st} - \bar{g}_{Na}m^3h(V_m - E_{Na}) - \bar{g}_{Ca}c^3(V_m - E_{Ca}) - \\ & (\bar{g}_K n^4 + \bar{g}_{K,A}a^3h_A + g_{K,Ca})(V_m - E_K) - \bar{g}_L(V_m - E_L)]/c \end{aligned} \quad (3.17)$$

The maximal conductance \bar{g}_{ion} describes the permeability of the respective ion channel while the E_{ion} stands for the voltage generated by ionic chemical diffusion currents.

The gating variables m, h, c, n, a for the voltage sensitive ion channels Na^+ , Ca^{2+} , non-inactivating K^+ , and inactivating K^+ , are formulated in Hodgkin-Huxley model style and follow the kinetic equation:

$$\dot{x} = [\alpha_x(1 - x) - \beta_x x]$$

In contrast, the ligand based K^+ ion channel of equation 3.17 is activated by the concentration of Ca^{2+} ions:

¹¹A-Type potassium channels are having an *inactive* state. They are referred as fast inactivating voltage gated outward current K^+ channels.

$$g_{K,Ca} = \bar{g}_{K,Ca} * \frac{([Ca^{2+}]_i / (Ca^{2+})_{diss})^2}{1 + ([Ca^{2+}]_i / (Ca^{2+})_{diss})^2} \quad (3.18)$$

where $(Ca^{2+})_{diss}$ is the dissociation constant and $[Ca^{2+}]_i$ is the actual Ca^{2+} ion concentration. Fohlmeister et al. (1990) assume that the ion concentration is kept on a constant value by an ion pump (Ca^{2+} -pump) following the equation:

$$\frac{d[Ca^{2+}]_i}{dt} = \frac{-3 * I_{Ca}}{2Fr} - \frac{([Ca^{2+}]_i - [Ca^{2+}]_{res})}{\tau_{Ca}} \quad (3.19)$$

where I_{Ca} is the current generated by inflowing Ca^{2+} ions and $[Ca^{2+}]_{res}$ is the residual level of Ca^{2+} ion concentration. In case $[Ca^{2+}]_i$ exceeds the $[Ca^{2+}]_{res}$, the pump will consequently sequester exceeding ions with the time constant τ_{Ca} . F is the Faraday constant, $3/r$ is the ratio of surface to volume of a spherical soma (Fohlmeister et al., 1990; Fohlmeister and Miller, 1997).

As a result of later researches, also a model for retinal ganglion cell of endothermic animals (cat and rat) was presented by Fohlmeister et al. (2010). However, the underlying retinal ganglion cell model used in this thesis is based on Fohlmeister and Miller (1997).

3.4 Compartment Model

Neuronal cells typically consist of different sections (e. g. , dendrites, a soma, and an axon). Every part has got its own geometric and biophysical properties. Also within a section, there might be differences, e. g. , in the first section of an axon proximal to the soma there are regions having much higher density of ion channels compared to regions distal from the soma. (Fried et al., 2009)

To take different properties into account, a neuron can be divided into multiple connected compartments (see figure 3.4). For every compartment, it is possible to define the exact biophysical mechanisms and dynamics, further, geometric properties like diameters or the topology related to other compartments (or an electrode for example) can be considered.

In general, a single compartment is modelled as active or passive cable model (see also section 3.1). However, in a multi compartment model also currents between neighbouring compartments must be taken into account. These currents are referred as axial currents. Between two neighbouring compartments, the intracellular resistivity is modelled by the resistance of the solution. In a multi compartment model, the single compartments influence each other along the full structure. This make the mathematical solution more complicated. However, because of the spatial discretization reached by the compartment, this method allows to model spatial effects like

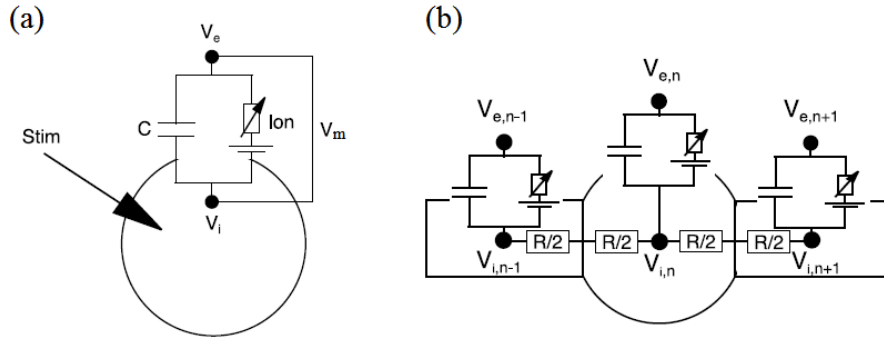


Figure 3.4: On the left (a), a single compartment modelled by cable model with a stimulus current, a capacitive current, and an ionic current. On the right (b), a neuronal cell is divided into n compartments connected to each neighbour by resistors in axial direction (figure modified from Werginz (2016)).

injected currents at some region in the neuron, or an extracellular potential gradient along the surface established from an external stimulus.

3.5 Activating Function

An extracellular stimulus will establish an electric field in the extracellular space. This field influences the extracellular potential of every compartment inside the field.

A concept to approximate the influence of the electrical field to cylindrical and uniform neuronal sections modelled by a multi compartment model, is the activating function introduced by Rattay (1986). It is derived from the cable model assuming given extracellular potentials for every compartment (McNeal, 1976). It shows regions of depolarization and hyperpolarization in a cylindrical neuronal section (Rattay, 1986, 1990, 1999):

$$f_n = \left[\frac{V_{e,n-1} - V_{e,n}}{R_{i,n-1}/2 + R_{i,n}/2} + \frac{V_{e,n+1} - V_{e,n}}{R_{i,n+1}/2 + R_{i,n}/2} + \dots \right] / C_n \quad (3.20)$$

The function of x and t is the second derivative of external membrane voltage along a neuronal section. $V_{e,n}$ is the external voltage of the n^{th} compartment which is exposed to the external field, while $R_{i,n}$ is the intracellular resistance. For more details see also section 4.2. Positive values indicate depolarized regions along the fibre while negative values show hyperpolarized regions (see figure 3.5). The activating function also shows the influence/effects of the electrode to neuron distance. An angle¹² of around

¹²Independent of fibre properties, the conductivity of the extracellular fluid, or stimulus amplitude.

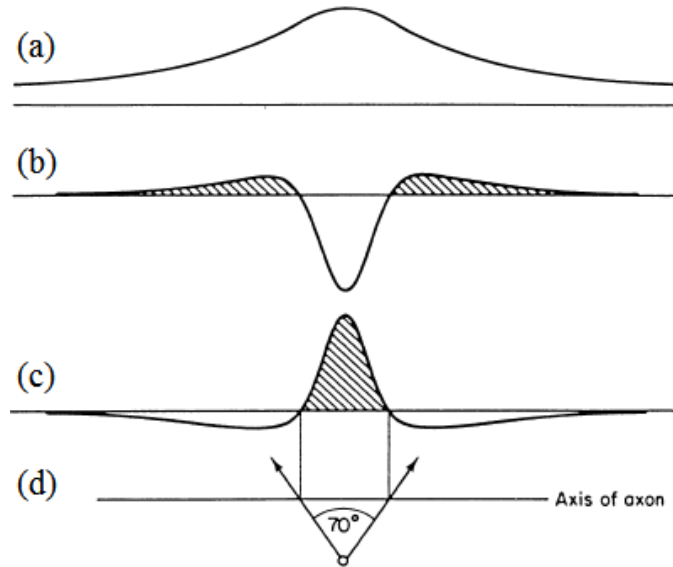


Figure 3.5: Results of the activating function on an extracellular stimulation. Shaded areas are depolarized regions. (a) shows the extracellular potential V_e for an anodic extracellular stimulation along the fibre. In (b) the changes of polarization for an anodic stimulation are approximated by the activating function f_n . (c) shows the activating function for a cathodic stimulus. In (d) the position of the electrode is marked, further the angle of around 70° indicates the borders between de- and hyperpolarized regions as resulted by the activating function (figure and parts of caption from Rattay (1990)).

70° at the electrode allows to estimate the borders between opposite polarized regions along the fibre. The length of the polarized region next to the electrode is growing with distance.

3.6 Longitudinal and Transversal Modelling

Another way of modelling extracellular stimulation is the calculation of the extracellular potential V_e for every compartment in a multi compartment model. Doing so will let the stimulus directly influence the membrane potential V_m . This method is applicable for different kinds of electrodes¹³.

An extracellular stimulus will establish a particular electric field in the 3D space. Knowing the topology (distance to electrode(s)) of every compartment in space, the extracellular potential influencing the surface of a compartment can be taken into account. The potential on the outside of a cell membrane strongly depends on the amplitude of the stimulus, the

¹³E.g. point micro-electrode, electrode arrays, plate electrodes.

distance electrode to compartment, the conductivity of the extracellular medium, and the position of the second (ground) electrode which also defines the form of the electric field. By using this way of modelling not only longitudinal, but also transversal currents (perpendicular to axis of the neuron) can be considered.

Therefore, longitudinal or transversal modelling is determined by the arrangement of neighbouring compartments of the modelled neuron in space. A cylindrical structure has a given natural axis along its length, this is the longitudinal modelling direction. The cross-sectional area is modelled in transversal direction. Also, the position of the electrode in relation to the neuron in case of extracellular stimulation may determine if it is a longitudinal or transversal modelling (see figure 3.6).

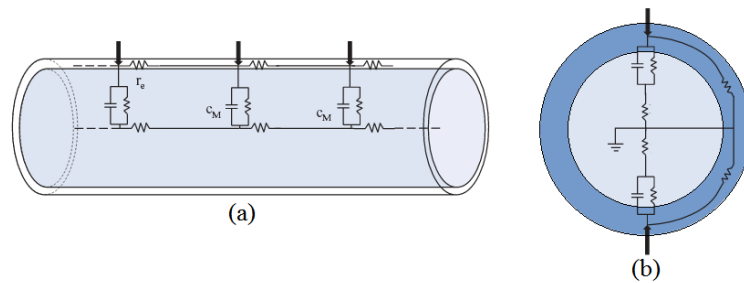


Figure 3.6: Longitudinal versus transversal extracellular stimulation. Figure (a) shows a classical multi compartment model of a cylindrical neuronal section modelled in longitudinal direction with three compartments. Figure (b) shows two compartments in transversal direction of a cylindrical neuronal section (figures from Meffin et al. (2012)).

Chapter 4

Blocking Phenomena

As already outlined in section *Electrical Stimulation* (see section 2.5), there are limitations in extracellular electrical stimulation. The stimulus strength must be within certain limits, otherwise an action potential might not be initiated or propagation is stopped. This chapter will give an overview about the conditions and reasons why action potentials may be blocked by a neuronal cell.

4.1 Stimulation Window

Primary target of extracellular stimulation is the initiation of an action potential. While the stimulus shall only irritate/disturb the cell, the initiation and propagation of the action potential shall be based on the cell's own mechanisms and dynamics. Because of several limitations, the applied stimulus must meet certain criteria to excite a neuronal cell.

An extracellular electrical stimulus must influence the neuronal cell with sufficient strength. A stimulus is creating an electric field which is determined by the current amplitude, the resistance of the medium, and geometric conditions. Therefore, the current amplitude of a stimulus must fit the distance to the target cell (current-distance relation) to create sufficient strength. Further, a neuronal cell has regions of different excitability. So, the stimulus also needs to target a region suitable for initiating an action potential. (Rattay, 1990)

The electric field establishes potential gradients to which the neuronal cell is exposed to. The form of the field lines determines the extracellular potential for every region of the neuronal cell. The form of the field can either support or prevent an action potential and its propagation. The shape of the electric field is determined by the type of stimulation (mono- or bipolar stimulation), geometry of stimulation, and the type of the electrode¹⁴.(Rattay, 1986, 1990; McIntyre et al., 2004b)

¹⁴Like point-, spherical-, plate-electrodes, or an electrode array.

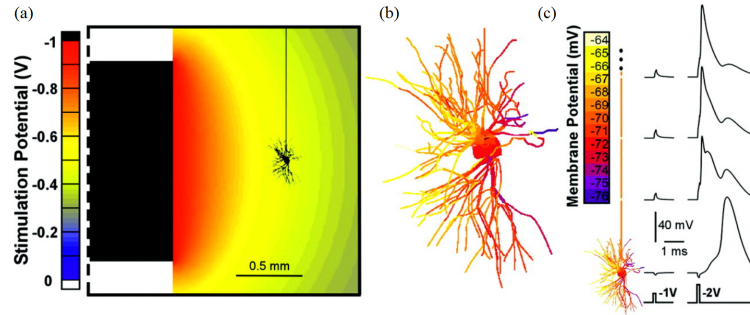


Figure 4.1: Electrical field established by an extracellular electrode and its influence on a neuronal structure. The deep brain stimulation electrode (indicated by the black area) in the left figure (a) generates an electric field shown with coloured field lines. A neuronal structure with dendrites, a soma, and an axon is placed inside the field. In the middle figure (b), the influences of the electrical field to the membrane potentials at different locations along the neuron are shown. Right (c), results (V_m) at different locations of two short $0.1ms$ impulses are shown, a sub-threshold impulse of $-1V$ and a supra-threshold impulse of $-2V$ (figure and parts of caption from McIntyre et al. (2004a)).

As shown in figure 4.1(c) for the weak stimulus, the first limitation of the stimulus window is the lower limit. In this case, the applied voltage in relation to the distance between electrode and neuronal structure does not result in a strong enough stimulus to initiate an action potential. More detailed, the stimulus had not enough strength to influence the membrane voltage at any excitable region of the neuron in a way that voltage sensible Na^+ ion channels did open. This is called sub-threshold stimulation as the voltage threshold for the Na^+ ion channels is not reached.

As visible in the second stronger stimulus, an action potential is propagating inside the neuronal cell. Here, the current-distance relation is causing a membrane voltage high enough to activate the voltage gated Na^+ ion channels. This is called supra-threshold stimulation, the stimulus is within the stimulation window.

But there is also an upper limit. Here the physics are more complicated. The absolute upper limit is given by the fact, that a too high stimulus amplitude can destroy the neuronal structure of a cell (Durand, 1999).

However, also below the threshold of cellular damage, the stimulus might not result in an action potential. Two different theories explaining the physical principles of the upper limit can be found in literature. One is the *Anodal Surround Block* or cathodic block phenomenon (for details see section 4.2) which basically states, that a strong depolarized region because of electrical stimulation will also cause strong hyperpolarizations in the neighbouring regions. The hyperpolarized regions are preventing the propagation of an action potential (Ranck, 1975; Rattay, 1990). The other phenomenon is the

Stimulation Upper Threshold (for details see section 4.3) which states, that a very strong stimulus is causing a reversal of the Na^+ current flux (Na^+ outflux instead of Na^+ influx) at a depolarized region, therefore an action potential is not initiated in the first place (Boinagrov et al., 2012).

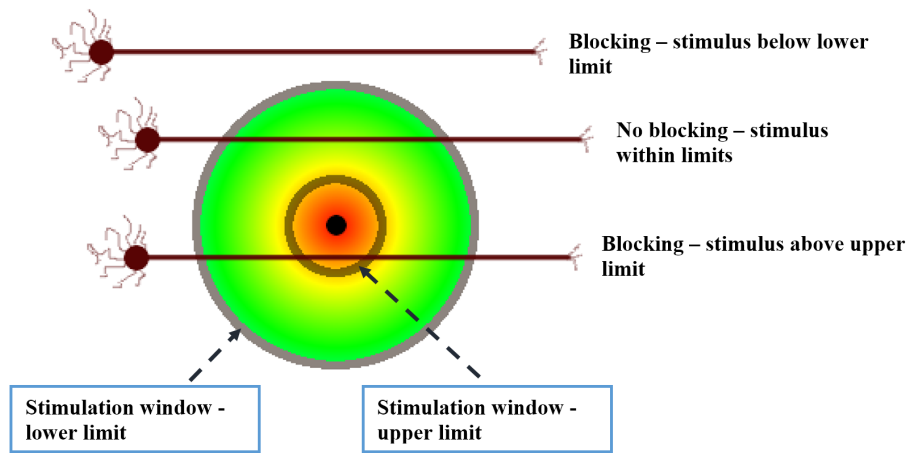


Figure 4.2: Stimulation window for extracellular stimulation, the point source electrode is in the center. Only the axon within the window will initiate an action potential that propagates. The axon near the electrode is blocked because of the upper limit, the axon outside of the relevant electric field because of the lower limit (figure according to Rattay (1990) and Ranck (1975)).

While these blocking phenomena may be seen as limitation in extracellular stimulation, they also can be used to apply selective stimulation. Selective stimulation tries to excite only certain neuronal target cells, while other cells shall not fire, or even be actively blocked to avoid excitation.

In retina neuroprostheses electrode arrays are used for the spatial stimulation of the retina. While these arrays already reach a rather high resolution (micro-electrodes per area), the achievable resolution might be lower because of electric cross-talk. Electrical cross-talk means interference of one site (micro-electrode) to other sites in parallel stimulation (Matteucci et al., 2016). These interferences are caused by crossing and partly summing up electric fields. One way of actively inhibiting non-target cells would be to stimulate those cells by currents above the upper limit so a block is caused (Barriga-Rivera et al., 2017).

4.2 Anodal Surround Block

The *Anodal Surround Block* is a blocking phenomenon which only exists at extracellular stimulation. An action potential will be initiated at a depolarized region, but, in case of the stimulation strength is above a certain

limit, hyperpolarized regions next to the depolarized one will prohibit the propagation of the action potential along the fibre. The basic concept of the *Anodal Surround Block* or cathodic blocking phenomenon was described by Ranck (1975) as:

”With extracellular stimulating electrodes, for any outward current that locally depolarizes a fiber there must be an inward current elsewhere that will hyperpolarize the fiber.”

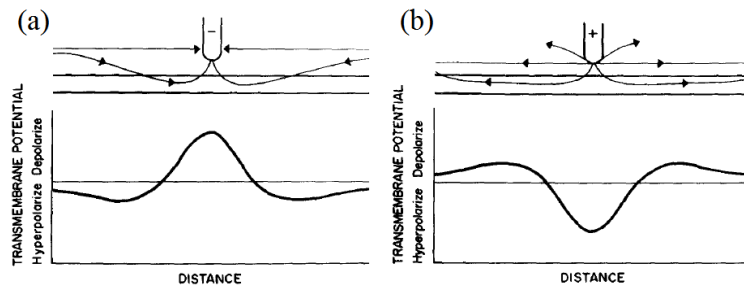


Figure 4.3: Current flow of a cathodic (a) and an anodic (b) stimulated cylindrical axon. Second electrode is not shown, its distance is assumed to be far away from stimulating electrode. Distance from electrode to axon is different for cathodic (larger distance) and anodic (smaller distance) stimulation. Anodic stimulation is less effective than cathodic, assuming the same stimulus amplitude (figure modified and parts of caption from Ranck (1975)).

Currents always must be in equilibrium as stated in Kirchhoff’s first law:

$$\sum_{k=1}^n I_k = 0 \quad (4.1)$$

This very basic rule for electrical circuits has a huge impact on the neuronal behaviour in case of extracellular stimulation. While there are different kinds in the exact setup of extracellular stimulation (like geometry of electrode, bipolar stimulation, electrode arrays, etc.), here the effects of a micro-electrode (point source with its ground far away from stimulation site) for cathodic and anodic stimulation are discussed in detail.

4.2.1 Electric Field

Before analysing the mechanism and dynamics of a neuronal cell influenced by an electric field, the temporal electric field created by the stimulus needs to be taken into account. An electric field generates a potential gradient in the space a neuron is placed in, and therefore, the extracellular potential V_e of the neuronal cell is directly determined by the field during stimulation.

The square pulse current I_{st} is generated in the extracellular space containing extracellular medium having the resistivity ρ_e . The resistivity is defined by the concentration of ions but also by other tissue packed in the extracellular space and has the unit $[\Omega \cdot cm]$. The distance to the ground electrode is assumed to be infinite which will result in a spherical electric field around the electrode. By considering Ohm's law $V = R \cdot I$, the distance r to a neuronal cell membrane, the spherical field with a surface area $4\pi r^2$, and distance to ground to be ∞ , the external potential V_e (relative to ground) can be approximated by (see also Rattay (1990)):

$$V = R \cdot I \rightarrow V = \frac{\rho_e \cdot I_{st}}{4\pi r^2} \quad (4.2)$$

$$V_e = \int_r^\infty \frac{\rho_e \cdot I_{st}}{4\pi r^2} dr \rightarrow V_e = \frac{\rho_e \cdot I_{st}}{4\pi r} \quad (4.3)$$

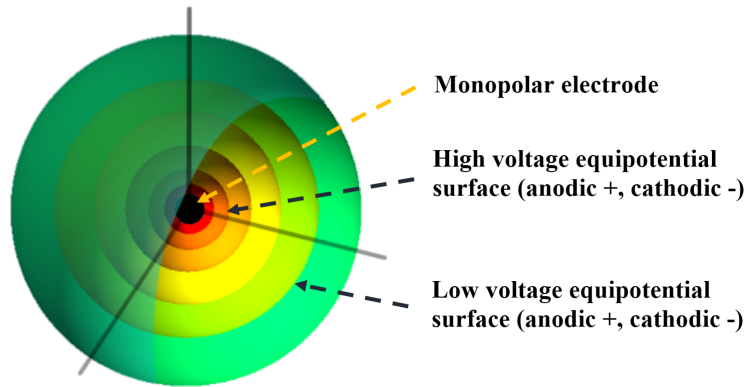


Figure 4.4: Equipotential surfaces of a monopolar electrode in space. In case of cathodic stimulation, the potentials are negative, in anodic stimulation positive. The voltage drop follows an exponential decay which leads to high voltage drops near the center electrode while voltage drops in the periphery are low.

4.2.2 Cathodic Stimulation

Considering the resulting spherical equipotential surfaces (see figure 4.4), it is obvious that there is (nearly) no possible geometric structure of a neuronal cell where the whole cell membrane is exposed to the same extracellular potential. The same gradient which is established in the extracellular space, will also influence the intracellular potential, but, the intracellular potential is trying to balance out all gradients within the dielectric isolating cell membrane (Gauss' law). Additionally, to those intracellular currents which

tries to reach equilibrium again, there are capacitive currents because of a changed ion distribution at the outer surface of the cell membrane. And, in case of leakage currents or opened ion channels during the stimulus, also transmembrane ionic currents will influence the intracellular potential. All these currents will lead to local depolarizations and hyperpolarizations in the neuronal cell at the same time during a stimulus (Ranck, 1975; Rattay, 1990).

As shown in figure 4.5, the cathodic stimulus will depolarize a neuronal structure below the electrode. The location along the fibre showing the largest depolarization will be the one with the shortest Euclidean distance to the electrode. The neighbouring regions will be hyperpolarized. The exact locations of different polarizations are only dependent of the distance between electrode and neuron, the angle of 70° indicates the region which will have a depolarization (Rattay, 1990). The magnitude of polarizations depends on the stimulation strength. While in depolarized areas an action potential may be initiated by opening Na^+ ion channels, a strongly hyperpolarized area next to the local trigger zone may prevent the propagation of the action potential. This depends on how strong the hyperpolarization actually is (Ranck, 1975).

4.2.3 Activating Function

Taking the extracellular potential as given¹⁵ the dependency membrane currents to membrane voltages can be investigated. The external potential for a monopolar point electrode is approximated by $V_{e,n} = \frac{\rho_e \cdot I_{st}}{4\pi r_n}$ (see equation 4.3) for every compartment. For a homogeneous fibre with constant diameter d this leads to (see also section 3.4, derivations from McNeal (1976) and Rattay (1986, 1990)):

$$\dot{V}_{m,n} = [-i_{ion,n} + \frac{d\Delta x}{4\rho_i l} \cdot (\frac{V_{m,n-1} - 2V_{m,n} + V_{m,n+1}}{\Delta x^2} + \frac{V_{e,n-1} - 2V_{e,n} + V_{e,n+1}}{\Delta x^2})] / C \quad (4.4)$$

with ρ_i for internal resistivity, C the membrane capacitivity, Δx the distance between two compartments, and l the node length (correction for myelinated fibres, in unmyelinated fibres $l = \Delta x$). This equation is simplified for cylindrical neuronal sections separated into compartments of equal length. According this equation, the stimulation influence can be reduced to (Rattay, 1990):

$$\frac{V_{e,n-1} - 2V_{e,n} + V_{e,n+1}}{\Delta x^2} \quad (4.5)$$

¹⁵By the stimulus amplitude, the current-distance relation, and the extracellular resistivity.

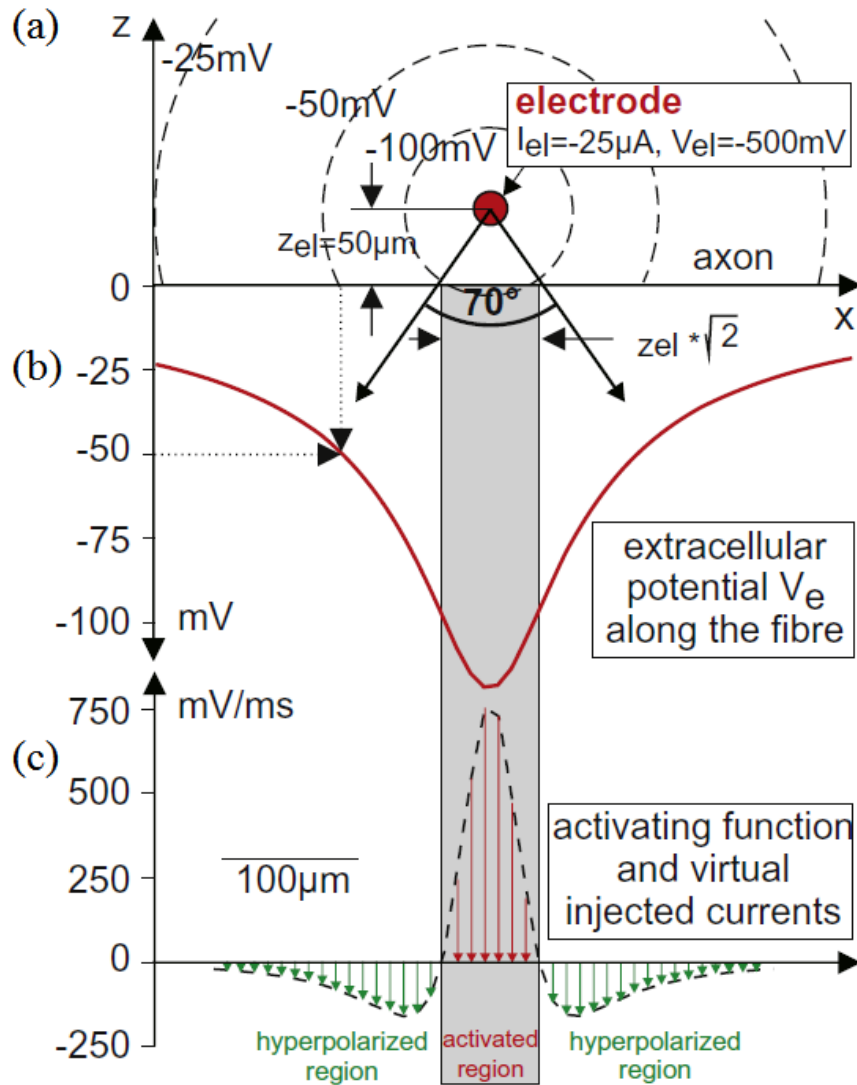


Figure 4.5: *Anodal Surround Block* during cathodic stimulation. (a) shows the geometry of the extracellular stimulation, the point source electrode is $50 \mu\text{m}$ away of an axon. Around the micro-electrode, the equipotential lines are indicated. In (b) the extracellular potential V_e along the fibre is shown. (c) shows the depolarized area of the membrane potential in the 'activated region'. The flanks to the right and left of the 'activated region' are hyperpolarized. Propagation of a possible initiated action potential in the depolarized area depends if it can overcome the hyperpolarized regions next to the depolarization. If not, the signal is blocked by the anodal surround block (figure and parts of caption from Rattay et al. (2012)).

which is the second difference quotient of the extracellular potential along a neuronal fibre. Assuming unmyelinated fibres ($l = \Delta x$) and $\Delta x \rightarrow 0$ leads to the activating function which is the slope of the membrane potential when exposed to an electric field from a point source with given extracellular potential $V_{e,n}$ for every compartment n :

$$f_n = \frac{d\Delta x}{4\rho_i l} \cdot \frac{V_{e,n-1} - 2V_{e,n} + V_{e,n+1}}{\Delta x^2} / C \rightarrow f = \left[\frac{d}{4\rho_i} \cdot \frac{\delta^2 V_e}{\delta x^2} \right] / C \quad (4.6)$$

$$f_n = \left[\frac{V_{e,n-1} - V_{e,n}}{R_{i,n-1}/2 + R_{i,n}/2} + \frac{V_{e,n+1} - V_{e,n}}{R_{i,n+1}/2 + R_{i,n}/2} + \dots \right] / C \quad (4.7)$$

This form, which is reduced to the extracellular potential $V_{e,n}$, the intracellular resistance $R_{i,n}$, and the membrane capacity C , allows to estimate the depolarized and hyperpolarized areas at extracellular stimulation. The border between these regions is given by an angle of around 70° from the electrode. This angle (see figure 4.5 shadowed area) is independent of fibre parameter or exact composition of extracellular medium (Rattay, 1990). Also, this angle indicates, that the length of the de- or hyperpolarized area nearest to the electrode depends on the distance between the electrode and the neuron. A near electrode creates only polarizations with short length, while a distal electrode results in long regions of polarizations.

4.2.4 Magnitude of Polarizations

The magnitude of hyperpolarization (areas under the activating function) will be less than the magnitude of depolarization. But in case of a stimulation strength several times higher than the minimum strength necessary to initiate an action potential, the magnitude of hyperpolarized areas will block the firing of the neuron (Ranck, 1975).

The magnitudes of de- and hyperpolarization depend on the current-distance relation (see figure 4.6):

- **Current-distance relation in z-direction:** The resistivity of the extracellular medium will weaken the stimulus strength along its way down the z-axis. The decay of voltage is exponential. A short distance will lead to a high extracellular potential at the neuron. The longer the distance between the electrode and the neuron, the lower the maximum potential at the cell membrane.
- **Current-distance relation in x-direction:** Considering the spherical equipotential surface areas around the electrode, it is obvious that the extracellular potential on a cell membrane is highest at the position with lowest distance to the electrode (z-axis). Left and right to the highest potential, the potentials will become lower with distance in x-direction.

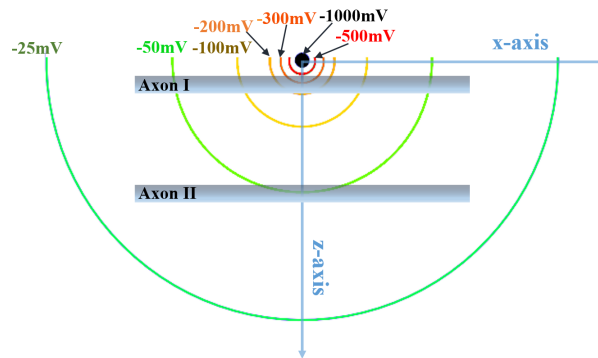


Figure 4.6: Cathodic stimulation with a point electrode of $-1000mV$. The equipotential lines indicate the spherical electric field and distances between them are in equivalent scale. Axon I near to the electrode has an extracellular potential of nearly $-300mV$ in its center, on the terminals only around $-40mV$. The potential gradient established on the surface is in a range of around $260mV$. This results in high magnitudes of de- and hyperpolarization. Axon II has an extracellular potential in the center of around $-50mV$, on the terminals around $-40mV$. On same length, axon II is only confronted with a potential gradient of around $10mV$.

A cylindrical neuronal structure placed in the vicinity of an electrode will reflect those potential gradients on its surface. The nearer it is placed, the higher the differences in the extracellular potential will be along the fibre. High differences in potentials will lead to high capacitive currents which will directly influence the magnitudes of de- and hyperpolarized areas.

4.2.5 Anodic Stimulation

When stimulating with anodic currents, the stimulus will create an even more positive extracellular potential. This leads to a hyperpolarization in regions next to the electrode which makes an action potential impossible there.

Taking a look at the activating function for anodic stimulation, one will see the strong hyperpolarization next to the electrode, but the potential gradient on the outside of the cell membrane leads to depolarizations left and right of the hyperpolarized region. This is mainly caused by capacitive currents induced by the electric field. While the hyperpolarized region nearest to the electrode cannot initiate an action potential, the two depolarized regions might do so.

4.3 Stimulation Upper Threshold

Another blocking hypothesis recently presented by Boinagrov et al. (2012) is the *Stimulation Upper Threshold*. Basically, it states that an action poten-

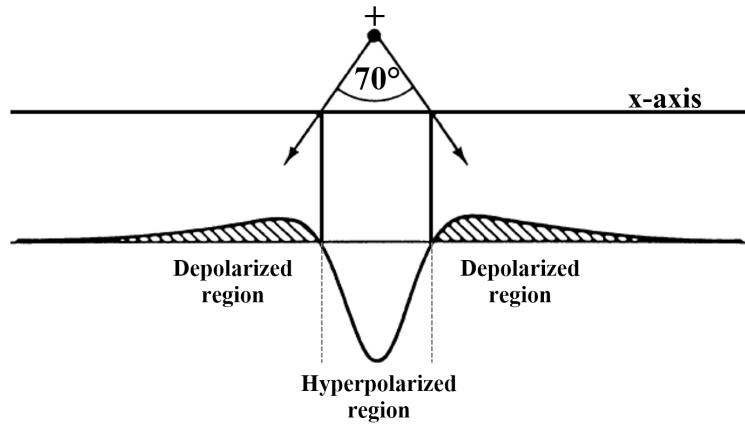


Figure 4.7: Anodic stimulation, the region within the 70° limit is hyperpolarized, as V_e is getting more positive and therefore the membrane voltage V_m will be more negative. In the hyperpolarized region no voltage gated ion channels will open. Next to the hyperpolarized area, there are depolarized areas mainly because of capacitive current flows. In this two regions, action potentials can be initiated if threshold voltage of voltage gated ion channels is reached (figure modified from Rattay (1990)).

tial is not triggered in first place at all if the extracellular cathodic stimulus strength is above a certain threshold. The reason is a reversal of Na^+ currents in the depolarization region because of the strong depolarization (Boinagrov et al., 2012):

”Computational modeling of RGC stimulation indicated that the upper threshold is due to reversal of the sodium current at high levels of depolarization, which was further confirmed in experiments with the low-sodium medium.”

The *Stimulation Upper Threshold* was investigated in-vitro on retinal ganglion cells of wild-type Long-Evans rats. After preparation of the retina, cathodic extracellular stimulations were performed and the soma was recorded by patch-clamp technique. The results were compared with a one-compartment model of a spherical soma (Boinagrov et al., 2010) using mechanisms and dynamics of the Fohlmeister and Miller (1997) model (see section 3.3). (Boinagrov et al., 2012)

4.3.1 Sodium Current Reversal

The sodium ion is positive charged (Na^+), therefore the electric force $\vec{F}_{Na,e}$ will move the Na^+ ion towards a negative potential. As the intracellular space of a resting neuronal cell is more negative than the extracellular space,

Na^+ ions are driven by electrical force into the cell in case of open ion channels.

Further, the Na^+ concentration in extracellular space is several times higher than in intracellular space (Pfützner, 2003). Chemical diffusion force $\vec{F}_{Na,d}$ will also drive Na^+ ions into the cell in case of open ion channels. Therefore, both forces $\vec{F}_{Na,e}$ and $\vec{F}_{Na,d}$ have the same direction¹⁶ and are pointing inside the neuronal cell during resting state. The total force for Na^+ ions is¹⁷:

$$\vec{F}_{Na} = \vec{F}_{Na,e} + \vec{F}_{Na,d} \quad (4.8)$$

Assuming the Na^+ concentration is always higher in extracellular space compared to intracellular space there will never be a current reversal because of chemical diffusion force $\vec{F}_{Na,d}$. In fact, the concentrations will slightly change because of the cells activity, but mechanisms like the sodium/potassium pump will ensure the concentration difference is more or less stable. Therefore, the sign of $\vec{F}_{Na,d}$ will never change.

While $\vec{F}_{Na,d}$ only knows one direction, the electric force $\vec{F}_{Na,e}$ is changing its direction as soon as membrane potential becomes positive ($V_i > V_e$). This happens during an action potential when V_m is shortly depolarized in the positive range, but also during cathodic stimulation where a strong stimulation strength will rise the V_m not only above the threshold voltage but even in the positive range. However, a changed sign of $\vec{F}_{Na,e}$ alone is not sufficient to get a reversal of the total force \vec{F}_{Na} . The magnitude of $\vec{F}_{Na,e}$ must be greater than $\vec{F}_{Na,d}$. Therefore, following two conditions must be fulfilled to get a sodium current reversal:

$$\text{sgn}(\vec{F}_{Na,d}) \neq \text{sgn}(\vec{F}_{Na,e}) \wedge |\vec{F}_{Na,e}| > |\vec{F}_{Na,d}| \quad (4.9)$$

For a given extra- and intracellular concentration of Na^+ ions, the equilibrium voltage E_{Na} (which is proportional to $\vec{F}_{Na,d}$) is given by the Nernst potential (Nernst, 1888):

$$E_{Na} = \frac{R \cdot T}{z \cdot F} \cdot \ln \frac{[Na]_e}{[Na]_i} \quad (4.10)$$

with R denotes the gas constant, T the temperature, F the Faraday's constant, and z the valence of an ion ($z = 1$ for Na^+). The concentrations for extracellular and intracellular space are given by $[Na]_e$ and $[Na]_i$. Therefore, a Na^+ current reversal happens if:

$$V_m > E_{Na} \quad (4.11)$$

¹⁶Nowadays cell outward currents are usually denoted with a positive sign while inward currents are defined by a negative sign.

¹⁷Additional forces like friction in the solution are ignored in this outline.

as the Na^+ current flow is defined as Hodgkin and Huxley (1952):

$$I_{Na} = g_{Na} * (V_m - E_{Na}) \quad (4.12)$$

As long as the membrane voltage V_m is less than the Nernst potential E_{Na} there will be an inflow of Na^+ ions into the cell. If V_m exceeds the Nernst potential E_{Na} the conditions of 4.9 are fulfilled, instead of an inflow there is an outflow of Na^+ ions through open ion channels - a sodium current reversal. The Na^+ Nernst potential E_{Na} is typically in the range of 35 – 50mV which also defines the upper threshold limit because of Na^+ current reversal (Boinagrov et al., 2012).

4.3.2 In-vitro Stimulation

Boinagrov et al. (2012) reported data from 26 cell recordings (of 16 prepared retinas). The exact settings of stimulation and recording are shown in figure 4.8.

The experiments were performed with a fixed stimulus duration in a high sodium artificial cerebrospinal fluid (ACSF). First, the current was increased until the lower limit of the stimulation window was reached resulting in short latency action potentials. Then, the current was increased again until the upper threshold was reached, no action potential was generated any more. While in the beginning with a current below lower limit no cell was generating an action potential, inside the stimulation window all cells responded with action potentials on the external stimulus. With increased current the upper threshold limit was reached, the cells started to block until all cells were not firing any more (results see figure 4.9). The thresholds between different cells varied significantly. (Boinagrov et al., 2012)

Further, the strength-duration relationship was investigated (results see figure 4.11 left graph). The lower and upper thresholds were measured by varying duration and amplitude of the stimulus, each stimulation was either assigned as 'spikes' or 'no spikes'. Near the thresholds, assignment was done by evaluating the probability for elicitation, in case it was $> 50\%$ it was assigned as 'spikes'. The strength-duration relation gives a good indication of the stimulation window with the corresponding lower and upper thresholds. (Boinagrov et al., 2012)

The hypothesis that the block is caused by a sodium current reversal was tested by exchanging the high sodium ACSF perfusion medium with a low sodium perfusion medium. For some cells the upper threshold decreased by a factor of 1.67 ± 0.33 , while the resting potential did not change. (Boinagrov et al., 2012)

4.3.3 Computational Modelling

The results of the in-vitro stimulation were also cross-checked with a computational model based on the Fohlmeister and Miller (1997) model (see

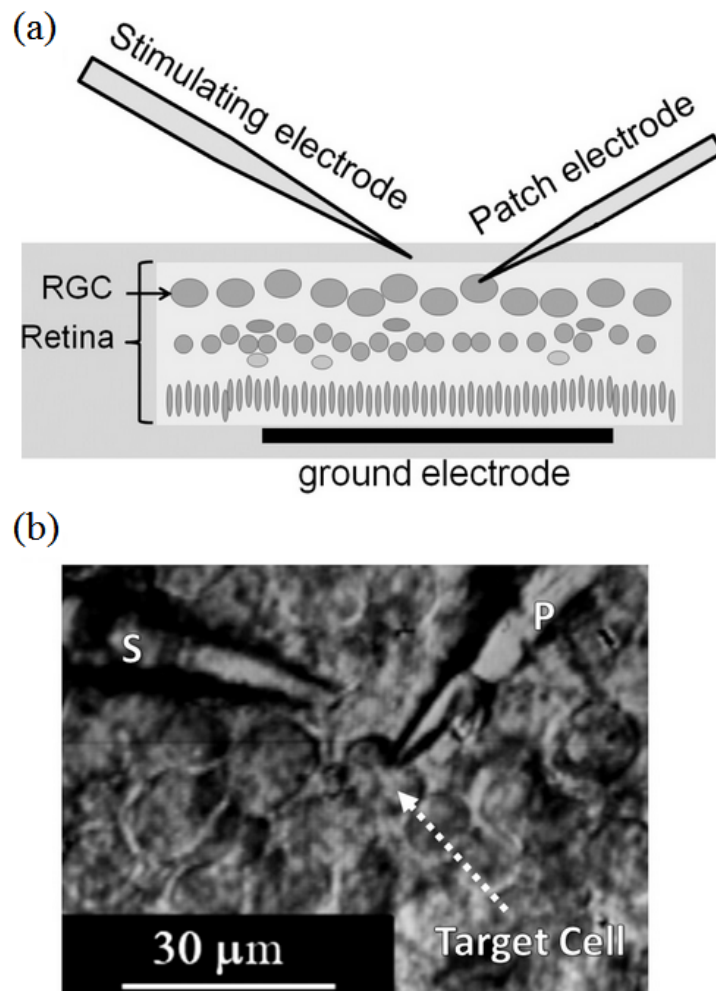


Figure 4.8: In-vitro extracellular stimulation of retinal ganglion cells. (a) depicts the experiment with a prepared rat retina placed in an artificial cerebrospinal fluid (ACSF) in a perfusion chamber with the retinal ganglion cells up. A patch electrode is placed directly on the soma to perform cell recording. The stimulation electrode was placed $25 \pm 15 \mu\text{m}$ away from the soma which generates cathodic rectangular pulses. A long wire as ground electrode was placed in the petri dish. (b) shows a microscope image of the experiment (figure and parts of caption from Boinagrov et al. (2012)).

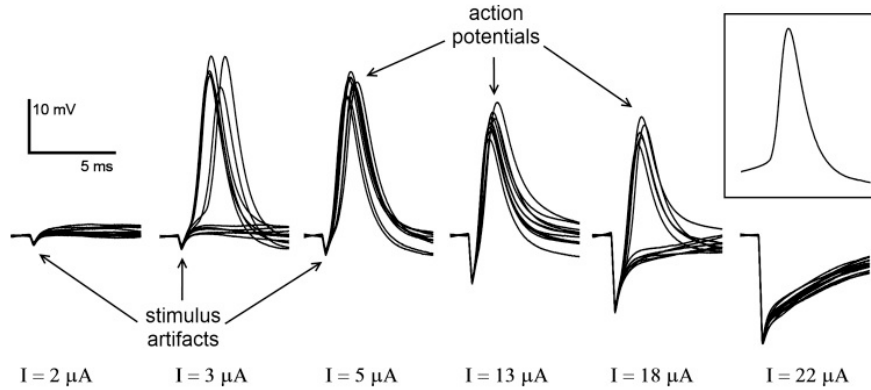


Figure 4.9: In-vitro extracellular stimulation of retinal ganglion cells. All stimuli were generated for a fixed duration of $0.2ms$, the current amplitude was increased. Left recordings show stimulation below lower threshold current ($2\mu A$). At $3\mu A$ most of the cells are firing, at $5\mu A$ all stimulations initiated an action potential. At $18\mu A$ around half of the cells are not initiating an action potential any more, at $22\mu A$ all cells are blocking (figure and parts of caption from Boinagrov et al. (2012)).

section 3.3) for salamander retinal ganglion cells (Boinagrov et al., 2012). The soma was assumed to be spherical. The model is a single-compartment model (symmetric distribution of Na^+ ion channels) with an extension to define an asymmetric distribution of Na^+ ion channels in the soma cell membrane. The asymmetric Na^+ ion channel distribution allows to mimic the very excitable axon region proximal to the soma (Boinagrov et al., 2010, 2012).

The modelled soma was stimulated with rectangular monophasic pulses and strength-duration relationships were investigated with following results (see figure 4.11 right graph) (Boinagrov et al., 2012):

- **Symmetric model, cathodic pulse:** At Na^+ conductance of $\bar{g}_{Na} = 85mS/cm^2$ the strength-duration curve matched quite well to the experimental data, lower conductance of $\bar{g}_{Na} = 50mS/cm^2$ shows a mismatch because of intersecting lower and upper threshold at around $55ms$.
- **Asymmetric model, cathodic pulse:** The model produced results comparable to experimental data but also to the symmetric model with the difference of lower thresholds. The lower thresholds are resulted as the electrode was placed at the pole which has a 10 times higher Na^+ ion conductivity. This led to a higher magnitude of depolarization during stimulation because of the high Na^+ ionic current passing the channels during the stimulus.

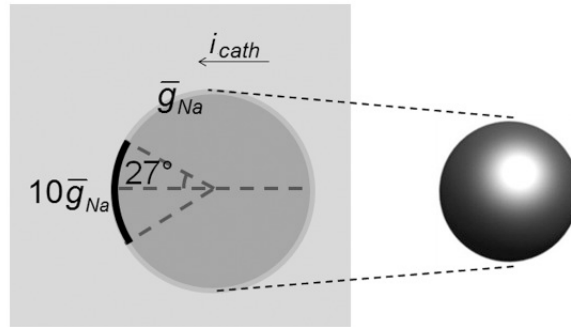


Figure 4.10: Asymmetric single compartment model of a spherical soma used to cross-check the in-vitro test results. The conductivity for Na^+ ion channels at the majority of the soma surface is defined as \bar{g}_{Na} . The region defined by the angle of 27° represents the surface area of the axon hillock. The axon hillock region is located on the depolarized pole of the soma, its surface portion was assumed to be 5% of the total soma surface area. Its conductivity was set 10 times higher (therefore $10 \cdot \bar{g}_{Na}$) compared to the conductivity of the majority of the soma surface (figure and parts of caption from Boinagrov et al. (2012)).

- **Asymmetric model, anodic pulse:** During anodic stimulation, the pole modelled with high density of Na^+ ion channels will hyperpolarize, while the opposite pole modelled with the lower Na^+ conductance is depolarized. The results are very similar to the symmetric model with low conductivity at cathodic stimulation.

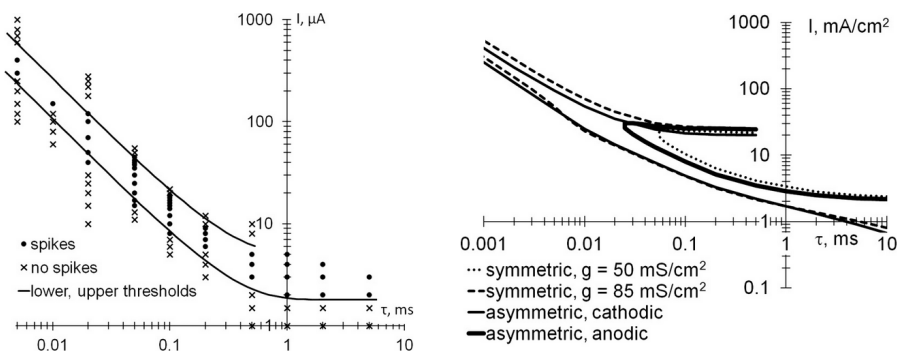


Figure 4.11: Retinal ganglion cells strength-duration relationship. Left, results of in-vitro experimental data, right data from the computational model (figure and parts of caption from Boinagrov et al. (2012)).

4.4 Controversy

Actually, there is a controversy if the *Stimulation Upper Threshold* distinguishes from the *Anodal Surround Block* (see Rattay (2014) and Boinagrov and Palanker (2014), but also Matteucci et al. (2016)).

In a first analysis of the *Stimulation Upper Threshold* by Rattay (2014), a retinal ganglion cell was stimulated in a multi compartment model using mechanisms and dynamics of the Fohlmeister et al. (1990) model. The retinal ganglion cell was modelled with a spherical soma, an axon hillock, a region called sodium band (having very high density of Na^+ ion channels), an axon, and a dendrite. While the soma was modelled in transversal direction, all other neuronal structures were modelled in longitudinal direction. (Rattay, 2014)

The results of this stimulation showed a blocked action potential in the soma at high stimulus amplitudes as reported by Boinagrov et al. (2012), however, a propagating spike was recorded in the axon anyway. The key essence of Rattay (2014) is, that blocking at high currents depends mainly on the electrode position relative to the axon. (Rattay, 2014)

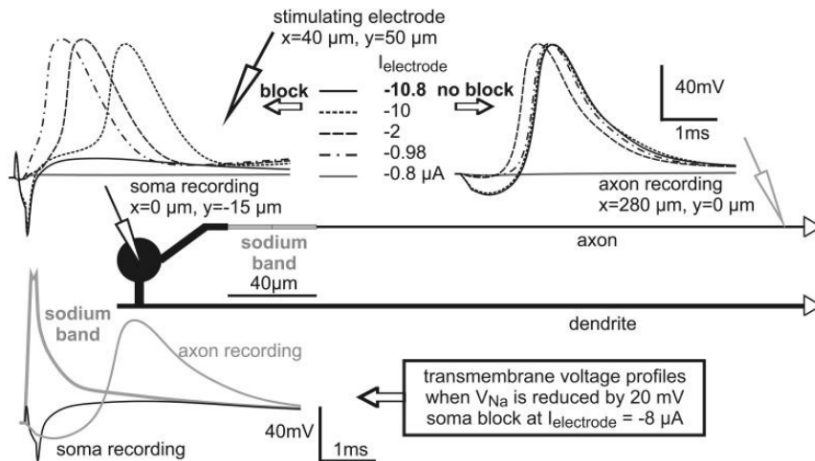


Figure 4.12: Multi compartment model of a retinal ganglion cell. The soma consists of 3 departments in transversal direction while the rest of the structures are modelled in longitudinal direction. While the recordings of the soma produced no action potential at $10.8\mu A$, the axon recordings show an action potential for $10.8\mu A$ (figure and parts of caption from Rattay (2014)).

In the reply of Boinagrov and Palanker (2014) it was stated that the Na^+ current reversal of the *Stimulation Upper Threshold* can be clearly distinguished from the *Anodal Surround Block*, as the Na^+ current reversal will prevent an action potential generation in the first place, while the *Anodal Surround Block* will prohibit the propagation of a generated action potential (Boinagrov and Palanker, 2014).

Chapter 5

Neuron Software

*Neuron*¹⁸ is a software tool developed at Duke and Yale University. After first researches in decreasing the computational costs of solving the equations of the Hodgkin-Huxley model for branched neuronal cells (Hines, 1984), Michael Hines continued in exploring software techniques to simulate different geometries and dynamics. As a result, the predecessor of *Neuron* was created, a software named CABLE (Hines, 1989). CABLE already provided the interpreter language HOC which is used for creating and controlling a simulation.

Finally, in 1993 the open source software *Neuron* was introduced (Hines, 1993). It was written in C, contained a user interface to plot results, and included the interpreter language HOC. For extension of mechanisms and dynamics, the model description language NMODL is used (Hines, 1993).

Since the introduction, *Neuron* is widely used in the neuroscience community for different simulations on any kind of neuronal cells. It has a large user community and provides with ModelDB¹⁹ an online available database for computational neuroscience (publications and source codes of simulations written in *Neuron* but also other software environments).

Since 2009 *Neuron* provides all functionality also for the *Python* environment. This provides better interaction of *Neuron* with other software environments. Further, the capabilities of *Neuron* can now be used inside a modern software development environment (Hines et al., 2009). All functionalities of *Neuron* including extensions written in HOC and NMODL are also available when using *Python*. This way it is possible to create highly interactive neuronal simulation where all mathematical problems are solved by *Neuron*.

¹⁸See <https://www.neuron.yale.edu> for introduction and download.

¹⁹See <https://senselab.med.yale.edu/ModelDB> for specific models.

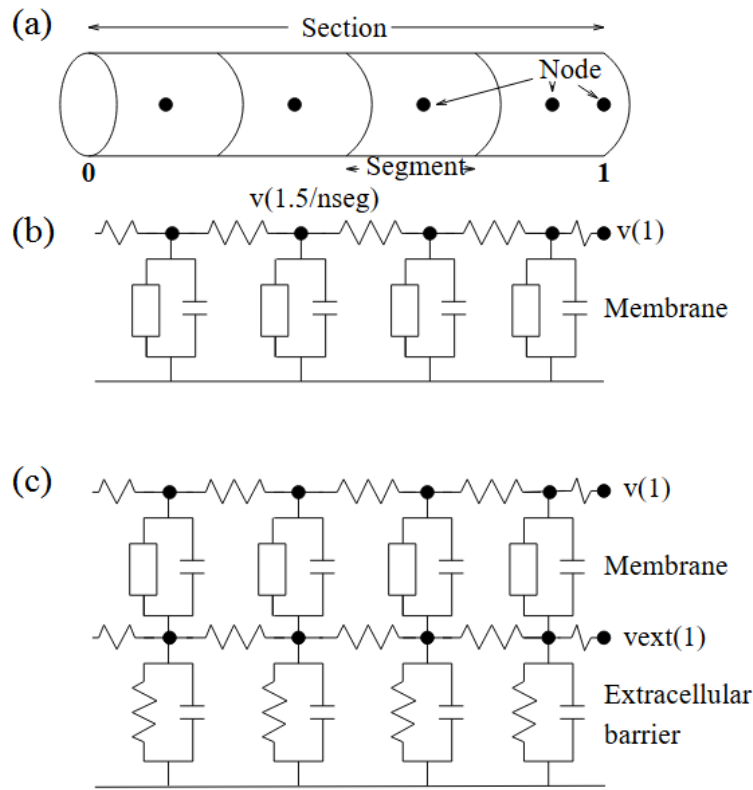


Figure 5.1: Morphology in *Neuron*. A part of a neuronal cell is modelled as cylindrical section and further divided into four segments (a). Each segment is represented by an electrical circuit, (b) shows the usual circuit with a resistor for a transmembrane ion channel and a capacitor for capacitive cell membrane currents. (c) shows an extended cable model using an additional extracellular layer for modelling extracellular stimulation or current flows at the outer cell membrane (figure and parts of caption from Hines (1993)).

5.1 Spatial Discretization

Neuron generally provides the mathematical solutions to solve complex neuronal models based on cable models (see section 3.1). While exact morphologies and topologies of cells are defined in *Neuron* (HOC or in *Python*), the exact mechanisms and dynamics are provided by using NMODL. The *Neuron* environment then mathematically solves the compartment models by bringing together the temporal, spatial, and biophysical dimensions of the modelled neuronal cell.

Besides the ability to create a multi compartment model, *Neuron* also provides common mechanism to stimulate neuronal cells, like voltage clamp or intracellular stimuli. Further, the standard *Neuron* user interface provides

many different tools to investigate results of a simulation in detail, also for very complex networks of neuronal cells.

Basically, the morphology of a cell is modelled by so called sections which again are separated into segments (see figure 5.1). Each segment provides its own geometry and an underlying cable model. Segments internally are connected by resistors which model the intracellular resistivity. The geometry of connected segments (compartments) defines the axis of the section.

The topology of a neuronal cell or of a network of cells is realized by connecting different section. Each section can be connected to one or more other sections. Connections are not only realized by connecting starts with ends, a child section can also be connected to any segment of the parent section.

While cylinders are the classical way of defining a section (and therefore also its segments are cylinders), *Neuron* also allows the creation of complex structures by using 3D point data. In this case, every segment can be defined by exact points in the Euclidean space. This results in frusta (truncated cones) which allow complex geometries in case of sufficient spatial discretization and provide good approximation of the surface area. (Carnevale and Hines, 2006)

5.2 Biophysical Mechanisms

Each section (and therefore also each segment) can be linked with different biophysical mechanisms. A biophysical mechanism is a mathematical description of the physical and biological behaviour of a neuronal section. In this sense, any extension of a section (e. g. , new layers, new parameters, new dynamics) are seen as mechanism. Common mechanisms are (Carnevale and Hines, 2006):

- **Extracellular:** This mechanism is included in *Neuron* and adds additional layers to include the extracellular membrane potential in every compartment (see also figure 5.1).
- **Ion channels:** Active ion channels which follow certain dynamics like voltage gated or ligand gated. Prominent example is the Hodgkin-Huxley model which is provided by *Neuron*, but also any other kind of ion channel is thinkable.
- **Active mechanisms:** Active current transport through the cell membranes like sodium/potassium pumps or calcium pumps.
- **Passive mechanisms:** Current transporting section without active behaviours.

Further, also some kind of helper mechanisms might be inserted, helping to store additional information and linkage to other mechanisms.

5.3 Temporal Discretization

The spatial discretization is defined by sections and segments, to simulate temporal behaviour, a temporal discretization is required. For this reason, the duration of a single time step (dt) is defined before running the model. The suitable time step duration strongly depends on the biophysical mechanisms and the results someone is interested. For example, the modelling of fast changing ion currents requires a higher temporal resolution than modelling the membrane voltage (Hines, 1993).

Neuron provides different integration methods, for a fixed time step dt two implicit methods are used (Carnevale and Hines, 2006; Hines, 1993):

- **Backward Euler:** A very stable method for first order differential equations with longer time steps. It is the default integration method of *Neuron* for quick analysing a cellular behaviour. The simulation error is proportional to the time step Δt .
- **Crank Nicholson:** This method provides a higher accuracy at shorter time steps with an error proportional to the square of the time step Δt^2 . However, this method has stability problems in case of small intracellular resistance for example.

Chapter 6

Methodology

To get inside views into the blocking phenomena of neuronal cells when applying an extracellular stimulus with high strength, a computational model was developed. The overall target is to draw conclusions of the physics of a neuronal cell during high amplitude extracellular stimulation.

The chosen model is a multi compartment cable model implemented in *Neuron*. The control of the model, but also all visualizations were realized in *Python*. The model implements the geometry and topology of a simplified retinal ganglion cell (Carras et al., 1992; Sheasby and Fohlmeister, 1999; Fried et al., 2009; Fohlmeister et al., 2010; Jeng et al., 2011; Rattay, 2014) stimulated extracellularly by a monopolar micro electrode. The mechanisms and dynamics are in Hodgkin-Huxley model style. More precisely, the model supports the original Hodgkin-Huxley model but also the Fohlmeister model. Additionally, a passive model can be assumed to get an impression of the direct effects of a stimulus to a neuronal cell.

Neuron is capable to deal with coordinates in $3D$ space, however, by an appropriate design of the retinal ganglion cell geometry and by dynamic adaptations of the cell geometry to the actual electrode geometry, it was possible to eliminate the 3^{rd} dimension y in space. The soma is assumed to have a spherical structure, its approximation was realized by using the $3D$ data points method of *Neuron* which results in an arrangement of truncated cones. Other structural elements like sections of the axon were realized by cylinders, or, in case of the tapering sodium channel band, by a conic element.

The realized model allows to analyse the cell behaviour in a systematic way. This was reached by a highly interactive user interface and additionally the possibility to run test procedures which produce tabular results stored in `.csv` files.

The biophysical properties were chosen according to actual research. However, there were slightly modifications to minimize computational costs. During the investigation of the blocking phenomena, morphological but also

biophysical properties were modified whenever it was useful for back checking hypotheses. Furthermore, during test procedures, different attributes were changed systematically to investigate correlations and coherences.

6.1 Cell Overview

The simplified retinal ganglion cell consists of following sections modelled in a multi compartment model. Described geometric properties in this section were extracted and adapted from Sheasby and Fohlmeister (1999), Fried et al. (2009), Fohlmeister et al. (2010), and Jeng et al. (2011):

- **Spherical soma:** The modelled soma of the retinal ganglion cell is assumed to have a spherical shape although in nature a wide range of complex 3D forms exists. Examining visual records of different retinal ganglion cells, it can be seen that the soma is not a perfect sphere, however, typically it is more spherical than cylindrical.
- **Axon:** The axon is modelled as a cylindrical shape with several taperings. It consists of different sections having different geometric and biophysical properties. The sections from proximal to distal of the soma are: axon hillock (AH), sodium channel band (SOCB), thin section (TS), and distal axon(DA). Geometrically, the single sections have different diameters and lengths, the sodium channel band is of conical structure, all other sections of the axon are modelled by a cylindrical structure. The axon gets thinner distal from soma, only at the last section (distal axon) there is a slightly increase of diameter again. The biophysical properties are determined by their ionic conductivity, especially the sodium channel band has a several times higher density of ion channels and therefore a much higher conductivity. The axon is connected on the eastern pole of the soma with a slightly bend directing to North before aligned horizontally directing to East again.
- **Dendrite:** A long cylindrical dendrite is included to mimic the branched dendrite network of a retinal ganglion cell. The dendrite leaves the axon on the southern pole vertically before heading to East and West. The dendrite is an active structure too, however, because of the low ion permeabilities it only has a minor relevance in exciting the retinal ganglion cell.

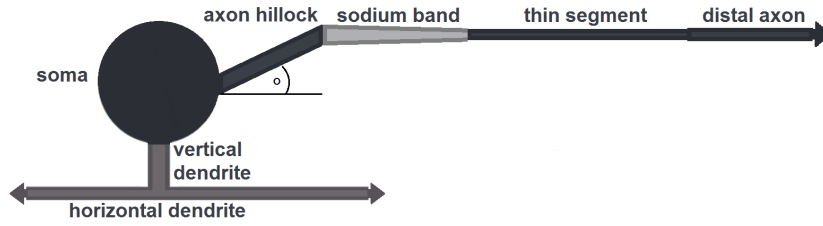


Figure 6.1: Schema of the morphology of the modelled retinal ganglion cell (not in scale). The axon is connected to the spherical soma at the eastern pole. The axon hillock is slightly inclining (inclination angle) in North-East direction before ending in the sodium channel band. The sodium band, the following thin section, and the distal axon are horizontally pointing to East. The dendrite is leaving the soma vertically at its south pole before ending in the horizontal dendrite.

6.2 Cell Morphology

The geometrical properties were combined and slightly adapted²⁰ from Carras et al. (1992), Sheasby and Fohlmeister (1999), Fried et al. (2009), Fohlmeister et al. (2010), Jeng et al. (2011), and Rattay (2014) (see table 6.1):

Property	Soma	AH	SOCB	TS	DA	VD	HD
Diameter d [μm]	20	3	3-0.8	0.8	1	4	2
Length l [μm]		40	40	90	150	10	150
Inclination angle [$^{\circ}$]		25					

Table 6.1: Geometric properties of the modelled retinal ganglion cell

The computerized topology (see figure 6.1) is based on visual analyses of tiger salamander retinal ganglion cells as presented by Toris et al. (1995). Starting at a spherical soma, the axon hillock section is leaving the soma at the eastern pole with inclination to the North-East. In the model this inclination is defined by an inclination angle. After the axon hillock the axon is pointing horizontally in eastern direction. The diameter is decreasing with distance from the soma. While the axon hillock still has a constant diameter, the sodium channel band is modelled by a conical shape getting thinner distal from soma. The following thin section has the lowest diameter

²⁰The lengths of the distal axon and the horizontal dendrite were massively reduced. This research is concentrating on the stimulation of the soma and the proximal axon regions like axon hillock, sodium channel band, and thin section. Modelling an axon or a dendrite considering the full length would increase the number of compartments a lot, and, with the number of compartments also the computational costs. In investigating the blocking phenomena, the stimulus electrode was only located near the soma, propagating action potentials were analysed until the end of the thin section.

before the axon diameter is slightly increasing again at the distal axon. In nature, the combined distal axons of all retinal ganglion cells form the optic nerve which passes visual information to the brain.

The strongly branched dendrites of a retinal ganglion cell as found in nature can have different forms and directions. In this research, the dendrite is modelled as an active structure (can initiate an action potential) but the densities of ion channels are low, so the dendrites are not the relevant sections which initiate or block an action potential. However, for the integrity of the model, a dendrite consisting of three sections was added to the model although it was considered in the results presented in this thesis. It is modelled by cylindrical structures leaving the soma on the southern pole and then pointing horizontally to East and West.

6.3 Cell Biophysics

The active cell mechanisms and dynamics are defined by ionic conductivities. Table 6.2 shows the standard ion conductivities as originally published for the two models used in this research. The standard ion channel conductivities as determined by Hodgkin and Huxley (1952) are based on experiments on the giant squid axon. The standard ion channel conductivities of the Fohlmeister model were determined for the tiger salamander ganglion cell (Fohlmeister and Miller, 1997).

The model developed in this research is including different sections of a retinal ganglion cell having different biophysical parameters. The determining ion conductivity for every section in this research is the one of the Na^+ ion channel \bar{g}_{Na} . All other conductivities were calculated based on the \bar{g}_{Na} and the original relations to each other as given in table 6.2. That means, based on a chosen ion conductivity \bar{g}_{Na} all other conductivities of the model were fitted under the condition that ratios between the single conductivities were kept as determined originally. Proceeding this way, the underlying model stays integer.

The Na^+ conductivities used as standard data in the Hodgkin-Huxley model and the Fohlmeister model (see tables 6.3 and 6.4) are based on researches of tiger salamander ganglion cells as presented by Sheasby and Fohlmeister (1999) and Jeng et al. (2011).

Model	\bar{g}_{Na}	\bar{g}_K	\bar{g}_L	$\bar{g}_{K,A}$	\bar{g}_{Ca}	$\bar{g}_{K,Ca}$
Hodgkin-Huxley model	120	36	0.3			
Fohlmeister model	50	12	0.05	36	2.2	0.05

Table 6.2: Standard ion conductivities as defined in Hodgkin-Huxley model and Fohlmeister model. All conductivities in [mS/cm^2]

The sodium channel band is assumed to have a 5 times higher Na^+ conductivity than the soma (for details see Sheasby and Fohlmeister (1999) or Rattay (2014) for example), Na^+ conductivities for the neighbouring sections of the sodium channel band were overtaken from Jeng et al. (2011) who considered anatomical findings of Carras et al. (1992) and Fried et al. (2009). This leads to following ion conductivities used in the Hodgkin-Huxley model (table 6.3):

Property	Soma	AH	SOCB	TS	DA	VD	HD
\bar{g}_{Na} (set)	80	70	400	100	70	25	25
\bar{g}_K (calc)	24	21	120	30	21	7.5	7.5
\bar{g}_L (calc)	0.2	0.175	1	0.25	0.175	0.06	0.0625

Table 6.3: Conductivities for Na^+ , K^+ , and leakage ion channels of the modelled retinal ganglion cell for the Hodgkin-Huxley model dynamics. While the \bar{g}_{Na} conductivity is set, the other conductivities are calculated based on the ratios as given by (Hodgkin and Huxley, 1952). All conductivities in [mS/cm^2]

Additionally to the basic Na^+ , K^+ , and leakage ion channels, the Fohlmeister model also implements following additional voltage gated channels: the inactivating A-type K^+ channel ($\bar{g}_{K,A}$) and the Ca^{2+} channel (\bar{g}_{Ca}). Further, another ligand gated K^+ channel $\bar{g}_{K,Ca}$ activated by the Ca^{2+} concentration in the intracellular space is considered (table 6.4):

Property	Soma	AH	SOCB	TS	DA	VD	HD
\bar{g}_{Na} (set)	80	70	400	100	70	25	25
\bar{g}_K (calc)	19.2	16.8	96	24	16.8	6	6
\bar{g}_L (calc)	0.08	0.07	0.4	0.1	0.07	0.025	0.025
$\bar{g}_{K,A}$ (calc)	57.6	50.4	288	72	50.4	18	18
\bar{g}_{Ca} (calc)	3.52	3.08	17.6	4.4	3.08	1.1	1.1
$\bar{g}_{K,Ca}$ (calc)	0.08	0.07	0.4	0.1	0.07	0.025	0.025

Table 6.4: Conductivities of the modelled retinal ganglion cell for the Fohlmeister model dynamics. While the \bar{g}_{Na} conductivity is set, all other conductivities are calculated based on the ratios as given by (Fohlmeister and Miller, 1997). All conductivities in [mS/cm^2]

The capacitance of the membrane is considered to be $C_m = 1\mu F$ in both models. The Nernst potentials for Na^+ , K^+ , and leakage current are $E_{Na} = 50mV$, $E_K = -77mV$, $E_L = -54.3mV$ for the Hodgkin-Huxley model, $E_{Na} = 35mV$, $E_K = -75mV$, $E_L = -62.5mV$ for the Fohlmeister model.

The extracellular medium is assumed as homogeneous ideal electrolytic solution of infinite size. Macromolecules as cells or other tissues in the extracellular space are not considered to cause any additional electrical effects²¹, therefore, the only property describing the extracellular space (ES) is the constant resistivity ρ_e ²². Same considerations apply for the intracellular space, except it is limited in volume by the geometry of the neuron. The resistivity for intracellular currents is given by ρ_i :

Property	Soma	Axon	Dendrite	ES
ρ [$\Omega \cdot cm$]	300	300	300	5050

Table 6.5: Resistivities of the neuronal sections and the extracellular space (ES)

6.4 Spherical Soma

The soma was modelled as a spherical structure. Basically, a spherical structure is hard to excite by electrical stimulation as it always has two poles with opposite polarizations while a stimulus is applied. Further, because of the geometry of a sphere, the intracellular potential will always be very close to be equipotential. When modelling a spherical structure, the geometry and its implications require special attention.

6.4.1 Membrane Potentials

A monopolar point electrode creates an electric field with spherical equipotential surfaces. The created potentials are dropping inversely with distance from the electrode. The surface of a spherical neuronal structure exposed to such an electric field will therefore also be confronted with different potentials. The pole nearest to the electrode will be influenced stronger than the opposite pole (see figure 6.2). The pole next to the electrode is called electrode pole from now on.

The sign of the extracellular potential along the spherical surface, will be positive in case of an anodic stimulus, negative in case of a cathodic stimulus. The magnitude of the potential gradient depends on the distance to the electrode, the diameter of the soma, and the amplitude of the stimulus

²¹In reality, macromolecules and tissue in the extracellular fluid will result in a non homogeneous resistivity. Further, also capacitive effects resulted by these structures would influence an extracellular stimulation.

²²The extracellular fluid is typically assumed to have a 3 times higher resistivity than the intracellular fluid. However, the retina is packed very tightly with retinal ganglion cells, bipolar cells, photoreceptors, and other cellular structures. The high cellular density in the retina leads to a very high extracellular resistivity ρ_e compared to the resistivity of the extracellular fluid only.

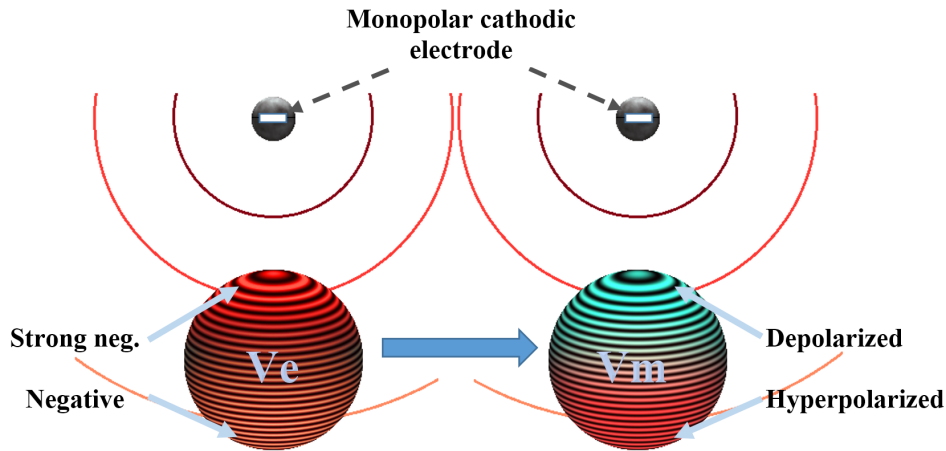


Figure 6.2: Comparison of the extracellular potential V_e versus the membrane voltage V_m of a spherical soma exposed to the electric field of a monopolar cathodic electrode. The spherical equipotential lines of the electric field are indicated by the coloured lines. Left, the surface of the soma will reflect the different extracellular potentials as created by the electric field on its surface. Therefore, the pole next to the electrode is stronger exposed to the electric field than the opposite pole. In cathodic stimulations, all extracellular potentials are negative. Right, the resulting membrane voltage V_m is indicated. The electrode pole is depolarized while the opposite pole is hyperpolarized. Somewhere between these two poles the membrane voltage is still in resting state V_r . The border between de- and hyperpolarized regions depends on the diameter of the soma and the distance between soma and electrode.

itself. As the membrane voltage is defined by $V_m = V_i - V_e$, the extracellular potential is directly affecting the V_m but not exclusively. The electric field also affects the intracellular potential V_i directly, further interaxial currents, transmembrane capacitive current, and ionic transmembrane current affects the V_i .

The geometry of a sphere is special. Because of its perfect symmetry, the electric field inside a conducting sphere is nearly zero (only some transmembrane forces will disturb intracellular potential slightly). An electric field describes the change in potential. In case of an electric field of zero, the potential must be equipotential²³.

Now, as described, the inside of the spherical cell is exposed to transmembrane electrical forces affecting the cell along the whole surface. However, because of the extracellular potential gradient from electrode pole to the opposite pole, the magnitude of the forces influencing the inside of the cell are not equal. Further, the inside of the cell is not a perfect conductor having

²³The electrical behaviour is described by Gauss's law. Different shapes of 3D structures are known as Gaussian surfaces.

a resistance of zero Ohm. These forces acting at different regions in the inside medium will also cause a slightly gradient of the intracellular potential. However, the electric forces inside the sphere which balance the potential will not allow the generation of a real intracellular potential gradient. Tests with the own model have shown, that differences in the intracellular potential are too small to detect in case of a soma diameter and intracellular resistivity ρ_i ranging in ranges as found in nature.

Therefore, the intracellular potential is seen as constant potential all over the inside of the spherical cell. The inside of the spherical soma is essentially equipotential (see for example Klee and Plonsey (1976) or Lee and Grill (2005)). The equipotential intracellular potential is established within such a fast duration, that in the temporal context of this model it must be assumed to be a step response.

Taking in mind the gradient of the extracellular potential V_e along the surface of the cell, and the equipotential intracellular potential V_i the membrane voltage $V_m = V_i - V_e$ is developing a depolarized and a hyperpolarized pole in case of a spherical shape. Note, while exposed to the electric field, the overall potential difference between V_i and V_e along the structure is the same as in resting state except of some ionic influences during the stimulus ($\bar{V}_i - \bar{V}_e \approx V_r$). Therefore, the magnitude of V_i must be between the maximum and minimum magnitude of V_e leading to a de- and hyperpolarization. The depolarized region is at the electrode pole in case of cathodic stimulation, at the opposite pole in case of anodic stimulation.

The depolarized pole is a potential local trigger zone for an action potential. In case an action potential is initiated, the electrical forces inside the structure will transmit those forces equally throughout the whole volume within a short time in the μs range. Therefore, if the spherical soma fires at the depolarized pole, the action potential is present at every position/segment in the soma within minimal delays.

6.4.2 Compartments

The Hodgkin-Huxley model and Fohlmeister model are characterized by conductivities \bar{g}_{ion} which are in the unit [mS/cm^2]. Therefore, the surface area of a modelled neuronal structure should meet the same area as in nature. Now, the spherical structure is already a simplification of the retinal ganglion cell soma. The modelling of a spherical shape by connected and stacked compartments can add another geometric inaccuracy. A reasonable spatial discretization will never result in a perfect sphere.

The usual shape to define a section in *Neuron* is a cylinder. In this case, only a length, a diameter, and the number of compartments are specified. Therefore, each compartment within a section is also of cylindrical shape. However, this method is suitable for a simplified axon or to define trees of dendrites. For translating complex cell networks into model data or to

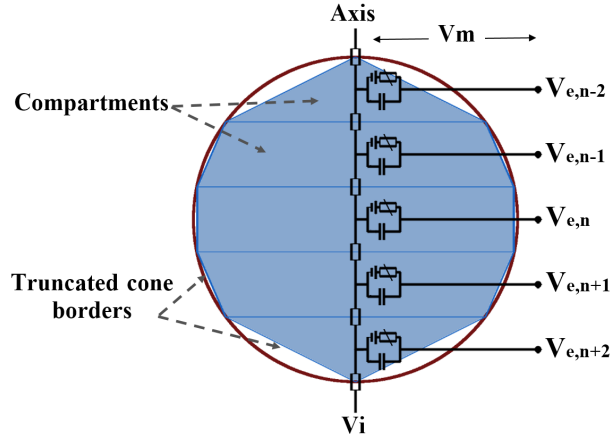


Figure 6.3: Schema of a spherical soma modelled in *Neuron* using 3D points and truncated cones. Here, a sphere modelled with 5 compartments is shown. Each compartment was defined by its x- and z-coordinates and its respective diameter. When the compartments are connected to each other, the outer surface borders are calculated automatically by *Neuron*. The total surface area of a section is the sum of all truncated cone surface areas. Also, the axis is shown which is perpendicular to the compartments.

define single complex 3D structures, *Neuron* also provides an additional way of creating neuronal sections. Each segment of a section is specified by its 3D coordinates along an axis in space and the respective diameter. Once all segments are defined, *Neuron* will connect them and calculates the surface area automatically. In case of using this method, truncated cones (frusta) are used instead of cylinders. The truncated cones will lead to an even and consistent surface. Further, also the total surface area of a section (the sum of every compartment's surface area) is more exact compared to stacked cylinders.

By choosing a sufficient number of segments, the spatial discretization of a sphere into truncated cones will create a nearly perfect shape. But, the surface area will always be less than the one of a real sphere. The surface area of a sphere is $A = 4\pi r^2$ resulting in an area of $A = 1256\mu m^2$ for a sphere with diameter $d = 20\mu m$. Using the 3D method of defining a shape in *Neuron* with 21 compartments, the total area of the section is $A = 1251\mu m^2$. The error is only around 0.4% which seems to be small enough for this research. If less error is required, the spatial resolution could be increased. However, this will result in higher computational costs.

6.4.3 Axis of Soma

In section 3.6 two different ways of modelling a cable model were introduced, the longitudinal and the transversal cable model. Cylindrical structures are usually modelled in longitudinal direction. However, a spherical shape as used for the soma has no distinct direction because of its symmetry. But, as the sphere will be exposed to an electric field, the axis is determined by the position of the sphere in relation to the electrode. A correct orientation of the cable segments is crucial for correct calculations.

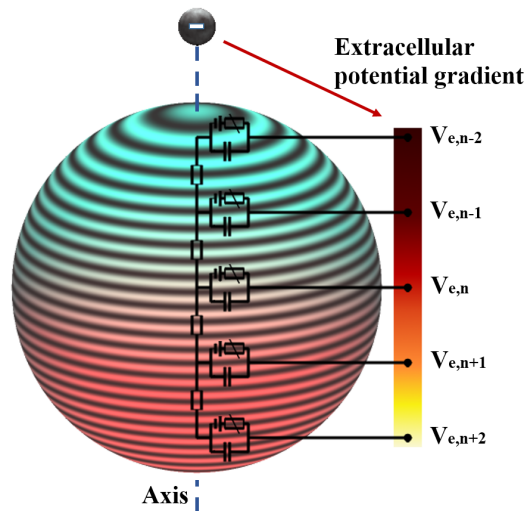


Figure 6.4: Compartments in a transversal extracellular stimulation. Every cable circuit of every segment has a corresponding connection to the extracellular potential. In the extracellular part of the cable model, the extracellular potentials which are based on the stimulus amplitude, distance to electrode, and the resistivity ρ_e are directly set for every compartment $V_{e,n}$. The extracellular potential gradient is shown on the right to the soma. The compartments are in transversal direction to the electrode (indicated by the cable model circuits). As the electrode creates a spherical electric field, the extracellular potentials $V_{e,n}$ represents the potential gradient along the surface of the spherical soma. The axis is in line with the electrode. The gradient on the sphere (every ring stands for one compartment) represents the membrane voltages $V_{m,n}$ showing a depolarized region at the electrode pole and a hyperpolarized region at the opposite pole.

Above in section 6.4.1 the distribution of the extracellular potential on a spherical surface was discussed in detail. There are two poles, the stronger influenced electrode pole and the opposite weaker pole. Every cable section of every compartment is connected to the extracellular space. To reflect the extracellular potential gradient as established at the surface of the sphere correctly, the axis of the soma must be in line with the center of the point electrode. Only a transversal model can represent the potential gradient

correctly.

Taking a closer look at the transversal model as shown in figure 6.4, the extracellular potentials are calculated by considering the transversal distance from electrode to every compartment, the stimulus amplitude, and the extracellular resistivity ρ_e . This results in an extracellular gradient in transversal direction as indicated in the right of the figure. Any other orientation of the axis would not reflect the transversal expanding electric field. The direct and indirect effects of the electric field will then lead to depolarized and hyperpolarized regions at the soma. The structure of the spherical surface in figure 6.4 shows the corresponding compartments/segments as they would be in 3D space, the colourings at the surface indicate depolarized (blue) and hyperpolarized (red) regions along the spherical structure.

In this research, the position in space of the electrode is variable. For this reason, the axis of the soma will always be reoriented whenever the position of the electrode changes. This is done by rotating of the soma axis in the direction of the electrode²⁴. This reorientation ensures that the soma is always in line with the electrode so the extracellular potential gradient is reflected correctly by the model.

6.5 Cylindrical Structures

In general, all considerations about the effects of an extracellular stimulus to a spherical structure are also valid for the cylindrical axon and dendrites. However, there is one key distinction compared to the symmetrical soma: A cylindrical structure has a given natural longitudinal axis. The electrical forces which balance out the intracellular potential V_i are the same, but, because of the length and the resistance because of the small diameter, the timing to reach steady state is different. Further, the transmembrane transmitted forces are of different magnitude along the axis, it is likely they will prevent the intracellular potential to become nearly equipotential. Therefore, a slightly potential gradient inside the structure is established.

6.5.1 Membrane Potentials

The asymmetry of a cylinder has direct effects on intracellular current movements and the equilibrium state of electrical forces. For the theoretical discussion, a single compartment with infinite small length is assumed. Such a compartment has no volume, only a circular area. Like the spherical structure such a compartment needs to balance out all electrical forces acting on it. In case of a nearly constant extracellular potential around the

²⁴See also the research of Lu et al. (2008) who also used a multi compartment model with a rotated axis for the spherical soma.

cross-sectional area acting via dielectric transmembrane forces, also the intracellular potential across the area will be nearly in equipotential state²⁵.

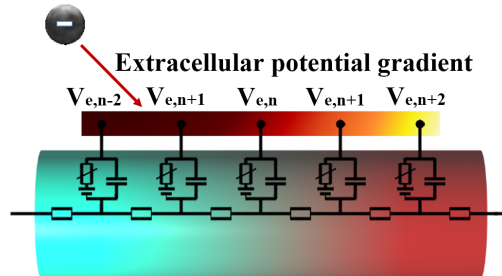


Figure 6.5: Compartments in a longitudinal extracellular stimulation. Every cable circuit of every segment has a corresponding connection to the extracellular potential. In the extracellular part of the cable model, the extracellular potentials which are based on the stimulus amplitude, distance to electrode, and the resistivity ρ_e are directly set for every compartment $V_{e,n}$. The extracellular potential gradient is shown above the cylindrical structure. The compartments indicated by the cable model circuits are in longitudinal direction to the electrode. As the electrode creates a spherical electric field, the extracellular potentials $V_{e,n}$ represents the potential gradient along the surface of the cylindrical axon having the outer left compartment $n - 2$ nearest to the electrode. The color gradient along the cylinder surface represents the membrane voltages $V_{m,n}$ showing depolarized regions in the vicinity of the electrode (left side) and hyperpolarized regions far away of the electrode (right side).

Now, every compartment of infinite small length has two neighbouring compartments which also interacts electrically. In equilibrium state a single compartment therefore needs to balance out not only the transversal electrical forces transmitted via the dielectric cell membrane, but also the longitudinal electrical forces from the neighbouring compartments transmitted by conduction. In case of even distributed extracellular surface potentials, the cylinder would also develop an equipotential intracellular potential V_i . However, in case there are extracellular potential gradients present along the longitudinal direction, also gradients in the intracellular potential will be established.

In case of monopolar extracellular stimulation which establishes a spherical electric field, the membrane potential $V_m = V_i - V_e$ is therefore composed by two potential gradients along the cylindrical structure. As the extra- and intracellular potential are not cancelling out each other, the membrane potential is characterized by a strong polarization next to the electrode and

²⁵There are models which consider the transversal direction too, this is especially necessary when investigating uneven distributed electric fields around a cylindrical structure or when analysing the influence of currents next to the cell membrane in the extracellular space.

two neighbouring regions having opposite polarization. Note, while exposed to the electric field, the overall potential difference between V_i and V_e along the structure is the same as in resting state except of some ionic influences during the stimulus ($\bar{V}_i - \bar{V}_e \approx V_r$). With longitudinal distance away of the electrode, the influence of the electric field becomes weaker, the membrane potential is converging to the resting voltage V_r . In case of cathodic stimulation (see figure 6.5), the region most influenced by the stimulus is depolarized, its two neighbouring regions are hyperpolarized. At anodic stimulation, there is a strong hyperpolarized region near the electrode followed by two depolarized regions next to it.

A depolarized region is a potential local trigger zone for an action potential. In case of cathodic stimulation an initiated action potential must overcome the two hyperpolarized regions first, otherwise the propagation of the action potential does not take place.

As this model does not consider any myelination along the axon, the effects of stimulation are very good approximated by the activating function²⁶.

6.5.2 Connection to Soma

As described in section 6.2 and figure 6.1, the axon will leave the soma at the eastern pole of the soma, the dendrite at the southern pole. However, in a multi compartment cable model the connection is realized by specifying the position along the axis of the parent structure (the soma in this case) where the terminal start of the child structure (axon or dendrite) is connected to²⁷. In this model, the direction of the soma axis is not fixed. It will always be orientated in line with the electrode to ensure transversal stimulation. As the axon shall leave the soma at its eastern pole (the vertical dendrite at the southern pole), the corresponding position on the soma axis to connect the child depends on the actual soma axis orientation in space (see figure 6.6).

The implemented solution will therefore always determine the actual orientation of the soma axis. Based on the rotation and the position a child shall be connected to, the corresponding position at the axis of the soma is determined. A child then is connected to this particular position directly at the soma axis. This ensures that the interaxial currents between different

²⁶See section 3.5 and also section 4.2 for the principles of the activating function and details to the polarized regions resulted in a cylindrical neuronal structure exposed to an electric field.

²⁷The model created in *Neuron* will place all child sections according to the parent position automatically. *Neuron* considers the distances between segments on the modelled axis as this geometric information is required to calculate interaxial current flow. But the diameter of a section is not considered in the morphology, instead the resulting surface area is calculated once and assigned to each segment separately. Therefore, when connecting a child to a parent, it is always connected directly on the axis of the parent where the intracellular current flows.

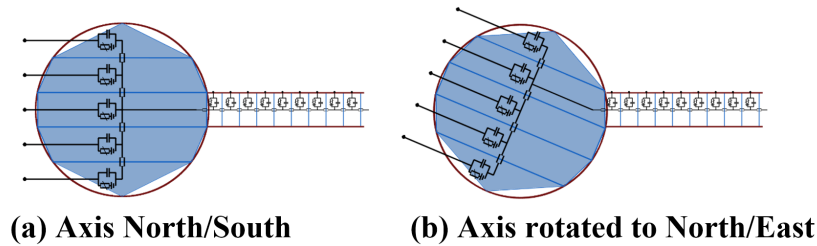


Figure 6.6: An axon connected to the eastern pole of a spherical soma. (a) shows an axis in North-South direction, therefore the axon is connected to the third compartment in the soma. (b) shows a slightly rotated axis to the North-East, therefore the segment of the soma representing the eastern pole of the sphere in space is the second segment from the top.

sections are considered correctly.

However, because all connections are realized along the axes, the resulting offsets in space need to be considered when dealing with geometric data like calculating the extracellular potential during an extracellular stimulation. For this reason, the model is dealing with a second coordinate system which considers all offsets in space compared to a pure cable model (see section 6.6.3).

6.6 Electrode

The electrode is considered to be a point source. The corresponding ground electrode is assumed to be infinite far away of the electrode. These assumptions will lead to a perfect spherical electric field established in the extracellular space.

To simulate extracellular stimulation with *Neuron*, different ways are thinkable²⁸. However, *Neuron* already provides two additional layers for the cable model which extend the model by extracellular potentials (see figure 5.1). The extracellular mechanism is deeply integrated in the *Neuron* environment, therefore, it was decided to use *Neuron*'s capabilities to deal with extracellular potentials directly.

6.6.1 Extracellular Mechanism

For practical usage of the provided extracellular mechanism of *Neuron*, some extensions were necessary. Generally, spatial and temporal discretization and solving the mathematical model shall be handled completely by the

²⁸A common way is to calculate the corresponding currents of an extracellular stimulus and inject these currents to segments of a neuronal structure.

mechanisms of *Neuron*. The own implementation is just setting up all necessary parameter so *Neuron* can perform its tasks. In case of the extracellular mechanism, the calculation and driving of the membrane potentials during the stimulus must be prepared for every segment. Callbacks or other communications during solving of the model between the *Python* code and *Neuron* itself should be avoided.

Therefore, parts and ideas from a sample program for extracellular stimulation published in the *Neuron* hot tips forum²⁹ by Ted Carnevale from Yale University were used and overtaken. In detail, the standard *Neuron* environment was extended by the `xtra.mod` mechanism which extends the functionality of every segment by:

- **Second coordinate system:** The coordinates of this mechanism are meant to represent the interpolated center of a segment in *Neuron*. Because of dealing with geometric space information, this coordinate system is also used to consider offsets between cable model coordinates and actual geometry. Therefore, any coordinate specified in this system represents the middle point of a segment in space considering actual dimensions of the neuronal structure.
- **Transfer resistance:** A transfer resistance R_x [$M\Omega$] will stand for the resistance between electrode and the reference position of the segment in extracellular space. It directly depends on the Euclidean distance between electrode and segment and the extracellular resistivity ρ_e .
- **Stimulus current:** A global variable for the stimulus current I_{st} will be added to every segment. This variable can be assigned by the model during solving.
- **Pointers:** There are two pointers for the extracellular potential V_e and for the membrane current density i_m . A pointer is used to link two *Neuron* variables by reference. In this case, the extracellular potential V_e (variable of the extracellular mechanism) is calculated by the transfer resistance R_x and the stimulus current I_{st} (variables of `xtra.mod`). Further, the contribution of the local membrane current because of the extracellular stimulation is reported back to the total membrane current (standard *Neuron* variable) for every segment.

When using the `xtra.mod`, respective coordinates needs to be calculated, further, for every segment the transfer resistance is set. Finally, the stimulus current I_{st} will be driven by the model. This is realized by specifying the current amplitude in combination with the timing of the stimulus (stimulus start time and duration). These information is the processed by

²⁹See <https://www.neuron.yale.edu/phpBB/viewtopic.php?f=28&t=168>.

Neuron automatically when solving the model³⁰. At every time step, based on the stimulus data and the transfer resistance defined before, the extracellular potential is calculated and included in the solution for the cable model equations.

6.6.2 Electrode Position

The mono polar electrode can be placed at any position (except inside a neuronal structure). The same coordinate system as used for all neuronal structures is used for the electrode too. However, this research's intention is to analyse extracellular stimulation near the soma and in the first regions of the axon proximal to the soma. So practically the electrode was mainly placed in the northern hemisphere above the soma (positive z-coordinate), in particular, above the soma itself, above the axon hillock, and lateral to the soma.

Moving the electrode position directly affects the geometry of all neuronal structures. As described in section 6.4.3 in detail, during modelling the axis of the soma is kept in line with the electrode. So, any change of the electrode position will cause a reorientation of the soma axis. This goes along with a reorientation of all other sections connected to the soma (see section 6.5.2).

In summary, it can be claimed that nearly the whole model setup needs to be recreated from the very beginning on to handle a position change of the electrode.

6.6.3 Electric Field

The spherical electric field is approximated by the equations 4.3 as given in section 4.2.1. As this research deals with a constant square pulse, the electric field is constant during the time a stimulus is applied.

As the extracellular membrane potential is calculated by model driving mechanisms of *Neuron* in combination with mechanisms of the `xtra.mod` file, the transfer resistance must be known for every segment. To calculate the respective resistance, the distance of a segment to the electrode must be gathered first. As already outlined, in a classical cable model as used by *Neuron* the real dimensions of a neuronal structure are not fully considered. Along the cable, only interaxial length information are of interest. So connections between neuronal structures are just realized by an electric circuit which ignores all dimensions of the structure except the interaxial distances between compartments.

As the coordinates used by the cable model are not suitable for calculating the distance of a segment to the electrode, the second coordinate system introduced with `xtra.mod` will store following information:

³⁰The *Vector play* functionality is used to drive the solving of *Neuron*.

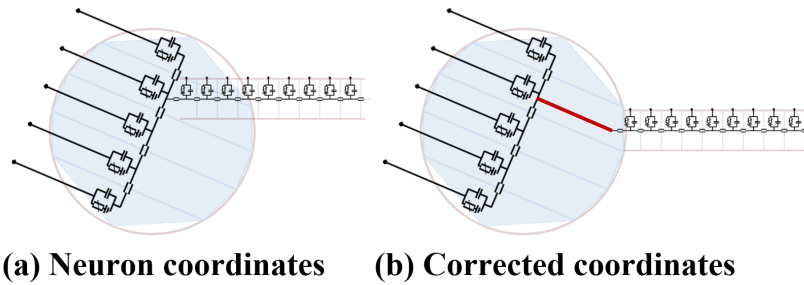


Figure 6.7: Schema of *Neuron* cable model coordinates versus real coordinates in space. (a) shows a soma and an axon section connected at the soma axis. (b) shows the real dimensions where the axon leaves the soma on the outside of the soma cell membrane. The red line in (b) is the correction in x- and z-dimension. The total correction includes the dimensions of the soma and offsets because of the rotated soma axis.

- **Neuronal structure coordinates:** For every segments its center is stored. This point (referenced as corrected coordinates, see figure 6.7) corresponds to the actual structure where child neuronal structures are attached at the parent's cell membrane and not at the center/axis.
- **Corresponding diameter:** Also, the corresponding diameter for the center of a segment is determined. As a segment is modelled either as a cylinder or as a truncated cone, the diameter at the center corresponds to the average diameter of the segment.

Using these geometric information, the Euclidean distance between the electrode and the segment can be calculated. Here it must be distinguished between a spherical structure and cylindrical/truncated cone structure:

- **Cylindrical structure:** Here the distance between electrode and segment center determines the extracellular potential affecting the segment. Although there will be a slightly gradient of extracellular potential along/around the surface of a single segment, because of the small diameter and the short length of a segment, the difference can be neglected. The average distance given by the center point of the is a good approximation to calculate the potential affecting the total surface of the segment.
- **Spherical structure:** The diameter of the soma is large compared to the diameters of all other structures. Further, the soma is modelled in transversal direction. Because of the spherical form of the soma, the distance between the electrode and the center of a segment is always shorter than the distance between the electrode and center

of the segment's surface where the electric field is actually affecting the segment (see figure 6.8). Therefore, the distance for calculating the transfer resistance R_x considers the corresponding diameter of the segment. The resulting distance will lead to a correct extracellular potential affecting the segment.

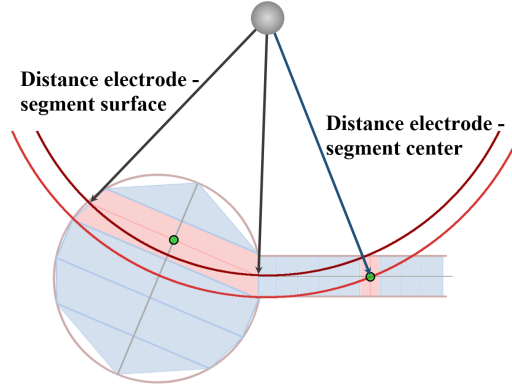


Figure 6.8: Distances used for calculating the transfer resistance R_x . The segment centers of the highlighted segments in the soma and axon are marked in green. For the axon, the distance between electrode and center is used to approximate the extracellular transfer resistivity (respectively the extracellular potential V_e). For the soma, the distance between electrode and segment surface center is taken. Note the equipotential lines of the electrode. They clearly indicate how much the extracellular potentials between segment surface center and segment axis center differ at the soma.

Under consideration of equation 4.3 and with the known distance between electrode and segment, the transfer resistance can be calculated:

$$V_e = \frac{\rho_e \cdot I_{st}}{4\pi r} \rightarrow R_x = \frac{V_e}{I_{st}} = \frac{\rho_e}{4\pi r} \quad (6.1)$$

where r is the distance between electrode and segment. I_{st} is the stimulus current applied in the extracellular space with the resistivity ρ_e . The transfer resistance R_x is stored by an `xtra.mod` variable for every segment. During model execution `Neuron` calculates the extracellular potential V_e by multiplying the transfer resistance with the stimulus current density i_{st} and the respective segment area A :

$$V_e = R_x * i_{st} * A \quad (6.2)$$

The resulted extracellular potential V_e is an active part of every segment's cable model and fixed to its value during the stimulation duration.

6.7 Neuron Models

Three different neuronal models are provided in this research. The active mechanisms of the Hodgkin-Huxley model and Fohlmeister model are used to analyse action potential initiation and propagation. Additionally, there is a passive model which is used to investigate the direct effects of an extracellular (or intracellular) stimulus without the influence of any ion channels.

While the Hodgkin-Huxley model and the passive models are integral parts of the *Neuron* environment, the Fohlmeister model had to be included to the standard installation. It consists of two files, the `fcm.mod` and the `capump.mod`³¹.

The downloaded Fohlmeister model file was extended by a voltage sensitive leakage channel with a constant conductivity \bar{g}_L according to the original publication of Fohlmeister and Miller (1997). Biophysical properties were set according to section 6.3.

For the Hodgkin-Huxley model, the biophysical properties of section 6.3 were applied for the Na^+ and K^+ ion channel conductances.

The passive model of *Neuron* contains a leakage ion channel. However, to see the effects of the extracellular stimulus on the neuronal structure without any ionic influence, the leakage channel can be disabled by setting the conductivity to zero ($\bar{g}_L = 0$).

6.8 Compiling of Neuron

The two model files of the Fohlmeister model (see section 6.7) and the additional mechanisms for extracellular stimulation provided by the `xtra.mod` file as described in section 6.6.1 had to be included in the standard *Neuron* software environment.

Neuron provides the possibility to compile a dynamic-link library `.dll` to extend the functionality of *Neuron*. Additional files created in the *Neuron* model description language NMODL will be translated into C-code which is finally compiled. The created *Neuron* `nrnmech.dll` is then again imported into the *Python* environment for using the additionally functionality in a *Python* script.

6.9 Neuron Recording

Neuron allows to record different data for every segment separately. Any data of interest to record must be specified beforehand. In a multi compart-

³¹Both files can be downloaded from the *Neuron* ModelDB <https://senselab.med.yale.edu/modeldb/>. There are several different projects available using those files, e.g., 'Salamander retinal ganglion cell: ion channels (Fohlmeister, Miller 1997)'. The naming of the files was changed in this project.

ment model consisting of several sections and a high spatial and temporal resolution, a high amount of data is resulted even for short simulations.

Nevertheless, it was decided to record all important data for every segment so detailed investigations and analyses are possible. To handle the resulted data, the user interface must support appropriate representation, further some algorithms allow automatic processing of the gained data. Additionally, results gained by automatic test procedures are exported into .csv files. Following data will be recorded during a simulation run:

- **Potentials and voltages:** Besides membrane voltage V_m , also extracellular potential V_e will be considered. Internally, also the intracellular potential V_i is calculated ($V_i = V_m + V_e$).
- **Current densities:** The total membrane current density i_m is further separated into i_{Na} and i_K current densities.
- **Gating variables:** The different gating variables m , h , and n are recorded, additional the total gating variable for Na^+ (m^3h) and K^+ (n^4) are calculated after *Neuron* has finished its calculations.

6.10 Action Potential Detection

The main questions for analysing lower and upper limit for extracellular stimulation are:

1. Was an action potential initiated for the chosen stimulus with certain current amplitude, duration, and distance to the neuron?
2. At which section/segment of the neuron the action potential was initiated first?
3. Did the action potential propagate along the neuron?
4. Was there some blocking at any position along the neuron?

Therefore, to analyse a huge amount of data, a method to detect action potentials automatically was required. First, very general definitions for an action potential were necessary which basically are:

1. The membrane voltage V_m must exceed $8mV$ at some time.
2. The duration of the membrane voltage V_m in the positive range must be longer than $0.1ms$.

There are no general definitions on how exactly an action potential is characterized. These two rules and the respective limits were defined based

on observations during implementation of the model. They are not too complex and will detect most action potentials correctly. Problems might only occur if two action potentials are overlapping (e. g., forward and back propagating action potential).

By applying these two conditions, an action potential can be found easily when analysing data after the stimulus. Nevertheless, there may be the situation that an action potential was already initiated or even completely generated during the stimulus itself. This especially happens during long stimulus durations.

These cases are difficult to handle as the membrane voltage during the stimulus includes also the extracellular potential ($V_m = V_i - V_e$) and its direct effects³². These direct effects which are causing de- and hyperpolarized regions will take place immediately when a stimulus is applied. After the stimulus ends these effects are reversed again. However, the membrane voltage after the stimulus will also include influences of transmembrane ionic currents taken place during the stimulus.

To handle also the timespan during the stimulus and the transition phase after the stimulus for automatic action potential detection, it was necessary to get rid of the direct effects and influences on the membrane voltage caused by the stimulus itself. Only electrical effects caused by currents through ion channels and interaxial current movements shall be left.

As the model mechanisms are based on a system of non-linear differential equations, it is nearly impossible to calculate these effects manually. Instead a filter was used which assumes that changes in the membrane voltage caused by direct effects of the stimulus itself are based on a linear time course.

To apply the filter, the delta of membrane voltage right after the stimulus starts ($\Delta V_{m,st,start}$) and after the stimulus ends ($\Delta V_{m,st,end}$) are determined. During the stimulus duration t_{st} the membrane voltage is corrected by subtracting the corresponding delta with respect to time t . The corrected membrane voltage ($V_{m,t,corr}$) is cleared by the direct effects of the stimulus. The linear change of these effects is considered by using the slope between $\Delta V_{m,st,end}$ and $\Delta V_{m,st,start}$ for voltage correction:

$$V_{m,t,corr} = V_{m,t} - (\Delta V_{m,st,start} + \frac{\Delta V_{m,st,end} - \Delta V_{m,st,start}}{t_{st}} * t) \quad (6.3)$$

The filter is applied for every segment separately to consider the individual direct effects of the stimulus. The resulting corrected membrane voltage will still include fragments of the direct effects. In reality, the temporal behaviour is non-linear. Therefore, the linear processing is only a rough approximation and not covering all aspects of changed membrane voltage.

³²Mostly the capacitive transmembrane currents and interaxial balancing currents influence the membrane voltage. But also voltage shifts because of active ion channels opening at some regions of the neuron will influence the membrane potential during the stimulus.

However, over the total duration the direct effects are cleared very effective, errors in the corrected membrane voltage because of the non-linearity are only of small magnitude. It is not likely that the automatic action potential detection is influenced by these errors too much.

Based on the corrected membrane voltages, any segment is analysed for initiated action potentials by applying above defined rules. All detected action potentials are stored together with the action potential timing and gating information for further analyses.

Once an action potential is detected, there is still the question left when it has started. Also here no general accepted rule can be applied. So it was decided to analyse the change in slope to get an idea of start and end of an action potential.

Using the already found maximum of the membrane voltage, and the temporal information when the action potential has crossed the zero-voltage line, the slopes (left and right flank of the action potential) around the maximum value are calculated. These slopes determined in the positive voltage range are assumed to be more or less equal also in the negative voltage range where the action potential has started.

The minimum slopes (one for depolarization, one for repolarization) are assumed to be 50% of the slope determined in the positive voltage range. Now, both flanks of the action potentials are investigated stepwise and checked for having at least the minimum slope. If at some point the minimum slope is not reached any more, this certain point is detected as start (left flank) or end of the action potential (right flank).

6.11 Automatic Test Procedures

For systematic investigations, the model is able to perform simulations based on defined test procedures. A test procedure contains an unlimited amount of single test cases. A test procedure is defined hard coded in *Python* by choosing all variables and their variations. Following variables are subject for variation between test cases:

- **Electrode Position:** The coordinates of the stimulus electrode.
- **Stimulus amplitude and duration:** The strength of the stimulus.
- **Neuronal Structures:** Definition which sections (soma, axon, dendrites) are considered in a test case.
- **Soma Radius:** Allows to vary the radius of the soma for systematic analysing lower and upper limits based on geometric properties.
- **Model Type:** The membrane mechanisms based on Hodgkin-Huxley model, Fohlmeister model, or passive model.

- **Resistivities:** Vary the intra- (ρ_i) and extracellular (ρ_e) resistivity.
- **Conductivities:** Vary the used conductivities (\bar{g}_{ion}) by a factor.

To define variations, different ways are available:

- **Fixed:** Sets a variable to a fixed value for every test case in the test procedure.
- **Values:** Allows to define manually a list of values for a certain variable.
- **Interval with step-width:** This option is used to define a sequence of values in a given interval with a given step-width.

Based on the definitions, all test cases are created under consideration of all possible variations³³. Then, successively each test case will be executed by the model. After each model execution, the model results are further processed on section and segment level to get a meaningful output. The most important analyses performed are:

1. Minimum and maximum membrane voltage V_m and extracellular potential V_e during the stimulus.
2. Distances and transfer resistances between electrode and section.
3. Number of detected action potentials in every section.
4. Segment(s) which initiated an action potential.
5. Timing of action potentials.
6. Gating variables and slopes during and after the stimulus.
7. Na^+ current and possible reversal during the stimulus.
8. Net flux of Na^+ currents during the stimulus.

To limit computational costs, there is no graphical representation of the results during executing a test procedure. Instead, a comma separated values file `.csv` will be created and stored. This file contains all definitions of every test case and the processed and prepared results of the model. This file can be used for further analyses and investigations over large amount of test data. In case graphical representation is required to analyse single test cases in the user interface, a test case can be repeated manually based on the data of the `.csv` file.

³³For example, three variables with 10 variations each will lead to 1000 test cases ($10 \times 10 \times 10$) in the test procedure.

6.12 User Interface

This model is concentrated on analysing the dynamic behaviours of retinal ganglion cells during extracellular stimulation. The dynamics are defined by a non-linear differential equation system. Because of the multi compartment approach, the high temporal discretization, and multiple measurements, special attention was paid in the graphical representation of results. All controls and visualizations were realized in *Python* 2.7.10, for user interface controls and containers the `tkinter` package was used, graphs were realized with the `matplotlib` environment.

The main window is intended to allow full control of the model parameters. Besides all options for extracellular stimulation, it is also capable to apply intracellular stimulation by injecting a defined current for a certain duration into any segment of the neuronal structure. This is mainly done to test the neuronal structure for correctness.

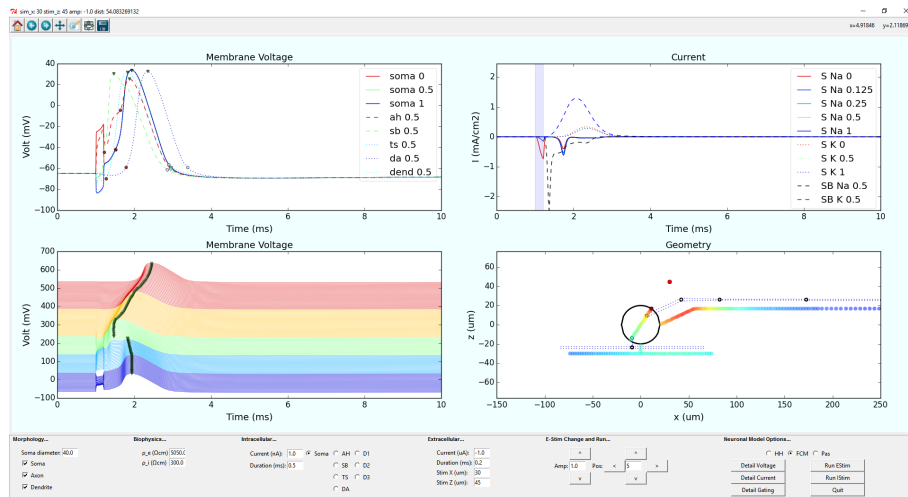


Figure 6.9: Main window of the realized model showing most important model results of a stimulation. While three of the graphs show model results, bottom right graph shows the actual geometric properties, the electrode position, and the influence of the electrode to the single sections of the neuron. All graphs are interactive by supporting panning and zooming. In the bottom frame, different options and parameters for the model can be set. Buttons allow the navigation to detailed model results. Also, new model executions (extra- or intracellular stimulation) are started from here.

After an extracellular stimulus is applied, the main window will give a general overview of the model results. In the main window following information are visualized:

- **Membrane voltage V_m :** Graphs of the membrane potential on distinctive positions of the neuronal structure are shown over time. Also,

detected action potentials and timing information are included in the graphs. Further, a second graph will show the membrane voltages of all segments over time. Here, the voltage is slightly shifted on the y-axis so the wave fronts are visible over the whole structure.

- **Current densities i_{Na} and i_K :** The main driving channel for depolarization is the Na^+ ion channel, the K^+ ion channel is responsible for repolarization. To get an overview of the dynamics, the currents are shown over time.
- **Geometric properties:** Another part of the main window will give a graphical representation of the geometric properties. Besides the neuronal structure also the electrode is shown. Further, the influence of the stimulus to every segment of the neuron is indicated by a color gradient along the axis of each section. Further, coordination of the cable model are shown additionally.

In case of further detailed investigations are necessary, there are three additional windows which provide insight views into the voltages, currents, and gating-variables. Here, special attention was paid in temporal aspects to visualize the dynamics of the neuronal cell. For this reason, a kind of movie-representation was implemented to navigate interactively through different data. A slider is used to navigate in time, the graphs containing the data are automatically adapted to the actual time step.

For highlighting the dynamics, data of the last several time steps are shown simultaneously. This gives a moving impression of the dynamics when sliding through time. The resulting graphs are generated over all compartments of the neuron (measurement (y-axis) to compartment (x-axis) for a single time step (slider)). Every graph created by this movie-representation additionally shows the gating variables of the Na^+ ion channels m and h as the gating-variables are the driving part for all electrical effects.

This movie-representation represents data of the dynamics in maximal temporal and spatial resolution. Further, the moving graphs give a very good understanding of the dynamic behaviour of the neuronal cell. Following detail windows are available:

- **Voltage details:** The membrane voltage V_m as well as the corrected membrane voltage $V_{m,corr}$ are shown for every compartment over time with shifted voltage to show the wave fronts. Two movie-graphs for the soma and the axon allow to navigate through the membrane voltage and additionally show the m and h gating variables of the Na^+ ion channels.
- **Current details:** Four movie-graphs show the total membrane current density i_m and the Na^+ current density i_{Na} for the soma and

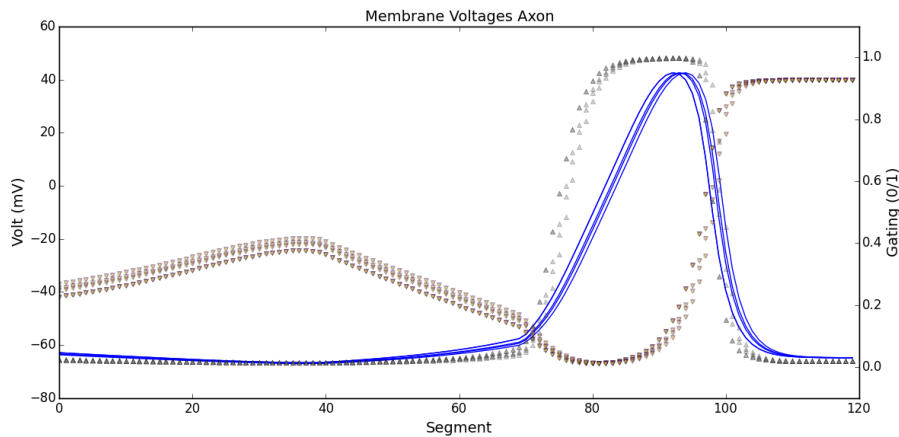


Figure 6.10: Graph generated by the movie-representation. An action potential is shown as it travels along the axon (blue lines) from left to right. The gray markers show the m gating, the violet markers the h gating. Here the interaction between the gating variables can be seen clearly. In segments the action potential has already passed (left) the m gatings indicate an already *closed* state, the h gatings are setting the *inactive* state to *active* again. In segments the action potential has not passed yet (right), the Na^+ ion channel is still *closed* by the m gatings, but the channel is not set to *inactive* state by h . In the segments just affected by the action potential, the transitions of m and h can be observed.

the axon. Additionally, the m and h gating variables of the Na^+ ion channels are shown.

- **Gating details:** This window shows the total Na^+ gating (m^3h) in different views. For every compartment the gating wave front is shown over time with shifted y-axis. Further, for some chosen regions of special interest the total Na^+ gatings are shown separately. Two movie-graphs visualize the total gating for soma and axon, additionally also the m and h gating variables are presented. To indicate the electrical effects caused by the total Na^+ gating, additionally the corresponding membrane voltage V_m is included in the movie-graphs.

The control panel in the main window allows to modify all relevant parameters for an extracellular stimulation. Further an intracellular current injection with a variable stimulus amplitude and duration can be performed for every section of the neuronal cell³⁴.

The most important parameters and options available on the user interface for extracellular stimulation are:

- **Model type:** Switching between the Hodgkin-Huxley model, the Fohlmeister model, or a passive model cell membrane behaviour.

³⁴The intracellular stimulus is always applied in the center of a section.

- **Geometry:** Allows to choose of which sections the neuron is composed of. Besides a full neuronal structure consisting of soma, axon, and dendrites, also the soma or axon can be stimulated alone. Also, combinations like soma with axon or soma with dendrites is allowed. Further the diameter of the spherical soma can be changed as the spherical structure and its size is of special interest for this research.
- **Stimulus properties:** Allows to set the current amplitude and duration of the extracellular stimulus. As well cathodic but also anodic extracellular stimulation is possible. For analysing model outcome for different current amplitudes in the user interface, the amplitude can also be changed by a defined step size (control via arrows). Each time the amplitude is changed in this way, the model is executed immediately.
- **Electrode position:** The x- and z-position of the electrode can be modified. For fast navigation, it can also be changed according a variable step size with immediate model execution (control via arrows).
- **Biophysical properties:** Allows to change the resistivities of the intra- and extracellular space.

Chapter 7

Results

During this research, different analyses were performed to get a better understanding of the mechanisms and dynamics of a retinal ganglion cell during strong extracellular stimulation. Besides analysing special cases by using the possibilities provided by the user interface of the implemented model, special attention was given to systematic analyses of the stimulation window in extracellular stimulation. In this context, different test procedures were created with the target to cover a broad range of test cases which may also be relevant in actual extracellular stimulation as done in neuroprostheses.

Geometrical and biophysical properties were used as described in section 6.2 and 6.3. However, sometimes one or more properties were varied to test a certain hypothesis. In this case, all changed properties are specified separately. The temperature was set to $T = 22^{\circ}C$, the temporal resolution used by *Neuron* to solve the differential equations was $dt = 10\mu s$.

7.1 Hypotheses

To start systematic analyses, a set of hypotheses were formulated beforehand. These hypotheses are partly of very general nature. However, when it comes to the blocking of a neuronal cell during or after an extracellular stimulation, things are getting complicated. There are several electrophysiological phenomena taking place at the same time. Further, there are different regions in the neuron which show different behaviours and additionally influence each other. And finally, temporal aspects like time constants in charging the cell membrane or voltage depending gating of ion channels play a role. Everything together, we are dealing with a very complex situation. The created hypotheses helped us to find an useful direction for our research:

1. An action potential can only be initiated when Na^{+} ion channels are open. An influx of Na^{+} ions through ion channels is precondition for initiation of an action potential.

2. A stimulus is opening ion channels in depolarized regions of a neuron (*open* state). Depending on the strength of impact and its duration, the stimulus might also trigger the *inactive* state of a Na^+ ion channel which closes a Na^+ ion channels again.
3. A spherical structure as the modelled soma are harder to stimulate than a cylindrical structure.
4. The intracellular potential of a spherical soma is assumed to be almost equipotential. An action potential in the soma is therefore present in every segment of the soma.
5. Direct electrical effects of a stimulus to a neuron are causing an immediate shift in the membrane voltages along a neuronal structure. Once the stimulus is turned off again, these direct effects are reversed. Any difference in the membrane voltages before the stimulus and right after the stimulus is caused by the active behaviour of a neuron during the stimulus or by ionic leakage current, therefore, by transmembrane ionic currents.
6. In normal conditions, Na^+ ions will influx in the cell through open channels. This influx causes a depolarization in the particular region. But a strong extracellular cathodic stimulus may not only open the Na^+ ion channels, it can also lead to a Na^+ current reversal at affected regions. This Na^+ reversal current will repolarize the particular region and therefore act against the stimulus³⁵. A Na^+ current reversal lowers the intracellular potential and will influence the dynamics of the retinal ganglion cell.

Further, based on these considerations, additional hypotheses according the upper limit of extracellular stimulation were formulated:

- **Normal stimulation strength:** The stimulus opens Na^+ ion channels in depolarized regions, additional Na^+ ions will influx. Because of the positive charged ionic influx, the depolarization is amplified. The time when Na^+ ion channels fully open is reached during or short after the stimulus. The strength of the stimulus or its duration will not cause the inactivation gate of the Na^+ ion channel to set the channel in *inactive* state (*h* gating) before the stimulus ends.
- **Strong stimulation strength:** The stimulus opens Na^+ ion channels. In the regions depolarized most, a Na^+ current reversal happens

³⁵The Nernst potential which is around $E_{Na} \approx 35 - 50mV$ for Na^+ ions in the cell environment describes the chemical diffusion force generated by ionic concentration differences. To overcome the diffusion force which is precondition for a Na^+ ion current reversal, the membrane voltage V_m must exceed the Nernst potential.

which acts against the stimulus. Because of the geometric properties of an electric field established by a point source, there also must be regions where Na^+ ions influx. An action potential is still possible as total Na^+ outflux is not strong enough to decrease the intracellular potential in a way an action potential is blocked.

- **Very strong stimulation strength:** The stimulus opens Na^+ ion channels. In the regions depolarized most, a Na^+ current reversal happens which acts against the stimulus. However, because of the strength and/or duration of the stimulus, the Na^+ channels are set to *inactive* state by the inactivation gate (*h* gating) before the stimulus ends. The *inactive* state prevents an action potential as the Na^+ ion channels are closed. Another theory explaining the prevention of an action potential would be a strong hyperpolarized membrane voltage after the stimulus because of a strong net outflux of Na^+ ions caused by a Na^+ current reversal. The hyperpolarization would eventually force the Na^+ ion channels to close immediately after the stimulus which blocks an action potential.

The above formulated theoretical considerations are only working hypotheses which are subject for systematic evaluation and verification. Besides testing for these hypotheses, we also needed to verify the correct behaviour of our model beforehand, especially the biophysical behaviour of the spherical structure. Therefore, before analysing the blocking phenomena of a retinal ganglion cell, the first results here are general tests of the model to prove its correct behaviour and to get a better understanding about the direct effects of the stimulus to the neuronal cell.

7.2 Direct Effects of Stimulus

To test for direct electrical effects on an extracellular stimulus, the membrane behaviour was set to be passive. In passive mode, no active mechanisms like ion channels or ion pumps are present. The effects of the electric field established by an extracellular stimulus to a neuronal structure are reduced to capacitive and interaxial currents.

7.2.1 Cylindrical Structure

In a first test, a cylindrical structure was stimulated by an extracellular stimulus perpendicular to the axis of the neuron. The neuron consisting of 1000 compartments is assumed to have a length of $l = 1000\mu m$ and a constant diameter of $d = 2\mu m$ (see figure 7.1). The electrode is placed $15\mu m$ above the neuron surface in *z*-direction. The stimulus was chosen to be cathodic $I_{st} = -1\mu A$ for a duration of $1.5ms$, the extracellular resistivity is $\rho_e = 5050\Omega \cdot cm$, the intracellular resistivity $\rho_i = 300\Omega \cdot cm$.

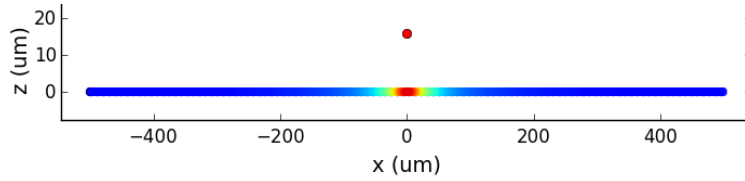


Figure 7.1: Electrode geometry of the extracellular stimulation. The electrode is placed $15\mu\text{m}$ perpendicular to the surface of a cylindrical neuron. The color gradient on the neuron depicts the impact strength V_e of the stimulus at the cell membrane.

After the stimulus is applied, the neuronal structure immediately responds on the electric field established by the stimulus. This will not only affect the extracellular but also the intracellular potential. According to the geometry of the stimulation and the cathodic stimulus, a depolarization takes place next to the electrode, while regions farer away of the electrode will be hyperpolarized (see figure 7.2). During the whole period of time when stimulating the neuron, the the membrane voltage V_m is slightly increasing.

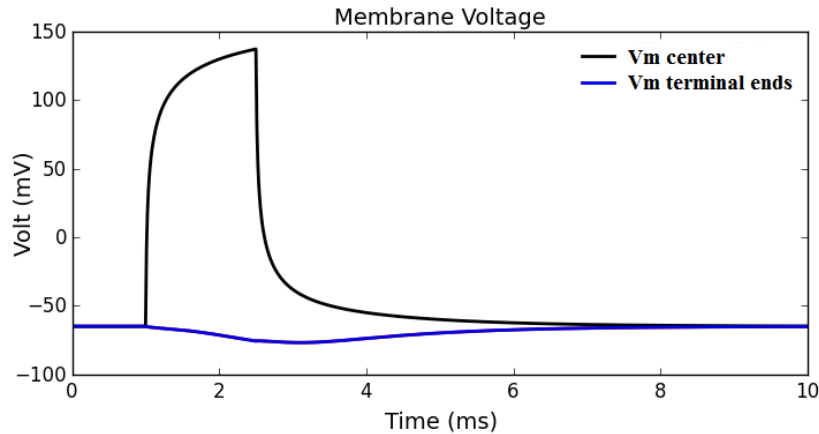


Figure 7.2: The membrane voltage V_m at the center of the neuron (black line) shows a very strong depolarized region. After an immediate step response rise after the stimulus has started, the membrane voltage is still slightly increasing while the stimulus is applied. The membrane voltages at the terminal ends of the neuron (blue line, V_m identical at left and right terminal ends) show slightly hyperpolarized regions.

To analyse the increasing membrane voltage during the stimulus at the center of the cylindrical structure, a closer look at the intra- and extracellular potentials must be taken (see figure 7.3). When the electric field is established, both, the extracellular potential V_e and the intracellular potential V_i are immediately (step response) affected. Both potentials are shifted accord-

ing to the strength of the electric field. While the extracellular potential V_e is not changing any more while the stimulus lasts, the intracellular potential V_i starts to balance out itself inside the structure. Note, the difference of the mean intracellular potential to the mean extracellular potential along the whole neuron is at every time equal to the resting voltage ($\bar{V}_i - \bar{V}_e = V_r$). This is caused by the passive mode which does not allow any ions to pass the cell membrane, therefore the average membrane voltage does not change in this simulation. However, the distribution of the intracellular potential may vary inside the cell at different times.

According to Gauss's law, the electric field of an isolated conductor in an electric field has the same magnitude at any position inside the structure. Now, the intracellular fluid is an electrolytic conducting medium, but in contrast to a metal conductor for example, it has a notable resistance. This is given by the resistivity ρ_i in $\Omega \cdot cm$. Because of the small diameter of $d = 2\mu m$, it can be assumed, that the balance in transversal direction is reached immediately after the stimulus started (step response). However, in longitudinal direction (along the x-axis of the neuron), the resistivity will play a crucial role for the interaxial currents which balance out the intracellular space. Comparing the two figures of 7.3, the one at $t = 0.02ms$ after stimulus shows a strong gradient in V_i along the neuron, while the intracellular potential V_i is on its way to steady state at $t = 1.02ms$. In steady state, there will still be a slightly gradient in the intracellular potential because electrical forces transmitted via the cell membrane will prevent equipotential state inside the cylindrical structure.

Assuming an intracellular resistivity of $\rho_i = 300\Omega \cdot cm$ and the size of the neuron $d = 2\mu m$, $l = 1000\mu m$, it takes more than $\tau > 3ms$ for the intracellular potential to reach the steady state and therefore the equilibrium state of the neuronal structure inside the electric field.

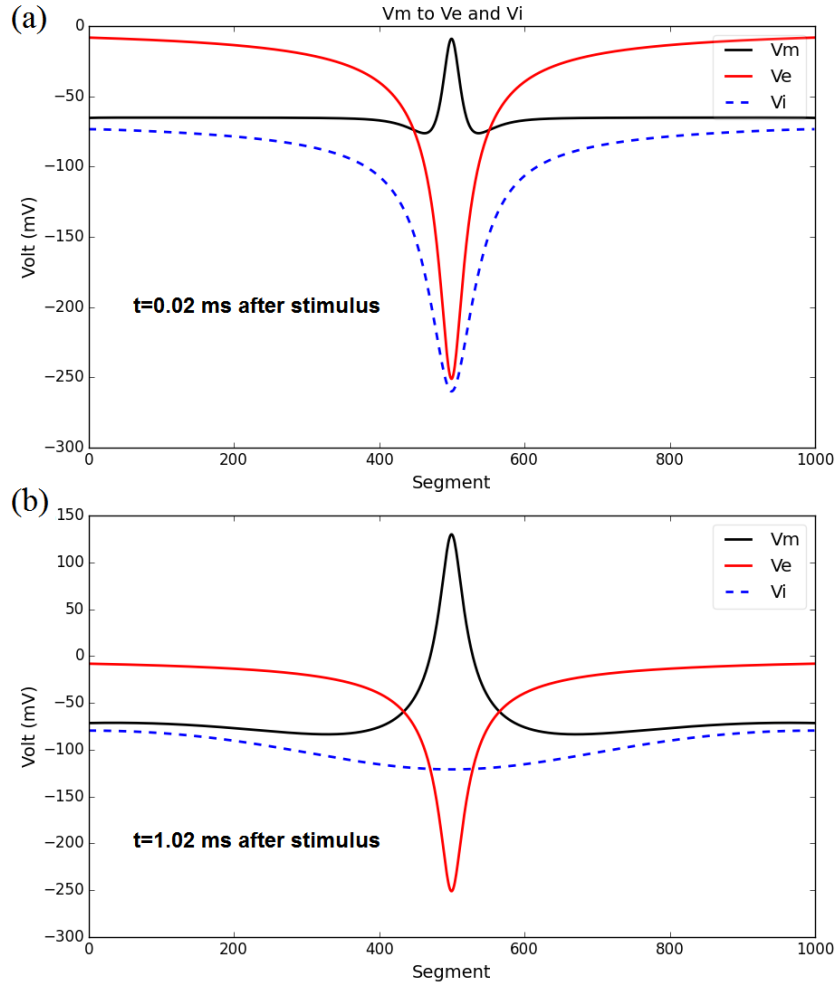


Figure 7.3: Membrane voltage V_m and the intra- and extracellular potentials V_i and V_e during the stimulus over all compartments. The upper graph (a) shows the stimulated neuron $t = 0.02ms$ after the stimulus was applied, the lower graph (b) $1ms$ later. At $t = 0.02ms$ the intracellular potential has reacted by an immediate response to the electric field. The V_i nearly has an identical shape like the V_e , only shifted by the resting voltage V_r . Here the membrane voltage already developed a depolarization region rising towards the positive range. Left and right to the depolarization, regions of hyperpolarization can be seen. At $t = 1.02ms$ the intracellular potential V_i already had $1ms$ time to balance out itself inside the neuron. There is a slightly potential gradient along the axis, but it is on the way to steady state. Because of transmitted electrical forces through the dielectric cell membrane, the intracellular potential will not reach equipotential state, a slightly gradient will persist. The membrane voltage V_m next to the electrode is strongly positive now. The membrane voltage is nearly inverse proportional to the extracellular potential. The difference over all segments $\bar{V}_i - \bar{V}_e$ is at every time during the stimulus equal to the resting potential V_r as no ions can enter or leave the cell in passive mode.

7.2.2 Spherical Structure

To analyse differences of a spherical structure, now, a spherical soma was stimulated by an extracellular stimulus. The electrode, electrode pole, and center of the sphere are in line. The diameter of the spherical soma consisting of 100 compartments is assumed to be $d = 20\mu m$ (see figure 7.4). The electrode is placed $15\mu m$ above the electrode pole of the soma in z-direction. The stimulus was chosen to be cathodic $I_{st} = -1\mu A$ for a duration of $1.5ms$, the resistivities are $\rho_e = 5050\Omega \cdot cm$ and $\rho_i = 300\Omega \cdot cm$.

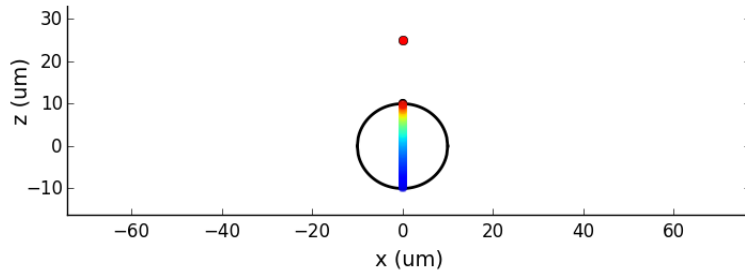


Figure 7.4: Electrode geometry of extracellular stimulation. The electrode is placed $15\mu m$ above the spherical soma. The color gradient on the soma axis depicts the impact strength of the stimulus for each segment.

After the stimulus is applied, the neuronal structure immediately re-sponds on the electric field established by the stimulus. This will not only affect the extracellular but also the intracellular potential. According to the geometry of the stimulation and the cathodic stimulus, a depolarization takes place at the electrode pole (at position 0 of the axis) while the opposite pole is hyperpolarized (position 1 of the axis). Somewhere in the northern hemisphere of the soma, the soma still must be at resting potential V_r . Exactly in the center compartment (position 0.5) the soma is already hyperpolarized (see figure 7.5). In contrast to the cylindrical structure, there is no change in the membrane voltage any more while the stimulus is applied. As the membrane voltage V_m is constant during the stimulation, it seems that the spherical structure is shifting its intracellular potential as a step response to the electric field.

Taking a closer look at the intra- and extracellular potentials during the stimulus (see figure 7.6), it can be seen, that the intracellular potential is already in (nearly) equipotential state at $t = 0.02ms$ after the stimulus. In the extracellular potential V_e the potential drop from electrode pole (segment 0) to the opposite pole is visible, the membrane voltage V_m is inverse proportional to the extracellular potential because of the constant V_i .

As seen in the previous section, the cylindrical structure needed some time to reach steady state after being affected by the electric field of the stimulus. As in the spherical case there must be a time constant for reaching

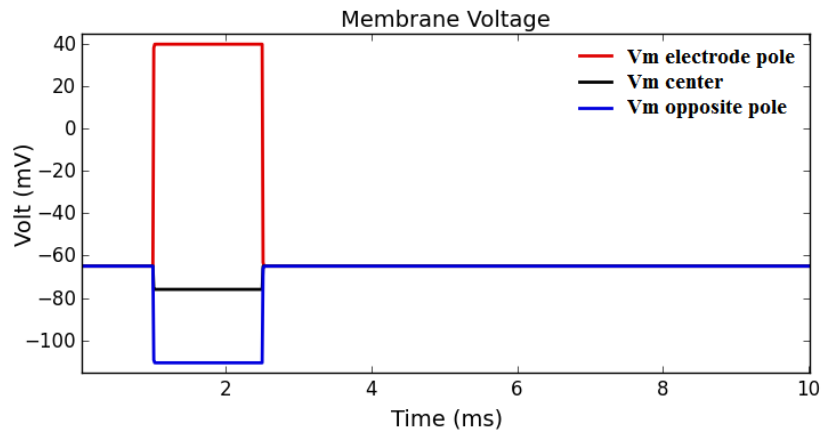


Figure 7.5: The membrane voltage at the electrode pole (red line) shows a very strong depolarized region. At the segment of the sphere's center (black line) there is a slightly hyperpolarized region, while at the pole with largest distance to the electrode the soma is strongly hyperpolarized (blue line). All recorded membrane voltages along the spherical structure show step responses to the electric field and stay constant while the stimulus is applied.

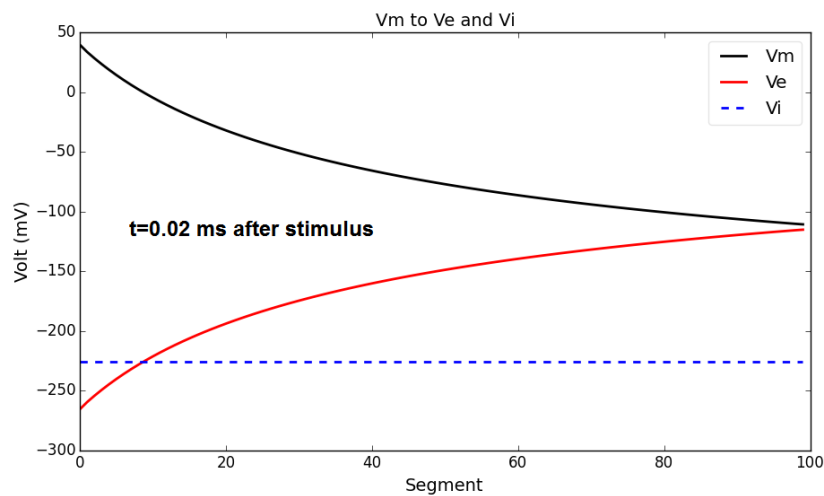


Figure 7.6: Membrane voltage V_m and the intra- and extracellular potentials V_i and V_e during the stimulus over all compartments. The graph shows the stimulated soma 0.02ms after the stimulus was applied. The extracellular potential is constant during the whole stimulus duration. At $t = 0.02$ the intracellular potential is already in almost equipotential state, therefore the neuron has reached its steady state. The mean difference over all segments $\bar{V}_i - \bar{V}_e$ is at every time during the stimulus equal to the resting potential V_r as no ions can enter or leave the cell in passive mode.

steady state too, the temporal resolution of the *Neuron* model was changed from standard $dt = 10\mu s$ to $dt = 0.1\mu s$.

Now, the big picture still looks the same, but when zooming in the μs range, it is clearly seen that also the intracellular potential V_i of the spherical structure is not all the time in its almost equipotential state (see figure 7.7). As for the cylindrical structure, first the V_i is directly affected (shifted) by the electric field. Then, following Gauss's law, the intracellular space is balancing out to reach steady state. In steady state the electric field inside the structure becomes zero. While the cylindrical structure needed approximately $\tau = 3ms$ to reach steady state, the spherical structure is reaching its steady state in a few μs . The reason is found in the perfect symmetry of a sphere. The force field of a single charge is spherical too, so inside a spherical structure there is an optimal force transmission. Further, the spherical space allows maximal movement of charges at shortest possible distances. Additionally, the cross-sectional area is huge compared to a cylinder which affects the resistance inside the structure.

In our model a soma with a diameter of $d = 20\mu m$ and an intracellular resistivity of $\rho_i = 300\Omega \cdot cm$ only requires approximately $\tau \approx 1.5 - 2\mu s$ for intracellular potential to reach its steady state (see figure 7.7 (a)). Doubling the diameter to $d = 40\mu m$ with $\rho_i = 300\Omega \cdot cm$ will lead to $\tau \approx 3 - 4\mu s$. Doubling the intracellular resistivity to $\rho_i = 600\Omega \cdot cm$ with a diameter of $d = 20\mu m$ also resulted $\tau \approx 3 - 4\mu s$ ³⁶.

These results also go conform with a research of Lee and Grill (2005) who modelled and laboratory tested spherical cells for temporal behaviour regarding the time to reach steady state when exposed to an extracellular electric field (see figure 7.8).

³⁶All cases were stimulated with same stimulus amplitude of $I_{st} = 1\mu A$ with an electrode distance of $15\mu m$. Results are not shown in this thesis.

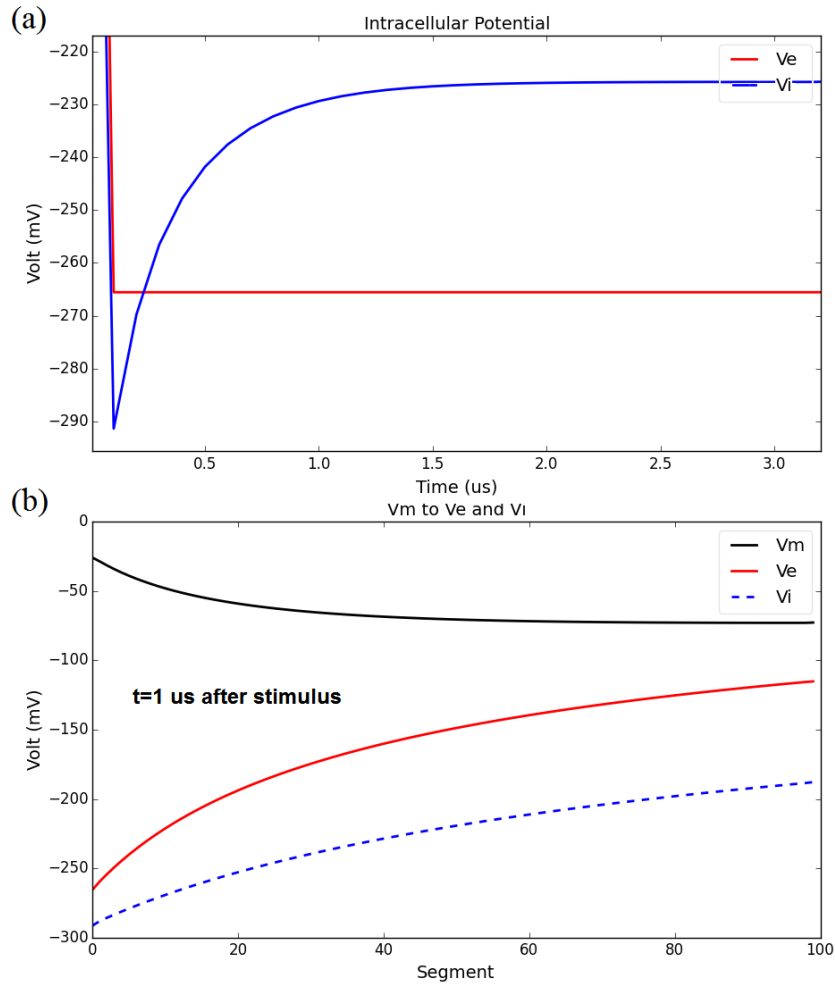


Figure 7.7: Model results with changed temporal resolution ($dt = 0.1\mu s$). The upper graph (a) shows the first $3\mu s$ of the intracellular potential V_i (blue line) and the extracellular potential V_e (red line) at the electrode pole. Here the temporal effects on the potentials induced by the electric field are visible. It takes around $2\mu s$ for the sphere to balance out the intracellular potential V_i and reach steady state. After balancing out the intracellular potential of the sphere is assumed to be equipotential. The lower graph (b) shows the V_i over all compartments at $t = 1\mu s$ after stimulus has started. The intracellular potential nearly has the same shape as the extracellular potential, both are shifted according to the strength of the electric field.

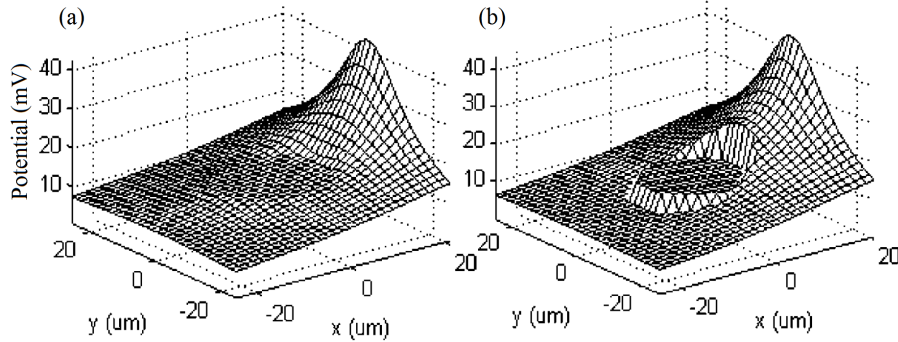


Figure 7.8: Potentials over time for an extracellular stimulation. At the center of the plane $(x, y) = (0, 0)$ a spherical structure with diameter $d = 20\mu m$ is placed. (a) shows the potential in space right after the electric field has been established. At this time, the potential across the membrane has a gradient as the membrane capacitance is not charged yet. The sphere has not reached steady state already. (b) shows the same simulation around $2.4\mu s$ later where the intracellular potential is already in equilibrium. Here, also the almost equipotential state of the intracellular potential of the spherical structure is nicely shown (figures and parts of caption from Lee and Grill (2005)).

7.3 Effects of Ionic Currents

In this section, the influence of ionic currents during the stimulation is investigated. For this reason, the same geometric properties for a cylindrical structure as taken in section 7.2.1 were applied. The cell membrane still got no active mechanisms, but in passive mode some leakage current channels were modelled. The Nernst potential for leakage channels was set to the resting potential $E_L = -65mV = V_r$. This implies ionic currents passing the cell membrane through the ion channels until the equilibrium state of $V_r = -65mV$ is reached. As conductivity $\bar{g}_L = 1mS/cm^2$ was assumed.

The neuron consisting of 1000 compartments is assumed to have a length of $l = 1000\mu m$ and a constant diameter of $d = 2\mu m$ (see figure 7.1). The electrode is placed $15\mu m$ above the neuron in z -direction. The stimulus was chosen to be cathodic $I_{st} = 1\mu A$ for a duration of $1.5ms$, the resistivities are $\rho_e = 5050\Omega \cdot cm$ and $\rho_i = 300\Omega \cdot cm$.

As the Nernst potential was chosen to be at resting potential of $V_r = -65mV$ the neuronal structure will be in steady state before a stimulus is applied. Once the electric field will establish de- and hyperpolarized regions along the cylindrical structure, also ionic transmembrane leakage current will flow. The leakage current tries to bring the cell back to its resting potential $V_r = E_L$. Segments actually having a membrane voltage V_m above the Nernst potential E_R will produce an ionic current which lowers the membrane voltage. Regions having a V_m below E_R are exposed to leakage

current which raises the membrane voltage. In figure 7.9 the solid lines show the membrane voltage V_m influenced by ionic leakage current compared to the case without any leakage channels (dotted lines). Because of the leakage currents, the whole cell structure is much faster in steady state again after the stimulus. In section 7.2.1 the time constant τ to balance the intracellular potential was given with $\tau > 3ms$ for a passive model. In figure 7.9 the cell also requires more than $3ms$ to come back to resting state after the stimulus ends (dotted lines). Having leakage channels, the cell is back in resting state after approximate $\tau \approx 1.5ms$ as the membrane voltage was already driven back to resting potential before the stimulus ended (solid lines).

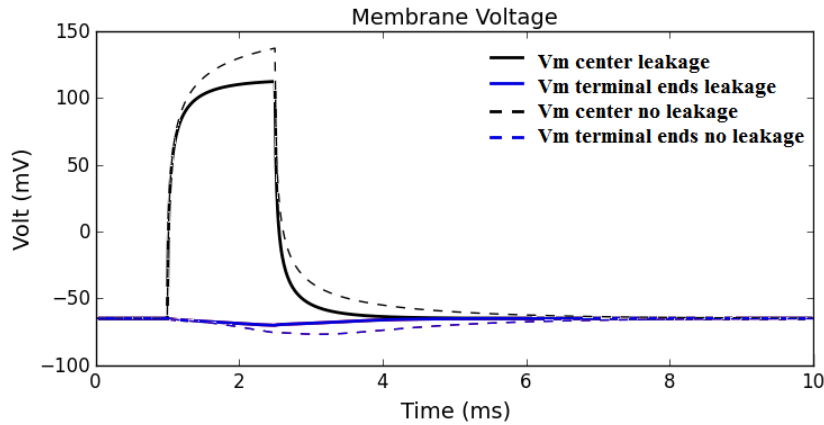


Figure 7.9: The membrane voltage at the center of the neuron (black line) shows a very strong depolarization. After an immediate peak after the stimulus has started, the membrane voltage is still increasing during the whole stimulus duration. The membrane voltages at the terminal ends of the neuron (blue line, V_m identical at left and right terminal ends) show slightly hyperpolarized regions. The solid lines show the influence of a leakage channel where any voltage above the Nernst potential of $E_L = -65mV$ is lowered by ionic transmembrane current flow and any voltage below E_L is raised. The dotted lines show the case of a passive membrane without any leakage channels as described in section 7.2.1 for the same geometry.

Note, in case of a spherical structure, the leakage current as set here would not make any difference in the results. As the Nernst potential E_L was assumed to be equal to resting potential $V_r = E_L$, the ionic transmembrane leakage currents are working against any voltage deviations to resting potential during the stimulus. But, as we learnt, the difference between mean intracellular potential and mean extracellular potential over the whole structure is also equal to the resting potential ($\bar{V}_i - \bar{V}_e = V_r$). So, any change in any compartment because of leakage current is immediately balanced out by the intracellular forces which establish an inner electric field of zero. As the time constant for a sphere is in the μs range (see section

7.2.2) no ionic leakage current effects are seriously changing the intracellular potential. Therefore, the intracellular forces keeping the equipotential state inside a spherical structure upright will overrule the effects of transmembrane ionic currents to the intracellular potential V_i and therefore also to the membrane voltage V_m .

Thinking about a mathematical model having active cell membrane behaviour, it is obvious that the sum of all ionic currents including leakage current must be in balance at resting state³⁷.

7.4 Stimulation Window Spherical Soma

For investigated the stimulation window of a spherical structure, the not very realistic case of a spherical soma without any other sections was assumed. An cathodic electrode was placed right next to the soma. For finding the stimulation window parameters the distance and amplitude of the stimulus were increased stepwise. The considered range for current amplitude was between $I_{st} = -1\mu A$ and $I_{st} = -150\mu A$. The range until $-10\mu A$ was analysed in $\Delta I_{st} = 1\mu A$ steps, for currents between $I_{st} = -10\mu A$ and $I_{st} = -150\mu A$ the step width was set to $\Delta I_{st} = 10\mu A$. The start position for the electrode was right next to the soma outer shell. The position of electrode z_{el} was increased in z -direction by $\Delta z_{el} = 1\mu m$ until the lower limit was reached (see figure 7.10).

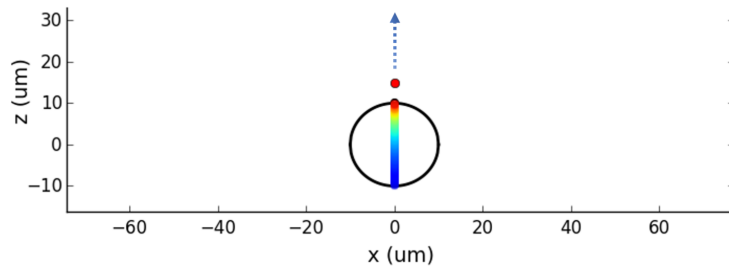


Figure 7.10: Geometry of extracellular stimulation. The electrode is placed near the electrode pole of a spherical soma and then moved in z -direction away of the soma.

Each combination of electrode distance and stimulus current amplitude was analysed regarding the generation of an action potential. The limits

³⁷This implies that the resting potential V_r for a mathematical cell membrane model is given at the voltage where all currents are cancelling out each other $\sum I_{ionic} = 0$. Besides the Nernst potentials and respective conductivities, also the gating variables influence the resting potential V_r . In resting state, the channels are normally not 100% closed. So, some transmembrane ionic current is also flowing when the cell is in resting state. The gating itself therefore also determines the amount of current flow.

were defined as:

- **Upper limit:** The smallest distance between the electrode and the soma electrode pole for a certain stimulus amplitude where an action potential was generated. Below this limit, no generated action potential was detected.
- **Lower limit:** The largest distance which just caused the firing of the soma. Above the limit, the stimulus strength is too weak to produce an action potential.

Each test case was automatically analysed for fired action potentials as described in section 6.10. It must be clearly said, that near the lower and upper limits for extracellular stimulation, there are cases where it is hard to distinguish if an action potential was generated or not. There is no general accepted definition for determining an action potential. All these questionable cases are characterized by having a very low maximum membrane voltage V_m ³⁸. Because of the intracellular resistivity, it is unclear if an action potential at such a low magnitude could possibly propagate. However, because the same rules for detection were applied for every single test case, it is assumed that possible misjudges should not have that high influence in the results as is a systematic error which only might shift the data a bit.

7.4.1 Geometric Relations Analysis

First, the stimulation windows for spherical neuronal structures having a diameter of $20\mu m$ and $40\mu m$ were determined by using Hodgkin-Huxley and Fohlmeister model mechanism. The results (see figure 7.11) show nearly identical stimulation windows for same diameters. In case the diameter is increased, also the range where stimulation is generating an action potential increases, but also the blocking area below the upper limit is larger for increased soma diameters.

Next, the correlation between amplitude I and the shortest distance D between electrode and cell in relation to the soma diameter d was investigated (current-distance relation, see section 2.5). After several linear regressions, it was clear there is a correlation which follows a polynomial function of second order for the stimulus amplitude:

$$y = a \cdot x^2 + b \rightarrow I_{approx,d}(D_d) = a \cdot D_d^2 + b \quad (7.1)$$

or, formulating it for the electrode distance, the current-distance relationship is approximated by a root function:

$$y = e \cdot \sqrt{x} + f, \{x|x > 0\} \rightarrow D_{approx,d}(I) = e \cdot \sqrt{abs(I)} + f \quad (7.2)$$

³⁸One condition for automatic action potential detection in this model is $max(V_m) > 8mV$. If this value is not exceeded at some time, a test case is marked as 'no action potential was generated'.

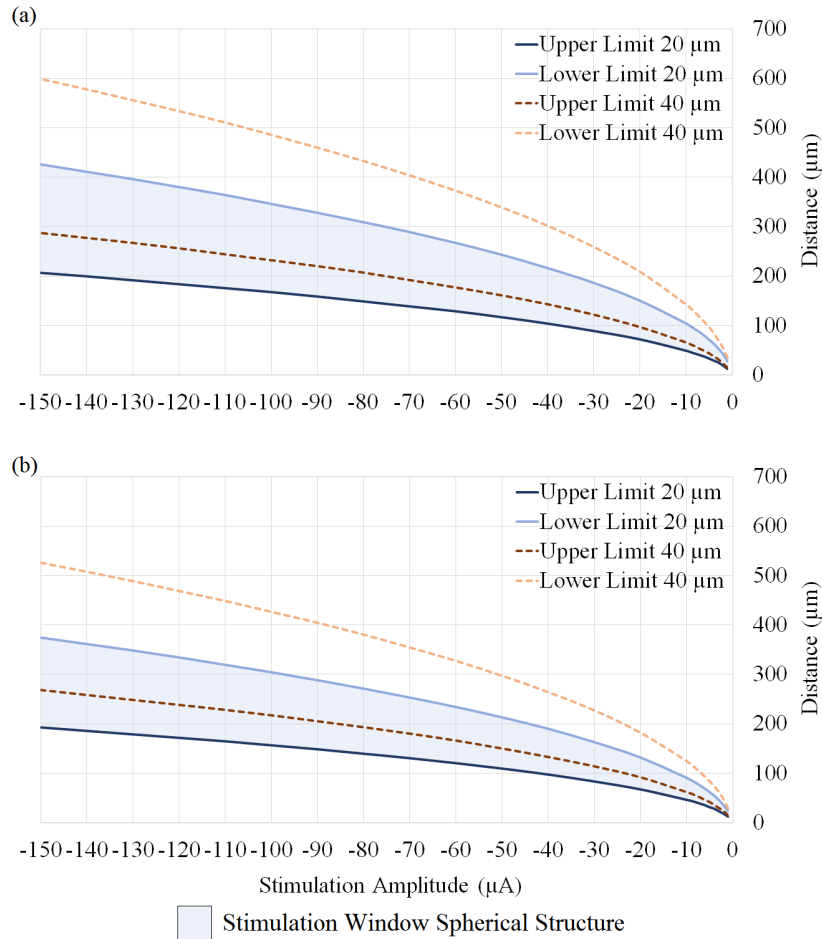


Figure 7.11: Upper and lower limits of a spherical soma stimulated extracellularly with a duration of $0.2ms$. The active membrane was modelled by a Hodgkin-Huxley model in (a), by a Fohlmeister model in (b). The x-axis represents the current amplitude applied reaching from $-1\mu A$ to $-150\mu A$. The y-axis is the distance from electrode to outer shell of the soma (distance electrode to electrode pole) in μm . The blue lines show the results for a soma having a diameter of $d = 20\mu m$. The resulting blue area indicates which configurations of stimulation amplitude and distance to soma (current-distance relation) generate an action potential. It describes the stimulation window for a soma diameter of $d = 20\mu m$. For comparison, the orange lines show the limits for the exact same conditions, but having a soma diameter of $d = 40\mu m$. Comparing (a) Hodgkin-Huxley model with (b) Fohlmeister model it is obvious that the Fohlmeister model stimulus window is slightly shifted down compared to the Hodgkin-Huxley model. So, the Fohlmeister model can be stimulated with higher strength but also stops earlier in firing action potentials at weak strengths.

where D is the electrode distance to the soma outer shell, I the corresponding stimulus current amplitude, and a, b, e, f are approximation coefficients which depend on the model, the diameter d of the soma, and the limit someone is interested in (upper or lower limit). The resulting approximations of the limit $I_{approx,d}$ or $D_{approx,d}$ are valid for a certain diameter d of the soma (see figure 7.12 and 7.13).

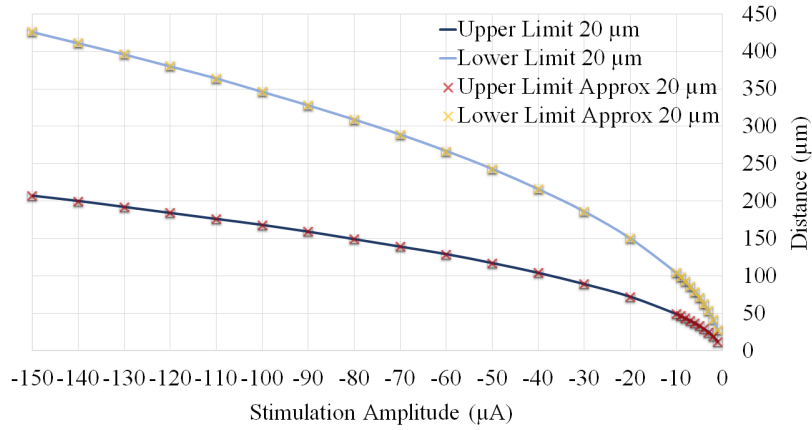


Figure 7.12: Stimulation window and its approximation of a spherical soma with $d = 20\mu m$ stimulated extracellular with a duration of $0.2ms$ and Hodgkin-Huxley model mechanism. The approximations for both limits were done in the form of equation 7.2.

Further, there is a relationship between the stimulation window and the diameter of the soma. If for a certain diameter d_0 the approximation coefficients are known, the corresponding curves can also be calculated for different diameters of the soma: double diameter stimulated with double current amplitude will lead to double distance:

$$I_{approx,d} = \frac{d}{d_0} \cdot I_{approx,d_0} \left(\frac{d_0}{d} \cdot D_d \right) \quad (7.3)$$

$$D_{approx,d} = \frac{d}{d_0} \cdot D_{approx,d_0} \left(\frac{d_0}{d} \cdot I \right) \quad (7.4)$$

Up to now, all test procedures were performed with a constant stimulation duration of $0.2ms$ with a focus on the current-distance relation. The second important factor determining the stimulation window is the strength-duration relation (see also section 2.5). For this reason, already performed test procedures as presented here, also were carried out by modified stimulation durations (see figure 7.14).

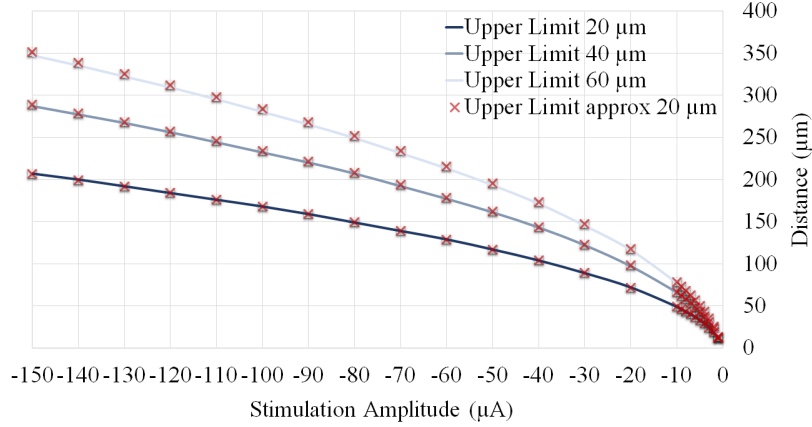


Figure 7.13: Upper limits of a spherical soma with diameters from $d = 20\mu m$ to $d = 60\mu m$ stimulated extracellularly with a duration of $0.2ms$ and Hodgkin-Huxley model mechanism. The approximation was calculated for diameter $d_0 = 20\mu m$ with equation 7.2. For diameter $d = 40\mu m$ and $d = 60\mu m$ the approximation for $d_0 = 20\mu m$ were rescaled by equation 7.4.

In general, a short stimulus duration allows the generation of action potentials for closer electrode positions. But when choosing too short durations, the stimulus might not last long enough to start the active mechanisms of the ion channels. The ion channels have delay times which need to be overcome either by enough current amplitude or by a long enough duration.

In contrast long stimulus durations, here the ion channels might already be closed again (or set to *inactive*) when the stimulus ends. In this case, the stimulation window also will cover only a small range of possible configurations which initiate action potentials.

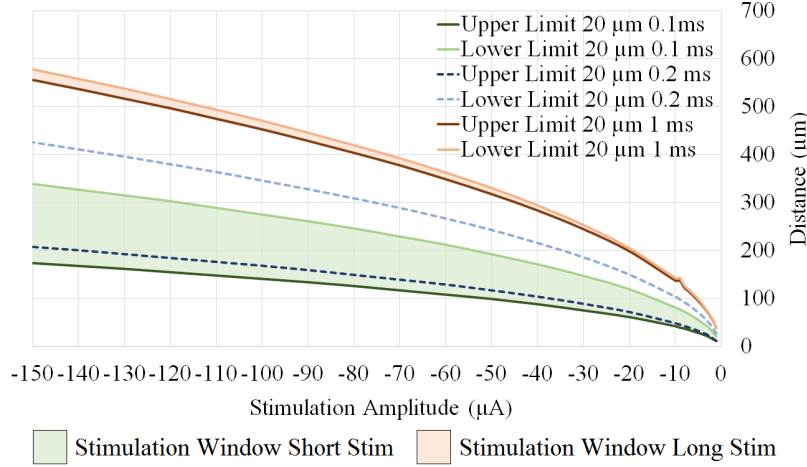


Figure 7.14: Upper and lower limits of a spherical soma with diameter $d = 20\mu\text{m}$ stimulated extracellularly. The active membrane was modelled by the Hodgkin-Huxley model. The durations of stimulation varied. Compared to the 0.2ms stimulus, the shorter 0.1ms stimulus results in a tighter stimulation window. An 1ms stimulus duration will result in an even much tighter stimulation window. At higher strength, the ion channels are already closed again when the stimulus ends. They are only kept in an *open* and *active* state just before reaching the lower limit. The possible configurations to initiate are only very limited.

7.4.2 Sodium Current Reversal

In a next analysis, the upper limits were investigated regarding current flow of Na^+ ions during the stimulus. The Nernst potential for sodium is $E_{\text{Na}} = 50\text{mV}$ for Hodgkin-Huxley model and $E_{\text{Na}} = 35\text{mV}$ for Fohlmeister model. This means, only if the membrane voltage V_m exceeds the Nernst potential E_{Na} at some local regions, the Na^+ current reverses (outflux of Na^+ ions) at these particular regions. This reversal will slightly repolarize the local region, so a Na^+ current reversal works against the stimulus. However, as we already know about the almost equipotential state inside a sphere, any change in intracellular potential will be distributed throughout the total volume within microseconds.

Figure 7.15 shows the stimulation windows of a spherical structure modelled by the Hodgkin-Huxley model and the Fohlmeister model. Additionally, the zones inside the stimulation windows were marked, where a Na^+ current reversal happened. A Na^+ current reversal is specified here as any Na^+ ion outflux flow which happens while the stimulus was applied. This

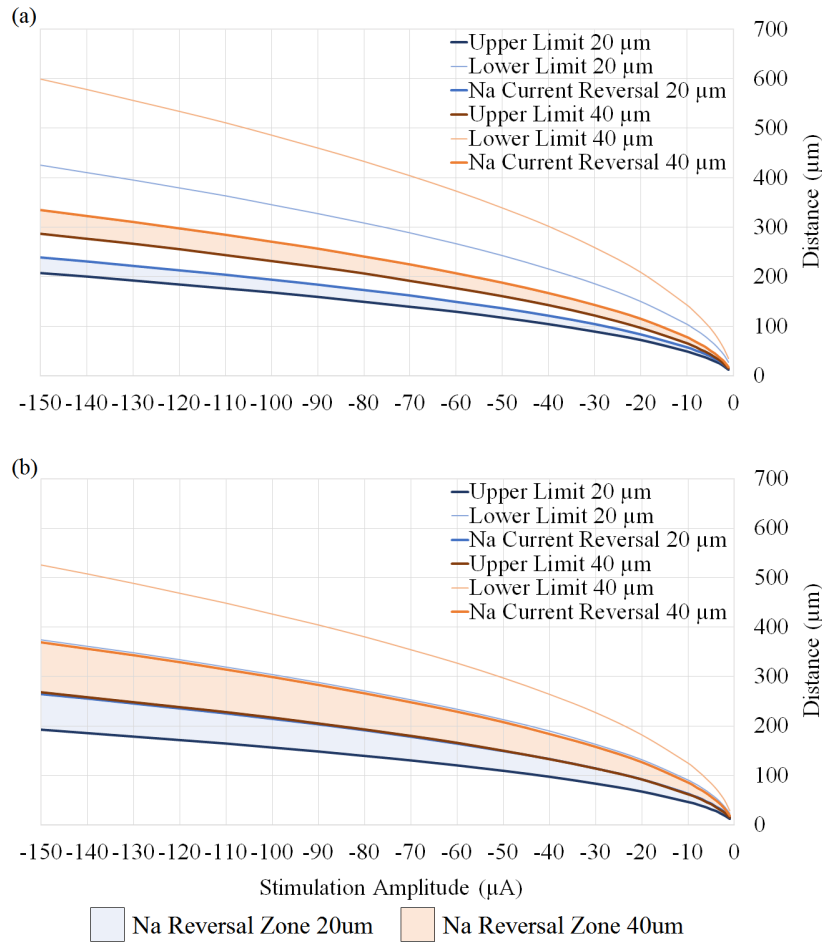


Figure 7.15: Upper and lower limits and zones of Na^+ current reversal of a spherical soma stimulated extracellular with a duration of 0.2ms . The active membrane was modelled by a Hodgkin-Huxley model in (a), by a Fohlmeister model in (b). The blue lines show the results for a soma having a diameter of $d = 20\mu\text{m}$ while the orange ones show limits for soma diameter of $d = 40\mu\text{m}$. The coloured areas (blue and orange) show zones within the stimulation window where action potentials were generated even though Na^+ current reversal occurred while the stimulus was applied. The shape of the current reversal limits follows the same paradigms as the upper or lower limit. The size of these areas seems to be constant, about 15% of the total stimulation window for Hodgkin-Huxley model and approximate 39% for Fohlmeister model.

means that at least at the compartment at the electrode pole³⁹ the membrane voltage V_m exceeded the Na^+ Nernst potential E_{Na} while the corresponding Na^+ ion channels were in *open* and *active* state.

When investigating the border/limit of the Na^+ current reversal region, it can be seen by the trend follows the same paradigms as the curves for upper and lower limits. Therefore, this limit could also be approximated by a polynomial function of second order (or a root function) as done for upper and lower limit. However, our interest was more focused on the portion of these zones within the stimulation window. So, for all recorded test cases, the percentage of the region within the stimulation window was determined:

$$NaReversalPerc = \frac{Na\ Reversal\ Area}{Total\ Area} \times 100 \quad (7.5)$$

Table 7.1 shows the determined proportions determined by considering extracellular stimulation current amplitudes between $-10\mu A$ and $-150\mu A$ (step width $-10\mu A$)⁴⁰. For the Hodgkin-Huxley model the soma diameters were $20\mu m$, $40\mu m$, and $60\mu m$. For the Fohlmeister model the simulated soma diameters were $20\mu m$ and $40\mu m$.

Model	NaReversalPerc	σ^2	σ_{mean}
Hodgkin-Huxley model	$15.27 \pm 0.06\%$	0.19%	0.34%
Fohlmeister model	$39.06 \pm 0.08\%$	0.20%	0.33%

Table 7.1: Determined percentages of areas within the stimulation window where a Na^+ current reversal occurred during cathodic stimulation. Additionally the variance and mean standarddeviation of the sample is given.

The determined percentages $NaReversalPerc_{HH} \approx 15\%$ for the Hodgkin-Huxley model and $NaReversalPerc_{FM} \approx 39\%$ for the Fohlmeister model should be investigated in detail. According to these results, the possible configurations to archive the generation of an action potential as given by the stimulation window also include many configurations which are causing a Na^+ current reversal at least at regions near to the electrode during stimulation.

³⁹Any Na^+ current reversal definitely occurs at the electrode pole which is the most depolarized region during cathodic stimulation. The Na^+ ion outflux at other compartments depends on the gradient of membrane voltage V_m along the axis of the soma.

⁴⁰The reason for not considering current amplitudes below $10\mu A$ is the little resolution in spatial data in this range. Step width for the electrode distance is always $\Delta z = 1\mu m$. For a soma stimulated with $I_{st} = -1\mu A$ and a diameter of $d = 20\mu m$ the distance between upper and lower limit is only $15\mu m$ (Hodgkin-Huxley model). Calculating any percentage within this resolution will not result in exact data. Still, also in the regions below $-10\mu A$, the calculated percentages are near to the total percentages calculated with data of higher stimulus amplitude.

Further it seems that the Na^+ current reversal limit is proportionally related to the stimulation upper limit. Further, the area within the stimulation window seems to be constant and independent of the soma diameter. Now we know, that the region around the upper limit is susceptible for providing some uncertainties regarding action potential detection. The detection of Na^+ current reversal itself is independent of the action potential detection. But when relating the limit for Na^+ current reversal only to lower limit which is not that endangered to contain uncertain information about action potentials, the results also show a proportional relationship and only a small variance.

Finally, some thoughts about the Na^+ current reversal. The detection of a Na^+ current reversal also includes scenarios where the membrane voltage V_m exceeded the sodium Nernst potential only slightly. Therefore, just a very limited amount of Na^+ ions could pass the cell membrane. But, there are also cases where these currents developed an ion flow of serious magnitude out of the cell. As shown in previous investigations in this thesis, there is more or less an equipotential state inside the spherical cell. Therefore, any local changes in potential because of ion currents are distributed over the full spherical volume within a short period of time in the μs range. Further, only because there is an outflux of Na^+ ions at the electrode pole, it does not mean there is a total Na^+ ion outflux during the stimulus. A sphere always has depolarized and hyperpolarized regions during the extracellular stimulus. If there is an outflux of Na^+ ions in the region around the electrode pole because V_m exceeded E_{Na} , there must be somewhere else regions where $V_m < E_{Na}$ and the Na^+ ion channels are open. At these regions there will be a Na^+ ion influx, the portion between in- and outflux regions depends on the gradient of extracellular potential V_e along the surface of the spherical cell.

So, in another analysis, the net current caused by transmembrane Na^+ ion movements during the stimulus was evaluated over the total volume of the sphere. The net transmembrane sodium current then was related to the upper limit and the Na^+ current reversal limit. Here, no distinct results were archived. For Hodgkin-Huxley model active mechanisms not a single current-distance relation for a stimulation duration of $0.2ms$ was found where an action potential was generated even though a net Na^+ ion outflux occurred during the stimulus. In contrast to the Fohlmeister model where a net Na^+ ion outflux during the stimulus did not necessarily prevent the initiation of an action potential (see figure 7.16).

While it is not surprising, that the limit for Na^+ ion outflux is near the upper limit, the huge differences between the Hodgkin-Huxley model and Fohlmeister model were not expected. In the Fohlmeister model, the upper limit and Na^+ net current outflux limit are nearly identical. Further, in Fohlmeister model the Na^+ outflux limit lies within the stimulation window, this means, there was an action potential created event though there was a

net outflux of Na^+ ions during the stimulus. In total contrast the Hodgkin-Huxley model: Here the Na^+ net current outflux limit clearly lies outside the stimulation window.

However, to give final judgements on the Na^+ current reversal flow and its contribution to active cell membrane dynamics, further evaluations are necessary. The limits for net Na^+ outflux and upper limit are very close together in the Fohlmeister model. But, the gatings which determine the upper limit are not based on pure physics but on probabilities. We believe these results are worth to be investigated in detail, but it is out of the scope of this thesis.

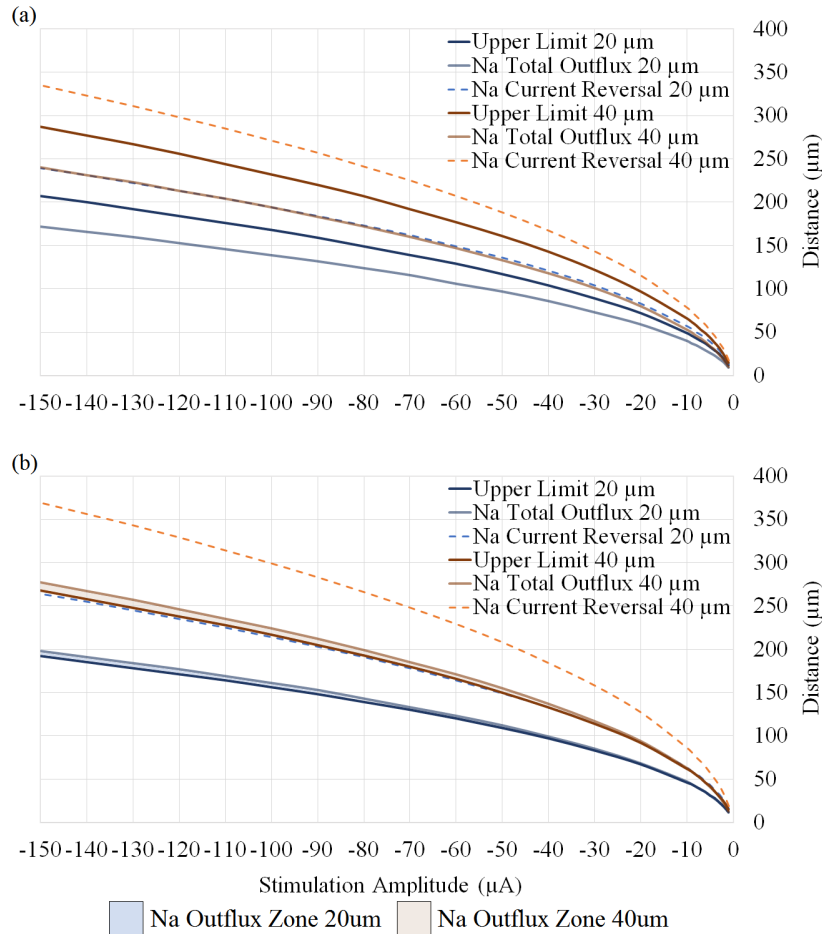


Figure 7.16: Upper limit, Na^+ ion net outflux zones within the stimulation window, and limits of Na^+ current reversal of a spherical soma stimulated extracellularly with a duration of $0.2ms$. The active membrane was modelled by a Hodgkin-Huxley model in (a), by a Fohlmeister model in (b). In the Hodgkin-Huxley model no Na^+ current net outflux was found within the stimulation windows. In contrast the Fohlmeister model, here configurations were found where a net outflux of Na^+ ions during the stimulus lowered the intracellular potential but the action potential was still initiated. These zones are very close to the upper limit.

7.5 Stimulation Window Retinal Ganglion Cell

In this last section, the extracellular stimulation of a retinal ganglion cell is simulated with a Fohlmeister model. As the dendrites are assumed to have only minor or even no effects on the results, they were not considered to decrease computational costs⁴¹. A cathodic electrode was placed right next to the soma. For finding the stimulation window parameters the distance and amplitude of the stimulus were increased stepwise. The considered range for current amplitude was between $I_{st} = -1\mu A$ and $I_{st} = -150\mu A$. The range until $I_{st} = -10\mu A$ was analysed in $\Delta I_{st} = -1\mu A$ steps, for currents between $I_{st} = -10\mu A$ and $I_{st} = -150\mu A$ the step width was set to $\Delta I_{st} = -10\mu A$. The start position for the electrode was right next to the soma outer surface. The position was changed by $\Delta z_{el} = 1\mu m$ in z-direction or $\Delta z_{el} = -1\mu m$ in x-direction until the lower limit was reached.

7.5.1 Electrode above Soma

First, the same electrode setup as in the previous section 7.4 was chosen for investigation. The electrode was placed above the soma and the electrode distance was increased in z-direction (see figure 7.17 (a)). Two different diameter of the soma were used, $d = 20\mu m$ and $d = 40\mu m$. At $d = 40\mu m$ the electrode pole is slightly above the axis of the soma in z-direction, at $d = 20\mu m$ the electrode is remarkable below the axon axis.

When analysing the results (see figure 7.17), for both cases an increased stimulation window can be spotted compared to a spherical soma only. At lower cathodic amplitudes (until approximately $I_{st} = -10\mu A$ for $d = 20\mu m$, $I_{st} = -30\mu A$ for $d = 40\mu m$) the retinal ganglion cell limits are more or less equal the the sphere limits itself, but at higher amplitudes there are remarkable differences. In case of a diameter of $d = 20\mu m$ significant more configurations will lead to an action potential, upper and lower limit are both rescaled accordingly. The greater range of stimulation can be easily explained by the shorter distance between electrode and axon regions⁴² compared to the soma regions. The axon (and here especially the proximal sodium channel band) is almost $7.5\mu m$ nearer (in z-direction for larger electrode distances) to the electrode than the electrode pole of the soma. Further, the sodium channel band is the most excitable region of the retinal ganglion cell in this model.

In case of $d = 40\mu m$ the lower limit for the retinal ganglion cell is almost the same as the one of soma only. Here the electrode pole and the sodium channel band axis nearly have the same z-coordinate. Totally different is the situation at the upper limit. The Na^+ ion channel conductivity \bar{g}_{Na} of

⁴¹This assumption is based on several comparisons done for different configurations in the model. However, it was not systematically investigated.

⁴²All electrode distances analysed here are related to the soma outer surface.

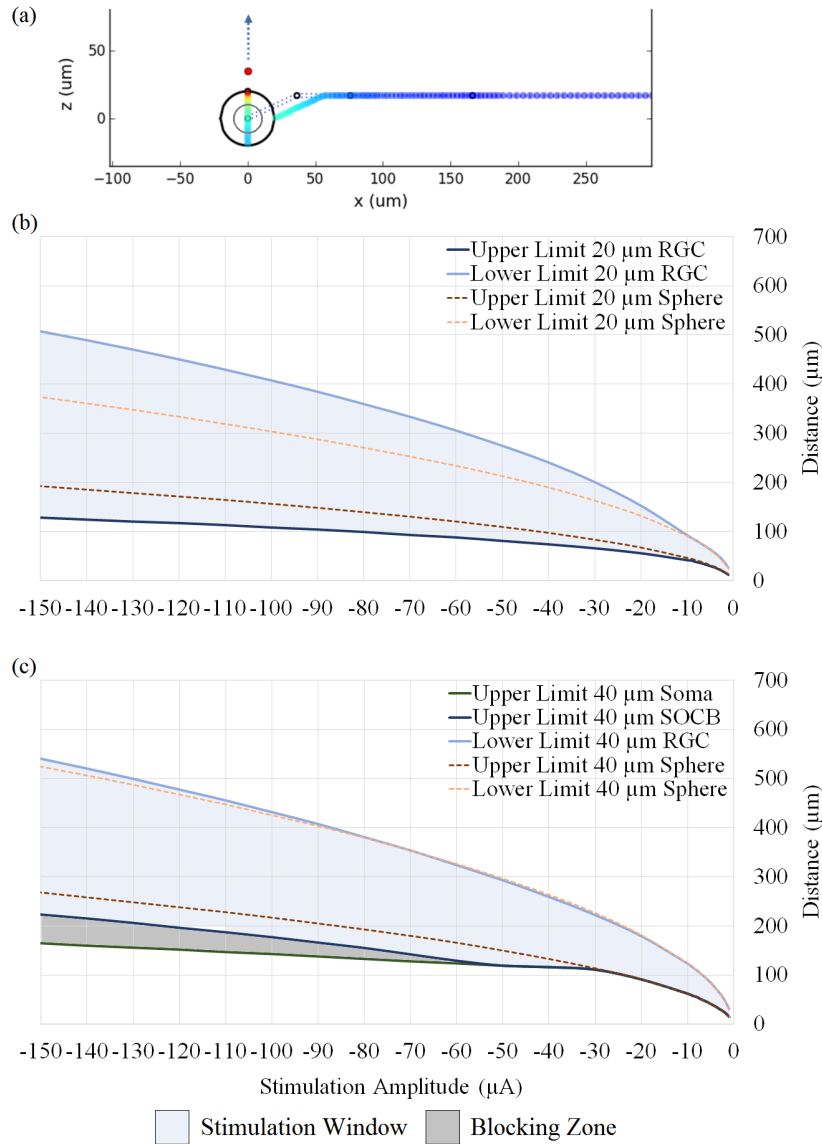


Figure 7.17: Upper and lower limits of a retinal ganglion cell (without dendrites) stimulated extracellularly with a duration of $0.2ms$. The electrode geometry with an electrode moved in z -direction away of the soma is shown in (a). The active membrane was modelled by a Fohlmeister model. The diameter of the soma is $d = 20\mu m$ in (b) and $d = 40\mu m$ in (c). The blue areas show the stimulation windows for the retinal ganglion cell while the orange dotted lines show the upper and lower limits for a soma only. At (c) the green line additionally shows an evaluation of the upper limit for the soma section of the retinal ganglion cell. In the soma blocking area (gray) action potentials were detected in the sodium channel band (SOCB) and thin section (TS) of the axon, but there were no action potentials detected in the soma itself.

the sodium channel band is 5 times higher than the \bar{g}_{Na} of the soma. At a stimulus amplitude of around $I_{st} = -30\mu A$, it can be clearly seen that the upper limit start to take a total different course than the limit for the spherical soma only. It seems like the axon section gets dominant in generating action potentials. For higher cathodic stimulation amplitudes starting with around $-50\mu A$ there is an additional limit. The gray zone in figure 7.17 shows configurations within the stimulation window of the retinal ganglion cell where no action potential was detected in the soma itself. It seems that there is an *Anodal Surround Block* preventing the propagation of the action potential back to the soma. Also a *Stimulation Upper Threshold* is thinkable, the soma is blocked because of the high stimulation strength and the strong hyperpolarization within the structure prevents a back-propagation of the action potential. Further, a combination of both blocking phenomena might be thinkable too. As there are still many uncertainties regarding the consequences of the Na^+ current reversal, no further analysis was done in this thesis.

In general, it must be said, that mostly all action potentials at higher amplitudes are not initiated in the soma firstly. Instead, the sodium channel band will mainly generate action potential which are propagating along the axon but also back into the soma.

7.5.2 Electrode above Axon Hillock

For the next test procedure, the configurations of the previous section were overtaken. The only difference is that the electrode is placed exactly between the soma and the sodium channel band. Therefore, the electrode was shifted in x-direction by around $\Delta x_{el} \approx 18\mu m + r_{soma}$ (see figure 7.18 (a)). As the electrode is exactly above the center of the axon hillock, the distances to soma and sodium channel band should be more or less identical. That means, that the nearest segments to the electrode of these sections are always exposed to almost the same stimulation strength. It is clearly expected, that the stimulation window is extended by this slightly shift of the electrode towards the axon.

Figure 7.18 shows the clearly increased stimulation windows for both soma diameters $d = 20\mu m$ and $d = 40\mu m$. In all test cases, the sodium channel band is the section which initiated the action potentials first. Further, there are *Anodal Surround Blocks* near the upper limit of the sodium channel band in both directions, soma direction and distal axon direction (gray areas in figure 7.18). At high stimulation currents, it can also be clearly seen that at certain stimulation strengths near the upper limit of the retinal ganglion cell the soma keeps blocking while the action potential already propagates along the axon. Here again, an *Anodal Surround Block*, a *Stimulation Upper Threshold*, or a combination of both phenomena are thinkable to prevent the action potential in the soma.

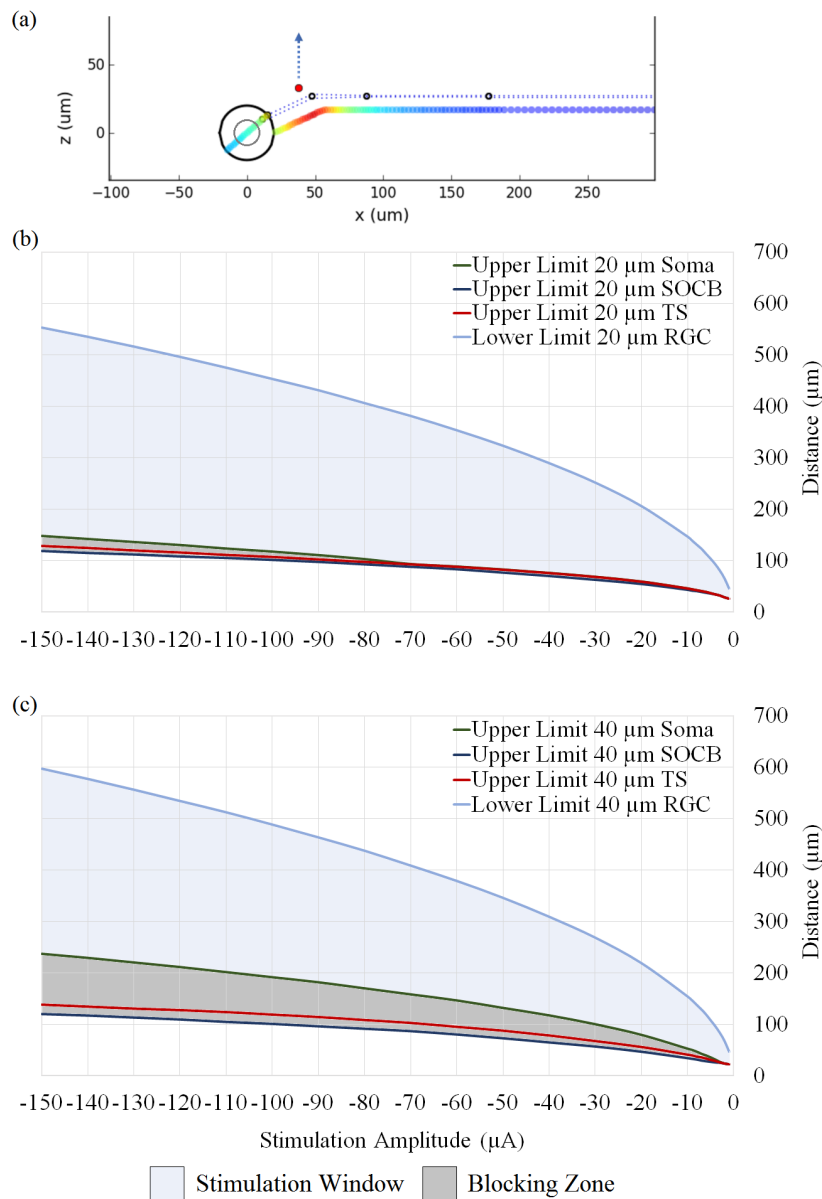


Figure 7.18: Upper and lower limits of a retinal ganglion cell (without dendrites) stimulated extracellularly with a duration of 0.2ms . The electrode geometry with an electrode moved in z -direction away of the axon hillock is shown in (a). The active membrane was modelled by a Fohlmeister model. The diameter of the soma is $d = 20\mu\text{m}$ in (b), $d = 40\mu\text{m}$ in (c). The blue areas show stimulation windows for the retinal ganglion cell where action potentials were detected in all sections. Besides the upper limit of the sodium channel band (SOCB), also the upper limit for the soma and the thin section (TS) are shown. The gray blocking areas indicate that action potentials were detected in the sodium channel band but not in the soma and/or thin section of the axon. The lower limit is identical for all sections.

7.5.3 Electrode lateral to Soma

In a last test, the electrode was placed next to the western pole of the soma and moved away of the soma in x-direction (see figure 7.19 (a)). In this arrangement, the soma is always nearer to the electrode than any axon section. However, it must be mentioned again, that no effects of the neuronal structures to the electric field itself were modelled. In reality, this configuration would cause disturbances to the electric field the axon is exposed to, as the soma is placed just between the electrode and the axon.

In figure 7.19 the results for a soma diameter of $d = 20\mu m$ and $d = 40\mu m$ are shown. The stimulation window is much larger compared to a spherical structure only. Also here the reason is found in the high conductivity \bar{g}_{Na} of the Na^+ ion channels in the sodium channel band. The upper limits are more or less identical, but the structure can be stimulated with weaker strengths compared to a sphere only and still will generate action potentials in distal axon sections. This results in an extended lower limit, especially for $d = 40\mu m$ the stimulation window has increased dramatically. The increased stimulation windows confirm our general hypothesis that a sphere is harder to stimulate than cylindrical structures.

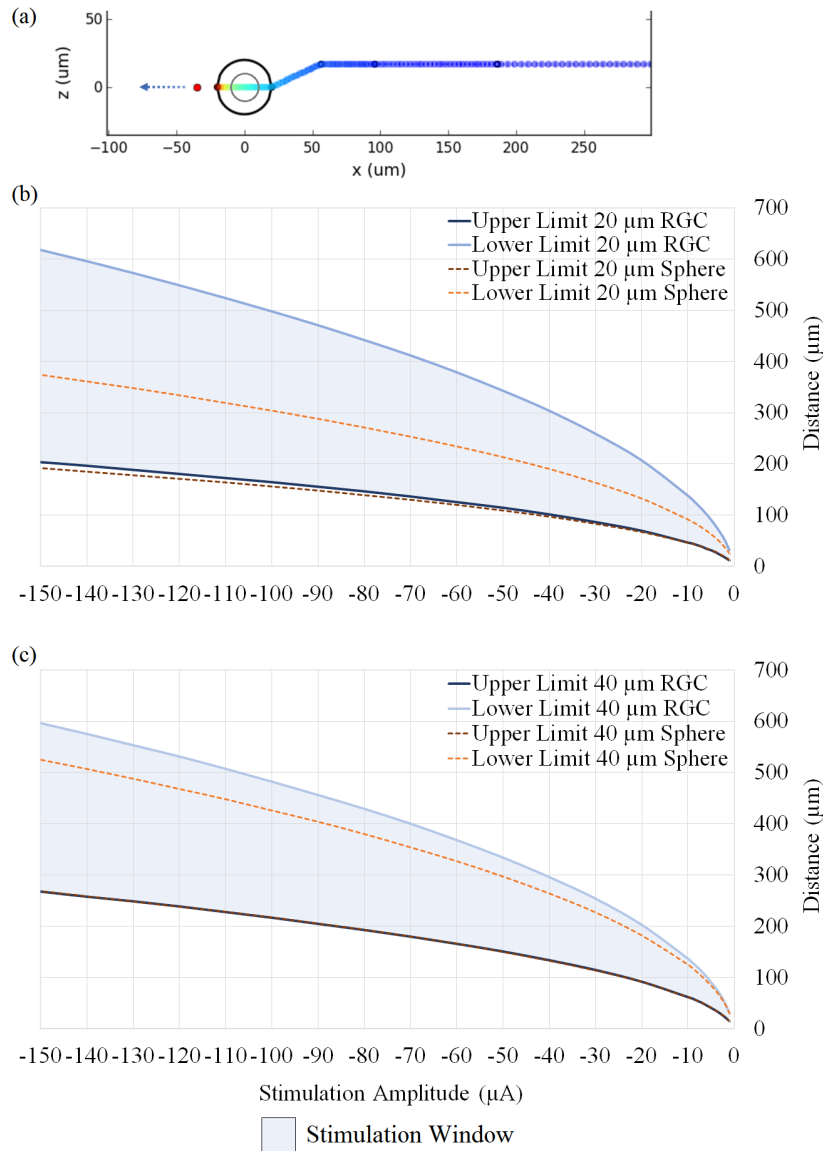


Figure 7.19: Upper and lower limits of a retinal ganglion cell (without dendrites) stimulated extracellularly with a duration of 0.2ms . The electrode geometry with an electrode moved in x-direction away of the soma is shown in (a). The active membrane was modelled by a Fohlmeister model. The diameter of the soma is $d = 20\mu\text{m}$ in (b), $d = 40\mu\text{m}$ in (c). The blue areas show stimulation windows for the retinal ganglion cell while the orange dotted lines show the upper and lower limit for a soma only. While the upper limit of the retinal ganglion cell is nearly identical to a spherical structure only, the total range of possible configurations for a successful stimulation is increased. The lower limit indicates that for this electrode geometry also much weaker stimulus strengths will produce propagating action potentials.

Chapter 8

Discussions

*“Each one of these cells
is as complicated as a city”*
- David Eagleman

Here, first analyses based on common and widely accepted mathematical models were performed. But it is always important to keep in mind that these models are mathematical descriptions of cellular behaviours as observed in experiments and are partly based on probabilities. Capacitive currents, current flows inside electrolytic solutions, diffusion forces, and electrical forces are studied for a long period of time and the physics are well known. But the dynamics of ion channels are extremely complex, everything takes place at a molecular level within macro-molecular complexes. Direct measurements are often technically not possible at all or are based again on probabilities. While our mathematical model gives us a good indication of the stimulation window of a retinal ganglion cell, experiments on real retinal ganglion cells are necessary to confirm and verify our results.

8.1 Summary

The provided results here only give a general overview of the blocking phenomena of an extracellular stimulated neuronal cell. The created retinal ganglion cell model in *Neuron* with its user interface and the possibilities in performing systematic test procedures allows very detailed investigations for varying test conditions. Further, the dynamics are presented in a good way to develop a good understanding of what is going on at different times and in different sections of a neuron.

However, the topic is complex and so is the generated data. The presented results are just covering some general aspects about blocking phenomena in extracellular stimulation. But to gather information, every systematic test procedure consisted of several 10000 simulations runs. Even

though the level of automated data analysis is high, still a lot of manual work is required to bring the results of all test cases and test procedures together for evaluation and analysis.

We investigated the behaviour of spherical neuronal structures during the extracellular stimulation out of a mathematical and computational point of view. While cylindrical axon structures are subject of investigations for many decades now, the researches concentrating on other geometric forms are not that present. However, special geometries like the more or less spherical soma in retinal ganglion cells may also influence the extracellular stimulations of neuroprostheses. Therefore, in the past few years investigations of non-cylindrical structures get in focus of research and we hope we also can contribute some little portion of knowledge to this field of science.

In some general tests, we have verified the behaviour of our model. The modelling of a spherical 3D structure with a 2D *Neuron* compartment model required extensively usage of different *Neuron* functionalities. The implementation took us some time and a lot of tests, however, in different publications and in the *Neuron* forum we finally always have found solutions for arisen problems. Now, we think that our solution can model the spherical structure of a retinal ganglion cell soma quite well. Comparing our model results to actual literature we could not find any remarkable divergences. Especially, we have shown that the inside of a spherical structure is almost in equipotential. Further the determined time constant to reach the steady state of a spherical cell exposed to an electric field in our cable model is comparable to experiments and results of 3D model found in literature.

Our investigations of the stimulation windows and the described blocking phenomena as presented here are just in the beginning phase. Up to now, only a limited outcome of our model was analysed in detail. Especially, the temporal behaviour of ion channel gating will get in focus for further research. However, already in these first analyses we were able to find relationships between different configurations of electrode geometry and diameter of a spherical structure. Further, for a spherical structure, we were able to approximate the stimulation window for different soma diameters based on data gathered for another soma diameter.

Furthermore, we were able to reproduce blocking phenomena during stimulation of a spherical soma only, but also for retinal ganglion cells without dendrites. Up to now, from a computational point of view, we can neither confirm nor preclude that a net Na^+ ion outflux because of a Na^+ current reversal during the stimulation prevents the action potential at high stimulation strength. For extracellular stimuli which influence different sections of a neuron with nearly same stimulus strength at the same time, we found blocking zones where either the soma or the soma and parts of axon are blocked. But, before the exact reasons for the blocking of the soma are not clarified, it is not possible to distinguish clearly between the *Anodal Surround Block* and the *Stimulation Upper Threshold* for all found configu-

rations which cause a neuronal block. Both phenomena or a combination of them might be responsible for partly blocking the neuronal structure. Out of a computational point of view, at the moment there are still many uncertainties regarding the consequences of the Na^+ current reversal on the generation or blocking of action potentials.

For final judgements on the origin of blocking far more analyses (with different computational methods and in experiments) are necessary. But we are very confident, that our model can support us to gather further detailed insight views about blocking phenomena at extracellular stimulation.

8.2 Further Work

First, the existing model should get additional functionality in doing automated data analysis to minimize the manual work in combining the test results. Further, our automatic action potential detection should be improved regarding detection of action potentials which are initiated and propagating while the stimulus is still affecting the neuron.

Further, more configurations for the stimulus itself should be implemented. Here, different pulse forms and trails are thinkable. Also an extension to stimulate more retinal ganglion cells simultaneously is foreseen to simulate the behaviour of a region of retina packed with many retinal ganglion cells.

In a next step a real *3D* model should be implemented which also considers the effects of the neuronal structures to the electric field established by a stimulus. Then, also other configurations for the stimulus (like stimulus trails, different geometries of the electrode) can be investigated in a real *3D* model environment. Results of a realistic *3D* model (for example the dynamics of an electric field) can flow back into the existing *Neuron* model.

Furthermore, all these computational efforts should be accompanied by experimental validation of the results in vitro on real retinal ganglion cell.

Bibliography

- Barriga-Rivera, A., Guo, T., Yang, C.-Y., Al Abed, A., Dokos, S., Lovell, N. H., Morley, J. W., and Suaning, G. J. (2017). High-amplitude electrical stimulation can reduce elicited neuronal activity in visual prosthesis. *Scientific Reports*, 7.
- Boinagrov, D., Loudin, J., and Palanker, D. (2010). Strength–duration relationship for extracellular neural stimulation: numerical and analytical models. *Journal of neurophysiology*, 104(4):2236–2248.
- Boinagrov, D. and Palanker, D. (2014). Reply to rattay. *Journal of neurophysiology*, 112(10):2666–2666.
- Boinagrov, D., Pangratz-Fuehrer, S., Suh, B., Mathieson, K., Naik, N., and Palanker, D. (2012). Upper threshold of extracellular neural stimulation. *Journal of Neurophysiology*, 108(12):3233–3238.
- Carnevale, N. T. and Hines, M. L. (2006). *The NEURON book*. Cambridge University Press.
- Carras, P. L., Coleman, P. A., and Miller, R. F. (1992). Site of action potential initiation in amphibian retinal ganglion cells. *Journal of Neurophysiology*, 67(2):292–304.
- Doyle, D. A., Cabral, J. M., Pfuetzner, R. A., Kuo, A., Gulbis, J. M., Cohen, S. L., Chait, B. T., and MacKinnon, R. (1998). The structure of the potassium channel: molecular basis of k⁺ conduction and selectivity. *science*, 280(5360):69–77.
- Durand, D. M. (1999). Electric stimulation of excitable tissue. In *The Biomedical Engineering Handbook, Second Edition. 2 Volume Set*. CRC press.
- Fohlmeister, J., Coleman, P., and Miller, R. (1990). Modeling the repetitive firing of retinal ganglion cells. *Brain research*, 510(2):343–345.
- Fohlmeister, J. and Miller, R. (1997). Impulse encoding mechanisms of ganglion cells in the tiger salamander retina. *Journal of neurophysiology*, 78(4):1935–1947.

- Fohlmeister, J. F., Cohen, E. D., and Newman, E. A. (2010). Mechanisms and distribution of ion channels in retinal ganglion cells: using temperature as an independent variable. *Journal of neurophysiology*, 103(3):1357–1374.
- Fried, S. I., Lasker, A. C., Desai, N. J., Eddington, D. K., and Rizzo, J. F. (2009). Axonal sodium-channel bands shape the response to electric stimulation in retinal ganglion cells. *Journal of neurophysiology*, 101(4):1972–1987.
- Gerstner, W., Kistler, W., Naud, R., and Paninski, L. (2014). *Neuronal Dynamics: From Single Neurons to Networks and Models of Cognition*. Cambridge University Press.
- Goldman, D. E. (1943). Potential, impedance, and rectification in membranes. *The Journal of general physiology*, 27(1):37–60.
- Hille, B. (1992). *Ionic Channels of Excitable Membranes*. Sinauer Sunderland, MA.
- Hines, M. (1984). Efficient computation of branched nerve equations. *International journal of bio-medical computing*, 15(1):69–76.
- Hines, M. (1989). A program for simulation of nerve equations with branching geometries. *International journal of bio-medical computing*, 24(1):55–68.
- Hines, M. (1993). Neuron - a program for simulation of nerve equations. In *Neural systems: Analysis and modeling*, pages 127–136. Springer.
- Hines, M., Davison, A. P., and Muller, E. (2009). Neuron and python. *Frontiers in Neuroinformatics*, 3:1.
- Hodgkin, A. L. and Huxley, A. F. (1952). A quantitative description of membrane current and its application to conduction and excitation in nerve. *The Journal of Physiology*, 117(4):500–544.
- Hodgkin, A. L. and Katz, B. (1949). The effect of sodium ions on the electrical activity of the giant axon of the squid. *The Journal of physiology*, 108(1):37.
- Jeng, J., Tang, S., Molnar, A., Desai, N., and Fried, S. (2011). The sodium channel band shapes the response to electric stimulation in retinal ganglion cells. *Journal of neural engineering*, 8(3):036022.
- Kandel, E. R., Schwartz, J. H., Jessell, T. M., Siegelbaum, S. A., and Hudspeth, A. J. (2000). *Principles of neural science*, volume 4. McGraw-hill New York.

- Kaniusas, E. (2012). *Biomedical Signals and Sensors I: Linking Physiological Phenomena and Biosignals*. Biological and Medical Physics, Biomedical Engineering. Springer Berlin Heidelberg.
- Klee, M. and Plonsey, R. (1976). Stimulation of spheroidal cells-the role of cell shape. *IEEE Transactions on Biomedical Engineering*, (4):347–354.
- Lee, D. C. and Grill, W. M. (2005). Polarization of a spherical cell in a nonuniform extracellular electric field. *Annals of biomedical engineering*, 33(5):603–615.
- Lu, H., Chestek, C. A., Shaw, K. M., and Chiel, H. J. (2008). Selective extracellular stimulation of individual neurons in ganglia. *Journal of neural engineering*, 5(3):287.
- MacKinnon, R. (2004). Potassium channels and the atomic basis of selective ion conduction (nobel lecture). *Angewandte Chemie International Edition*, 43(33):4265–4277.
- Malmivuo, J. and Plonsey, R. (1995). *Bioelectromagnetism: principles and applications of bioelectric and biomagnetic fields*. Oxford University Press, USA.
- Matteucci, P. B., Barriga-Rivera, A., Eiber, C. D., Lovell, N. H., Morley, J. W., and Suaning, G. J. (2016). The effect of electric cross-talk in retinal neurostimulationcross-talk in retinal neurostimulation. *Investigative ophthalmology & visual science*, 57(3):1031–1037.
- McIntyre, C. C., Grill, W. M., Sherman, D. L., and Thakor, N. V. (2004a). Cellular effects of deep brain stimulation: model-based analysis of activation and inhibition. *Journal of neurophysiology*, 91(4):1457–1469.
- McIntyre, C. C., Mori, S., Sherman, D. L., Thakor, N. V., and Vitek, J. L. (2004b). Electric field and stimulating influence generated by deep brain stimulation of the subthalamic nucleus. *Clinical neurophysiology*, 115(3):589–595.
- McNeal, D. R. (1976). Analysis of a model for excitation of myelinated nerve. *IEEE Transactions on Biomedical Engineering*, (4):329–337.
- Meffin, H., Tahayori, B., Grayden, D. B., and Burkitt, A. N. (2012). Modeling extracellular electrical stimulation: I. derivation and interpretation of neurite equations. *Journal of neural engineering*, 9(6):065005.
- Mulrone, S., Myers, A., and Netter, F. (2009). *Netter's Essential Physiology*. ClinicalKey 2012. Saunders/Elsevier.
- Nernst, W. (1888). Zur kinetik der in lösung befindlichen körper. *Z. phys. Chem*, 2(9):613–679.

- Nowak, L. and Bullier, J. (1998). Axons, but not cell bodies, are activated by electrical stimulation in cortical gray matter i. evidence from chronaxie measurements. *Experimental brain research*, 118(4):477–488.
- Pfützner, H. (2003). *Angewandte Biophysik*. Springer Physik. Springer.
- Ranck, J. B. (1975). Which elements are excited in electrical stimulation of mammalian central nervous system: a review. *Brain research*, 98(3):417–440.
- Rattay, F. (1986). Analysis of models for external stimulation of axons. *IEEE transactions on biomedical engineering*, (10):974–977.
- Rattay, F. (1990). *Electrical Nerve Stimulation: Theory, Experiments and Applications*. Springer Vienna.
- Rattay, F. (1999). The basic mechanism for the electrical stimulation of the nervous system. *Neuroscience*, 89(2):335–346.
- Rattay, F. (2014). On the upper threshold phenomenon of extracellular neural stimulation. *Journal of Neurophysiology*, 112(10):2664–2665.
- Rattay, F., Paredes, L., and Leao, R. (2012). Strength–duration relationship for intra-versus extracellular stimulation with microelectrodes. *Neuroscience*, 214:1–13.
- Rattay, F. and Wenger, C. (2010). Which elements of the mammalian central nervous system are excited by low current stimulation with microelectrodes? *Neuroscience*, 170(2):399–407.
- Sheasby, B. W. and Fohlmeister, J. F. (1999). Impulse encoding across the dendritic morphologies of retinal ganglion cells. *Journal of neurophysiology*, 81(4):1685–1698.
- Toris, C. B., Eiesland, J. L., and Miller, R. F. (1995). Morphology of ganglion cells in the neotenus tiger salamander retina. *Journal of Comparative Neurology*, 352(4):535–559.
- Werginz, P. (2016). *Neuronal activation characteristics in the electrically stimulated retina : a model-based study*. PhD thesis, Technical University Vienna.